Technische Universität München

Department Chemie

Fachgebiet Theoretische Chemie

Environmental Chemistry of Uranyl: A Relativistic Density Functional Study on Complexation with Humic Substances and Sorption on Kaolinite

Alena Kremleva

Vollständige Abdruck der von der Fakultät für Chemie der Technischen Universität München zur Erlangung des akademischen Grades eines

Doktors der Naturwissenschaften (Dr. rer. nat.)

genehmigten Dissertation.

Vorsitzer: **Univ.-Prof. Dr. J. P. Plank**

Prüfer der Dissertation:

1. **Univ.-Prof. Dr. N. Rösch**
2. **Univ.-Prof. Dr. K. Köhler**

Die Dissertation wurde am 18.08.2009 bei der Technischen Universität München eingereicht und durch die Fakultät für Chemie am 09.09.2009 angenommen.

Acknowledgments

I am deeply indebted to my supervisor Prof. Dr. N. Rösch from the Technische Universität München whose help, stimulating suggestions, and encouragement helped me in all the time of research and writing of this thesis.

I am heartily thankful to Dr. Krüger, whose encouragement, guidance and support from the initial to the final level enabled me to develop an understanding of the subject. I gratefully acknowledge his extended help in academic and nonacademic issues.

I offer my regards and blessings to Dr. Dassia Egorova, Dr. Ludmila Moskaleva, and Egor Vladimirov who supported me in many respects (professional and personal) during my stay in München and my work at TU München.

I am grateful to many of my colleagues for stimulating discussions as well as for pleasant work and nice time which we spent together: Dr. F. Schlosser, Dr. A. Matveev, Dr. A. Genest, Dr. R. S. Ray, Dr. S. Bosko, D. Başaran, S. Parker, and those not mentioned here whose presence was helpful and memorable. It is pleasure to thank my friends Elena Medvedeva, Eugenij Grabchak, Dr. Dominic Schupke, Dr. Claus Gruber for their friendship, support and confidence in me, which made my way through all ups and downs much easier.

I would like to thank my parents who inspired me for study and research all my life, who taught me never give up, and who always believed in me. Without them I would not be what I am today.

This thesis would not have been possible without deep support of my friend Ivan Nechaev. He deserves special mention for his love, care, and patience.

Finally, I would like to thank everybody who was important to the successful realization of this thesis.

to Ivan Nechaev

Content

Introduction

The migration and the transport of actinides, released from various sources to the environment, nowadays are of great concern.[1] The strong ability of actinides to from complexes with different natural organic macromolecules (humic substances) as well as organic and inorganic colloids allows the fast distribution of radioactive pollutants in an aquatic environment.[2] Contamination of aquatic natural systems, e. g. groundwaters, can lead to poisoning of drinking water, accumulation of radionuclides in plants, animals, and humans, etc. Preventing the contamination of groundwater and terrain from the results of anthropogenic actions will help to avoid numerous problems. In turn, understanding the environmental chemistry and the transport of actinide can help to avoid and solve these issues.

Long-living radioactive elements in nature derive from various sources. First, there is natural accumulation. Natural actinide isotopes are present in rocks and minerals, e.g. phosphates containing uranium or thorium. These places are known and most of them are used as mining sites for some naturally occurring radionuclides. There are natural deposits of uranium, for example, in Saskatchewan in Canada, in South Australia, in Kazakhstan. Uranium mining itself is more dangerous than other underground mining due to radon gas emitted by uranium ore and the elevated level of radiation. Besides, any mining site has an increased risk for contamination, not only for workers, but for people living nearby.

Another source is anthropogenic: actinides have been artificially produced starting from the middle of the last century. Actually, the use of several naturally occurring actinide isotopes has increased as well. In general, this happened due to the production and use of nuclear weapons and the nuclear power industry. Artificial or anthropogenic actinides are U-236, Pu-238, Np-239, etc.[3] About 2000 tons of Pu have been produced until now.[4] The amount of artificially produced actinides is larger than that occurring naturally, and they have occasionally been released into the environment.

Currently, the most pressing international problem of the nuclear industry with regard to establishing a long-term energy production plan is the disposal of nuclear waste,[5,6] which represents a possible source of permanent contamination. The composition of nuclear waste varies depending on the source of the waste and how it was treated. Nevertheless, uranium is the main component of spent fuel, ~ 94%, plutonium takes about 1 %, the rest are minor actinides (Np, Am, Cm) and fission products.[7] Therefore, uranium interaction in aqueous solution, with organic matter, mineral surfaces, etc. are intensely investigated. To protect our biosphere we need a long-term management strategy including storage, disposal and/or transformation of the waste into a non-toxic and faster decaying form. The radioactive waste has to be converted in such a form which will not react or degrade for a long time period. Also, it needs to be isolated from the biosphere. The timeframe needed for the isolation of waste repositories ranges from 10^4 to 10^6 years. For the moment only deep geological formations are seriously considered for such long periods. Many countries try to find an appropriate solution for a final rather deep and safe repository for high-level waste and spent fuel.[5,6] In the meantime storing high-level nuclear waste above ground for a century is considered appropriate as well, since it allows the material to be observed easily and any problems to be detected and managed.

The German Federal Ministry for the Environment, Nature Conservation and Nuclear Safety (BMU) has developed safety requirements for the final disposal of radioactive waste[8] and established criteria and procedures to be used in the site selection procedure. A long-term geological repository should fulfill the following requirements: (*i*) the integrity of the isolating rock zone must be ensured for a period of 1 million years; (*ii*) the pore water present in the geological rock zone must not in any case mix with groundwater; (*iii*) there should be no advective transport within the rock zone; (*iv*) secondary pathways leading to ingress of aqueous pollutant solutions from the isolation rock host must be excluded.[8] Based on these criteria, the BMU would like to compare one of the controversially discussed possible repositories in Germany, the Gorleben site, with other potential sites. Among those, clay is one option beside salt formations or granite for disposing radioactive waste. One of the possibilities of host rocks considered in Europe is the opalinus clay formation in Switzerland.[5] The sedimentary rock known as opalinus clay takes the form of a homogeneous layer, around 110 meters thick in the region of interest. It formed in a marine environment by deposition of fine silts that altered over geological timescales to a clay rock. opalinus clay layers can be found in Northern Switzerland, in various areas of Southern Germany and in France. This clay has very good sealing and isolation capacity, which is provided by microscopically small

plate-like clay minerals.[9] The surface-active particles can fix toxic substances over a long geological time period. The long-time behavior and engineering properties of opalinus clay are being investigated in Switzerland[5,9] and Germany.[6]

The security of a repository is not only related to the safety of the storage place itself, but also to pollution prediction and the ability to take action in case of any accident. Therefore, one needs to achieve a comprehensive level of knowledge and understanding of the interaction of radioactive materials with other substances. The ability to predict the migration behavior of waste materials as well as knowledge of their chemistry are essential for any risk assessment. To predict the behavior of pollutants in the environment, not only from waste materials, but also from mining sites and natural deposits of radioactive elements, one needs a rather deep understanding of the chemical mechanisms of migration, complexation, diffusion, adsorption, etc. In this context, an important goal currently is the accumulation of fundamental and applied knowledge about physical and chemical properties of hazardous elements, in particular actinides.

Various experimental and analytical methods are nowadays used to study actinide chemistry in natural systems: X-ray absorption spectroscopies (XANES, EXAFS),[10-25] nuclear magnetic resonance (NMR),[26,27] time-resolved laser-induced fluorescence spectroscopy (TRLFS),[28-32] Fourier transform infrared (FTIR) and ultraviolet-visible (UV-vis) spectroscopic methods,[13,16,33,34] surface complexation models,[35,36] batch experiments,[37,38] etc. Recently, also computational methods for characterizing actinide compounds and their reactions were greatly developed and have become popular.[39–47] They also contribute to such type of investigations.

In the present thesis two major problems of actinide interaction with the environment are investigated by computational methods: (i) complexation by organic matter in aquifer or soil and (ii) actinide adsorption at mineral surfaces. I studied the behavior of uranyl UO_2^{2+}, which is the chemically most stable form of U(VI). Uranium in general is the central element in the nuclear fuel cycle, as fuel of nuclear reactors and as major component of the final waste. Uranyl is a highly mobile ion; it readily forms complexes with organic and inorganic matter.[2] Furthermore, uranyl is the dominant uranium species in contaminated groundwater systems.[48] Besides complexation in solution, the interaction of uranyl with clay mineral surfaces may contribute to its accumulation or retardation. Thus, adsorption of uranyl by natural clays can influence its distribution in the environment.

The first part of the present work describes the complexation of uranyl with alcoholic groups of humic acids in solution.[49] The second part is devoted to uranyl adsorption at the

clay mineral kaolinite.[50,51] Both processes, complexation by humic acids (HAs) and adsorption on mineral surfaces, are genuine mechanisms which affect the mobility of actinide contaminants under natural conditions.

Part I – Complexation of uranyl with alcoholic groups of humic substances

1. Actinides in the environment

1.1 Solution chemistry of uranium

The most important oxidation states of uranium in a natural environment are 4+ and 6+. Compounds containing tetravalent uranium are insoluble, while those containing the stable hexavalent uranyl ion UO_2^{2+} are highly soluble and mobile.[1,2] Therefore, uranyl and its compounds were extensively studied. The structure in aqueous solution was determined as penta-coordinated aqua ion $UO_2(H_2O)_5^{2+}$ using LAXS[52] and EXAFS[13,16,53] techniques; quantum chemical[43,44] and molecular dynamics[54] studies confirmed this structure.

One of the important processes in solution is hydrolysis, which starts for the uranyl ion already at pH of the solution of ~2.[55] The formation of hydroxo complexes of uranyl competes with the complexation by organic and inorganic ligands. When examining the solution chemistry of uranyl, one should take into account the actual hydroxo compounds in a solution at a certain pH and uranyl concentration. The stoichiometric coefficients of various $(UO_2)_n(OH)_m$ compounds and their equilibrium constants were determined by experiment.[55,56] Using these constants, ionic strength of the solution, and initial concentration of uranyl one can determine the speciation of uranyl, which illustrates the variety of different hydrolysis products that co-exist at certain pH values of the solution. Generally, the concentration of the solvated uranyl ion drops with increasing pH until ~5–6. At nearly neutral pH mostly $(UO_2)_3(OH)_5^+$ is formed; at high pH $UO_2(OH)_4^{2-}$ is the dominating product before precipitation of uranyl as mixed oxides and hydroxides occurs.[55,56]

In solution the uranyl ion forms soluble complexes with carbonate, organic and inorganic substances.[57,58] Carbonates are important ligands since they are ubiquitous in the environment under aerobic conditions and have a high metal-complexing ability.[59] The presence of carbonato ligands significantly changes the speciation. Complexes of uranyl with carbonate ligands suppress hydrolysis, affect the complexation especially at high pH and hinder adsorption at pH ~8 and higher.[25,59] Mononuclear $UO_2(CO_3)_n$ compounds are formed around neutral pH and the dominant species $UO_2(CO_3)_3^{4-}$ is present in a wide pH range (>7).[60]

The interaction of uranyl with organic decomposition products, that are present in any natural water and soil, as well as the adsorption of uranyl at clay minerals are key processes for migration of uranyl.[2,57,58] The former is assumed to happen via oxygen donor centers, mostly of carboxylic groups, which are deprotonated at near neutral pH, and therefore have a negative charge that attracts metal cations. The complexation with organic matter will be discussed in more details in the subsequent Sections 1.2–1.3. The adsorption of actinides at mineral surfaces is a likely retardation mechanism. It also can reduce the oxidation state of actinides.[57,58] The second part of this work is dedicated to modeling the adsorption of uranyl at various surfaces of kaolinite, one of the simplest clay minerals.

1.2 Complexation by humic substances

The migration behavior of actinides in the environment depends on their oxidation state, the chemical speciation, redox reactions, sorption characteristics, the pH of the solution and many other environmental conditions.[2,57,58] The interaction of actinides with humic substances, present in solution, can enhance the migration of actinides or give rise to retention of some of them. Humic substances can also cause a reduction to lower oxidation states.[61] Natural organic matter can reduce, for example, Pu(VI) to Pu(IV) or Np(VI) to Np(V).[61] Polyelectrolytes are major organic species which play a role in the migration and immobilization of actinides in natural waters.[57,58]

Humic substances are organic polyelectrolyte macromolecules – the principal organic component of soils and waters. Humic substances can be distinguished by their solubility properties. They are divided into fulvic acids (FA), which are soluble at all pH values, humic acids (HA), which are soluble above pH ~3.5, and humin – the insoluble fraction at all pH values.[57] These three classes of compounds are not easily characterized because they have very variable compositions.

For polyelectrolytes in solution the increased ionization with increasing pH results in a strong intramolecular repulsion, and even uncoiling of the polymeric network.[58] Binding with

metal ions neutralizes the repulsion and allows a contraction of the macromolecule. As a result if sufficient metal ions are complexated, one finds compact molecules with a relatively hydrophobic exterior. This induces coagulation and precipitation of metal-humate complexes. If the amount of bound metal ions is not enough, complexes stay soluble and can migrate in environment.

Humic substances may also exhibit colloidal behavior due to their rather large size. An important property is that the diffusivity of an extended macromolecule is lower than when in coiled form. For example, in fresh water with low salt concentration humic acids are expected to be extended and their diffusion is slow, therefore, the diffusion of associated actinides is reduced as well. At variance, in waters with high salt content humic acids are more coiled and their diffusion is increased.[62] The result of such coiling is a decrease of the hydrophobicity, which together with the high salinity leads to aggregation and coagulation. Therefore, diffusion is hindered. In addition, humic macromolecules can form coatings on colloidal inorganic species and mineral surfaces and change their adsorption properties.[25] Actinides are expected to interact with these coated colloids and surfaces in the same way as with humic colloids.

1.3 Reactive groups of humic substances

Actinide elements interact most strongly via oxygen donor sites, therefore the binding to HAs is expected to occur via oxygen donor functional groups.[63] Table 1.1 shows the ranges of oxygen distribution for various functional groups of six samples of humic acids (HAs) and fulvic acids (FAs).[63] As one can see, carboxylic groups are prevailing.

The pK_a of humic polyelectrolytes varies with the degree of ionization as calculations at different points during a titration process show. At 50 % ionization of carboxylate groups, the pK_a was obtained at 3.6 for a variety of fulvic acids. For humic acids this value is ~ 4.8.[64] For the phenolic dissociation at 50 % ionization a pK_a value of ~ 9.8 was reported.[65] Thus, in most natural waters carboxylic groups are mostly ionized while phenolic groups remain protonated. Therefore, carboxylic groups are assumed primarily to mediate the interaction of HAs with actinides.[63,66] They can contribute to different types of complexes (bi- and monodentate, chelate). Because of their low pK_a values (< 7) they exhibit a strong propensity to form complexes with actinides in aqueous solution at low pH values (2 to 6), while polynuclear

Table 1.1. Oxygen distribution in functional groups of HAs and FAs.

Sample	$-CO_2H$	Phenolic	Alcoholic	C=O	OCH_3	Other
HAs	34-50 %	7-14 %	1-8 %	15-30 %	2-4 %	5-29 %
FAs	57-75 %	1-10 %	9-20 %	11-17 %	3-5 %	0-10 %

anionic products of uranyl hydrolysis (see Section 1.1) hinder complexation at higher pH values.[55]

Recently other functional units of HAs have been considered as complexation sites of actinides, among them amino groups[32,67,68] as well as alcoholic and phenolic hydroxyl groups.[13,31] Earlier studies of uranyl complexation by amino groups[69,70] favored the formation of chelate complexes between uranyl and amino acid. Therefore, the contribution of amino groups in complexation was suggested. In contrast, a recent study[32] did not find any evidence for the formation of chelate species that involve an amino group. In summary, the contribution of amino group in uranyl complexation by HAs is still under discussion.

The relatively high pK_a values of alcoholic (~14–15) and phenolic OH groups (~10) are one of the reasons why their role in actinide complexation may be less important. Recall that under natural conditions the pH is about neutral, ~7. Recently, phenolic OH groups attracted interest and were examined as complexation sites in natural and synthetic HAs for uranyl (VI) ions at pH = 2–4[13,31] and for neptunyl (V) ions at pH = 7.[10,71] Natural as well as synthetic HAs were modified to block phenolic OH groups by methylation.[31] First, all the carboxylic and alcoholic groups were permethylated in a methanol solution by diazomethane. Then, the permethylated HAs were reacted with NaOH to hydrolyze the ester groups. As a result, modified HAs exhibited blocked phenolic and other alcoholic OH groups, while carboxylic groups were demethylated.[31] Differences between complexes with carboxyl and phenolic groups may be discernible, when phenolic OH groups of HAs are blocked. Nevertheless, EXAFS results showed similar structure parameters (±1 pm) of uranyl complexes for original and modified humic substances at pH = 2.[13] However, the loading capacity of HA, representing the maximuml mole fraction of available complexing sites of HA, decreased when modified humic substances were compared at pH = 4 to their unmodified counterparts.[31] As a result, the reduction of the loading capacity demonstrates that phenolic OH groups contribute to uranyl complexation at pH = 4. Thus, blocking phenolic OH groups may change the complexation behavior of HAs and, hence, phenolic OH groups may be involved in complexation of actinides. Yet, the experimental methods used were not sensitive enough to demonstrate the contribution of phenolic OH groups in an unequivocal way.

Complementing experimental efforts, theoretical studies may help to rationalize the role of various functional groups. This thesis reports results of a computational study on uranyl complexation by alcoholic (aliphatic and phenolic) OH groups of humic substances.[49] Alcoholic groups were modeled with the help of small aliphatic and phenolic alcohols. These ligands can be regarded as models of complexation sites of humic substances. As both

phenolic and aliphatic OH groups are protonated under natural conditions, uranyl complexes with ligands in protonated and deprotonated form were compared. As alternative complexation mechanism that does not require deprotonated OH groups to be present in solution, deprotonation of ligands in the field of uranyl was explored. This work mainly presents structural parameters as well as complexation free energies and compares these results to those of experiments and other computational study of uranyl complexes with carboxylic groups.[72,73]

2. Computational approach

2.1 Computational details

Recently, quite a few computational studies have been devoted to actinide complexation in solution.[72-76] Suitable quantum chemistry methods[39-47] afford a reliable description of the relativistic electronic structure of rather large systems with heavy atoms. Solvent effects can be estimated with applying a polarizable continuum model (PCM);[41,43] however, for a reliable description of the solvation of uranyl complexes, in particular short-range solvent effects, it is necessary to treat the first hydration sphere explicitly in the quantum mechanical model.[41,43,77]

In the following, "first principles" scalar relativistic density functional calculations of uranyl complexes with aliphatic and phenolic alcohols are presented. All calculations were carried out with the Gaussian-type orbitals fitting-functions density functional method[78] (LCGTO-FF-DF) as implemented in the program PARAGAUSS 3.0.[79] Specifically, the scalar relativistic[40,80] second-order Douglas-Kroll-Hess (DKH)[81,82] all-electron approach to the Dirac-Kohn-Sham problem was used. Because all species examined exhibit a closed-shell electronic structure, effects of spin-orbit interaction were neglected.[83,84]

A two-step strategy was employed to determine structures and energetics.[76] First, structures were optimized with the local density approximation (LDA) of the exchange-correlation functional (VWN parameterization),[85] which is well known for furnishing accurate bond lengths of compounds with heavy elements.[76,84,86] For these LDA optimized structures, in a second step, energies were evaluated invoking the generalized gradient approximation (GGA) proposed by Becke and Perdew (BP).[87,88] Such GGA energies are more accurate, while binding energies determined with LDA functionals are generally overestimated.[86,89]

The Kohn-Sham orbitals were represented by flexible Gaussian-type basis sets, contracted in a generalized fashion using appropriate atomic eigenvectors. For U, a basis set of the size (24s, 19p, 16d, 11f)[90] was used, contracted to [10s, 7p, 7d, 4f]. The light atoms

were described by standard basis sets:[91] (9s, 5p, 1d) → [5s, 4p, 1d] for C and O,[91a,b] and (6s, 1p) → [4s, 1p] for H.[91a,c] The quality of these basis sets has previously been examined.[92] The performance of the actinide orbital basis sets was tested on the six- to four-valent oxocations, UO_2^{2+}, UO_2^{+}, UO_2, and on the halides, UF_6 and UCl_6. The deviations caused by the standard contraction were insignificant: less than 0.25 % or about 0.5 pm for bond distances and less than 1% for vibrational frequencies and binding energies.[92]

In the LCGTO-FF-DF method, the classical Coulomb contribution to the electron-electron interaction is evaluated via an approximate representation of the electron density; the corresponding Gaussian-type auxiliary basis set was constructed by a standard procedure.[78] The exponents of s and r^2 type functions were generated by scaling the exponents of the corresponding orbital basis. In addition, five "polarization exponents" each of p, d, and f type were added at each atomic center as appropriate. These exponents were constructed as geometric series with a factor 2.5, starting with 0.1, 0.2, and 0.3 au for p, d, and f type exponents, respectively. For U all three series were used; for C and O, only the p and d type series, and for H, only the p type series was applied. Thus, the auxiliary basis sets were (24s, $9r^2$, 5p, 5d, 5f) for U, (9s, $5r^2$, 5p, 5d) for C and O, (6s, $1r^2$, 5p) for H. Comparison with results of other DF calculations confirmed the accuracy of the current FF approach for actinide complexes.[84]

The grid for the numeric integration of the exchange-correlation functional was chosen as a superposition of atom-centered spherical grids.[93] All atomic grids featured 146, chosen such that angular integration is accurate to all components up to L = 19. There were 180 radial shells for U, 68 for O, 78 for C, and 61 for H. For typical complexes these grids comprise about 26000, 11400, 10000 and 9000 points for U, C, O, and H centers, respectively.

In geometry optimizations, the total energy was converged to 10^{-8} au, gradients were required to be less than 10^{-6} au. All stationary points of complexes (without a PCM environment) were confirmed as local minima by a normal mode analysis.

Long-range electrostatic solvation effects were taken into account using a PCM model, the COSMO variant[94-97] (conductor-like screening model), as implemented in the program PARAGAUSS.[77] In the COSMO approach the solute is placed in an empty cavity surrounded by of a dielectric medium. This solute cavity was constructed from overlapping atomic spheres with radii derived from van der Waals radii,[98] scaled by 1.2 (except for H); additional spheres were created according to the GEPOL algorithm.[99,100] The dielectric constant of water was taken as $\varepsilon = 78.39$. Short-range solvation effects were represented by direct inclusion of the first hydration sphere of uranyl at the all-electron level.

2.2 Evaluating of reaction energies

All complexes as well as ligand molecules were fully optimized in solution without any symmetry constraints. Zero-point energy (ZPE) corrections and thermodynamic corrections to the energies were estimated from the results of a normal mode analysis, carried out in the gas phase. Translational, vibrational, and rotational contributions to the energy and entropy terms of G_{gas} were calculated with the help of the corresponding partition functions.[101] Hence, all energies listed in the following are estimates of Gibbs free energies ΔG. Free energies of reactions were derived by means of a thermodynamic cycle.[101]

$$\begin{array}{ccccccccc} A_{gas} & + & B_{gas} & \rightarrow & C_{gas} & + & D_{gas} & & (\Delta G_{gas}) \\ \downarrow \Delta G_{sol} & & \downarrow \Delta G_{sol} & & \downarrow \Delta G_{sol} & & \downarrow \Delta G_{sol} & & \\ A_{aq} & + & B_{aq} & \rightarrow & C_{aq} & + & D_{aq} & & (\Delta G_{aq}) \end{array}$$

Calculated Gibbs free energies in the gas phase G_{gas} and solvation energies ΔG_{sol} of all systems were used to derive Gibbs free energies in solution: $G_{aq} = G_{gas} + \Delta G_{sol}$. Therefore, the Gibbs free energies of reactions were estimated as:

$$\Delta G_{aq} = \Delta G_{gas} - \Delta G_{sol}(A) - \Delta G_{sol}(B) + \Delta G_{sol}(C) + \Delta G_{sol}(D) + SSC,$$

where SSC are standard state corrections. Standard state corrections for the reaction free energies were accounted for by adjusting to the standard concentration of 1M for solutes. The corresponding standard molar volume is 1 l, and the standard pressure is 24.45 atm. The standard state for gas phase is a pressure of 1 atm. Solvation free energies $\Delta G_{sol}(X)$ were calculated according to the following reaction

$$X_{gas} \rightarrow X_{PCM}$$

This reaction can be divided into two steps, describing the transition between the different conventional standard states

$$X_{gas}\ (1\ atm) \rightarrow X_{gas}\ (24.45\ atm) \rightarrow X_{PCM}\ (24.45\ atm)$$

The free energy change of the first step is $\Delta G^1 = RT \ln (24.45/1)$, while the free energy of the second step is simply the solvation energy from a PCM calculation, $\Delta G_{sol} = E_{PCM} - E_{gas}$. As a result, the standard state correction for the solvation energy ΔG_{sol} for each molecule participating in a reaction is $RT \ln (24.45/1) = +8$ kJ mol^{-1}, except for water molecules. Water as a solvent has a different standard concentration of 55.34M, the standard molar volume is 0.018 l, and the standard pressure is 1354 atm. Thus, for each water molecule the corresponding standard state correction will be accounted as $RT \ln (1354/1) = +18$ kJ mol^{-1}.

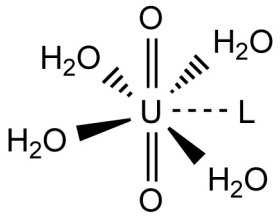

Figure 2.1. Schematic representation of five-fold coordinated uranyl with one ligand (L) coordinated in monodentate fashion. The equatorial plane is the plane perpendicular to the $[O=U=O]^{2+}$ moiety.

2.3 Models

Both experimental[13,14,16,53] and theoretical[43,45] results suggest a pentagonal coordination of the uranyl ion to be preferred. Therefore, in the present work, uranyl was assumed to exhibit five-fold coordination in all complexes studied. Thus, for monoligated complexes with alcohols four water molecules of the first coordination sphere of the uranyl were explicitly included in the quantum chemical model (Fig. 2.1).

Simple aliphatic alcohols were taken to model the corresponding complexation sites of HAs: methanol (MeOH), ethanol (EtOH), propanol (PrOH), and isopropanol (iPrOH). Both neutral and deprotonated forms of alcohols were considered as possible ligands. As examples of OH groups attached to aromatic fragments of HAs, I invoked phenol (PhOH) as well as ortho-hydroxy phenol (oPhOH, catechol), and para-hydroxy phenol (pPhOH, hydroxy-quinone). See Fig. 2.2 for a schematic representation of the neutral form of all ligands

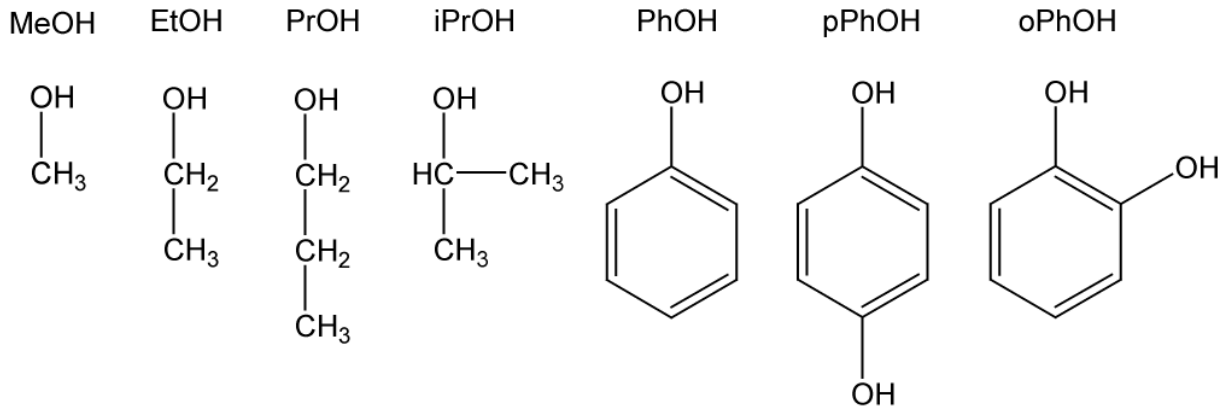

Figure 2.2. Schematic structures of various ligands in protonated form which were used to model alcoholic complexation sites of humic acides for uranyl. Aliphatic groups are modeled by methanol (MeOH), ethanol (EtOH), propanol (PrOH), and isopropanol (iPrOH); phenolic complexation sites are represented by phenol (Ph), para-OH-phenol (pPhOH) and ortho-OH-phenol (oPhOH, catechol).

examined. Besides alcoholic ligands, the neutral acetic acid CH_3COOH ligated to the uranyl in monodentate fashion was optimized for comparison. Results for acetate were already available.[72,73]

All model alcohol ligands studied offer a single OH group as complexation site, oPhOH being an exception. Two configurations have been considered for the two OH groups of ortho-hydroxy phenol (catechol): (*i*) an "out" isomer where the hydroxyl groups are pointing away from each other; (*ii*) an "in" isomer where one hydroxyl group forms a hydrogen bond with the second, Fig. 2.3. The energy difference of these two isomers was calculated at 5 kJ mol^{-1} in favor of the "in" isomer. Catechol in "out" conformation offers two identical complexation sites for uranyl, whereas the "in" conformation yields two *different* complexation sites (Fig. 2.3). However, during structure optimization of one of the corresponding uranyl complexes ("in1"), where uranyl is attached to the hydroxyl oxygen which donates to the hydrogen bond, the second hydroxyl group turned outward, and a complex with oPhOH in "out" conformation resulted. Note that the two different catechol complexes of uranyl, "in2" and "out", yield the same structure with $oPhO^-$ after deprotonation –complex "out" with $oPhO^-$ (Fig. 2.3). The corresponding complex with "in" configuration of the $oPhO^-$ ligand is possible only if uranyl complexates the deprotonated ligand. Thus, uranyl complexes with $oPhO^-$ may exhibit (*i*) configuration "out" if complexation takes place before

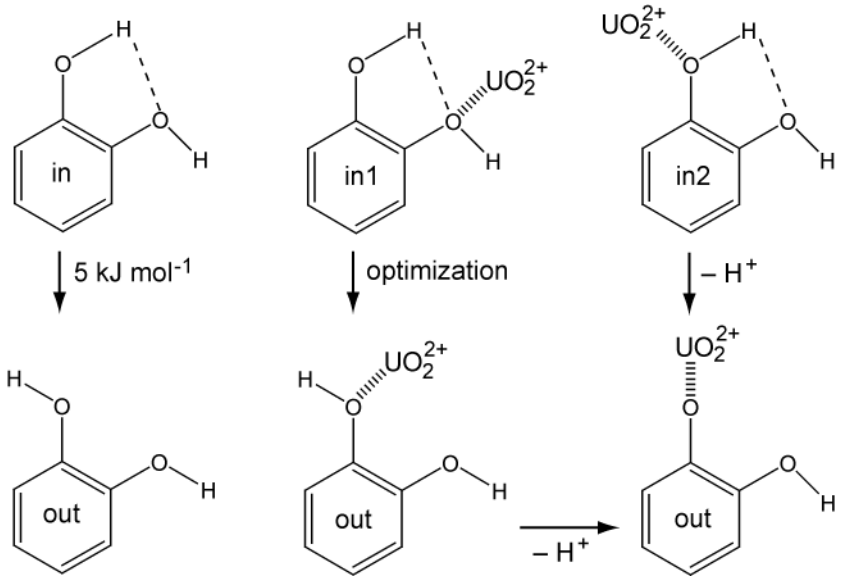

Figure 2.3. Schematic structures of two isomers of o-OHC_6H_4OH (oPhOH): "in" – one hydroxyl group forms a hydrogen bond with the second OH group; "out" – hydroxyl groups pointing away from each other. Three complexes of uranyl with neutral oPhOH isomers have been explored, one with out and two with in configurations (in1, in2). During optimization, complex in1 rearranged to isomer out. Deprotonation of uranyl-catechol complexes of either out or in2 configurations yield the same structure (bottom corner on the right).

deprotonation, (*ii*) configuration "in" if the ligand first looses the proton.

The monodentate complex of uranyl with oPhOH/O^- likely is not the ground state. Because of the high stability of five-member rings, a chelate conformation of the uranyl-catechol complex is expected to be more stable.[102] In the Section 3.1 and 3.3 mainly monodentate complexes will be compared, because these models represent single OH groups of humic acids. Nevertheless, chelate structures of catechol were modeled too and optimized in solution with C_s symmetry applied; these results are discussed in Section 3.4.

3. Results and Discussion

In the following first geometric, then energetic characteristics of uranyl mono- alcoholate and mono-alcohol complexes will be discussed. Whereas alcoholate groups offer natural complexating sites for actinide cations, the interaction of uranyl with protonated alcohol groups also was studied because this is the prevailing state at environmental conditions. Alcoholate complexes may also be obtained via intermediate alcohol complexes and deprotonation of the alcohol group which is facilitated in the field of uranyl.

3.1 Geometry parameters

Pertinent structural parameters of optimized complexes with aliphatic and phenolic ligands in solution are collected in Table 3.1: (*i*) axial bond length U-O_t, (*ii*) bond length U-O_c to the alcoholic ligand, (*iii*) the corresponding U-C distance, (*iv*) angle U-O_c-C, (*v*) the bending angle O_t-U-O_t of uranyl, (*vi*) the range of U-O_w bond distances to aqua ligands, and (*vii*) the average equatorial U-O uranium-ligand distance U-O_{eq} – an important parameter for comparison with experiment. Usually only axial bond lengths U-O_t and average equatorial distances U-O_{eq} are available from EXAFS studies.[11-13,15] In EXAFS, it is often not possible to resolve different types of equatorial U-O bonds because U-O_w distances are comparable to U-O_c distances of the ligands. The interpretation of the corresponding EXAFS data is normally based on a comparison with typical distances derived from X-ray diffraction on crystal structures.[11]

Table 3.1. Uranyl complexes $[UO_2(H_2O)_4ROH]^{2+}$ and $[UO_2(H_2O)_4RO]^{+}$ of aliphatic and aromatic alcohols ROH[a] in comparison to aqua and acetic acid ligands: structure parameters, distances in pm, angles in degree.

		U-O_t	U-O_c	U-C	U-O_w	U-O_{eq}	O_t-U-O_t	U-O_c-C
RO^-	OH^-	180	210[b]		237-246	237	172	
	MeO^-	181	209	324	241-247	237	177	136
	EtO^-	181	208	337	239-248	237	174	151
	PrO^-	181	208	346	238-249	237	168	169
	$iPrO^-$	181	208	347	239-249	237	168	170
	PhO^-	180	217	333	237-248	237	176	144
	$oPhO^-$, in	180	213	345	240-253	238	171	174
	$oPhO^-$, out	180	214	345	240-247	237	171	171
	$pPhO^-$	180	215	335	238-251	238	171	148
	CH_3COO^-, mono[c]	179	229	335	234-243	236	177	138
	CH_3COO^-, bi[c]	179	237	277	236-237	237	174	94
ROH	H_2O	178			235-238	236	171	
	MeOH	178	235	335	234-242	237	177	123
	EtOH	178	234	340	235-239	236	176	126
	PrOH	178	234	340	234-241	237	177	126
	iPrOH	178	233	343	235-242	237	178	128
	PhOH	178	246	352	233-239	238	178	131
	oPhOH, in2	178	245	350	234-237	237	178	130
	oPhOH, out	178	251	356	230-247	239	175	151
	pPhOH	178	245	352	234-240	238	178	132
	CH_3COOH	178	230	343	234-254	238	177	148
Exp.	HA sol.[d]	178(2)				237-240(2)		
	Blocked HA sol.[d]	178(2)				238-240(2)		
	Carb. ac. sol.[e]	179(1)		325(3)		237(1)		
	Catechol, pH=5[f]	178(2)				239(2)		
	Catechol, pH=10[f]	182(2)				237(2)		

[a] For the designations of the various alcohols ROH, see Figs. 2.2 and 2.3. [b] U-O bond to hydroxyl. [c] Ref. 72. [d] Refs. 13, 31. [e] Average over various α-substituted carboxylic acids, Ref. 32. [f] Ref. 15.

The upper part of Table 3.1 contains results for complexes with deprotonated ligands RO^-. Optimized geometries for uranyl complexes with MeO^- and MeOH are shown in the Figs. 3.1a and 3.1b. The axial U-O_t bond lengths of the complexes $[UO_2(H_2O)_4OR]^{+}$ are

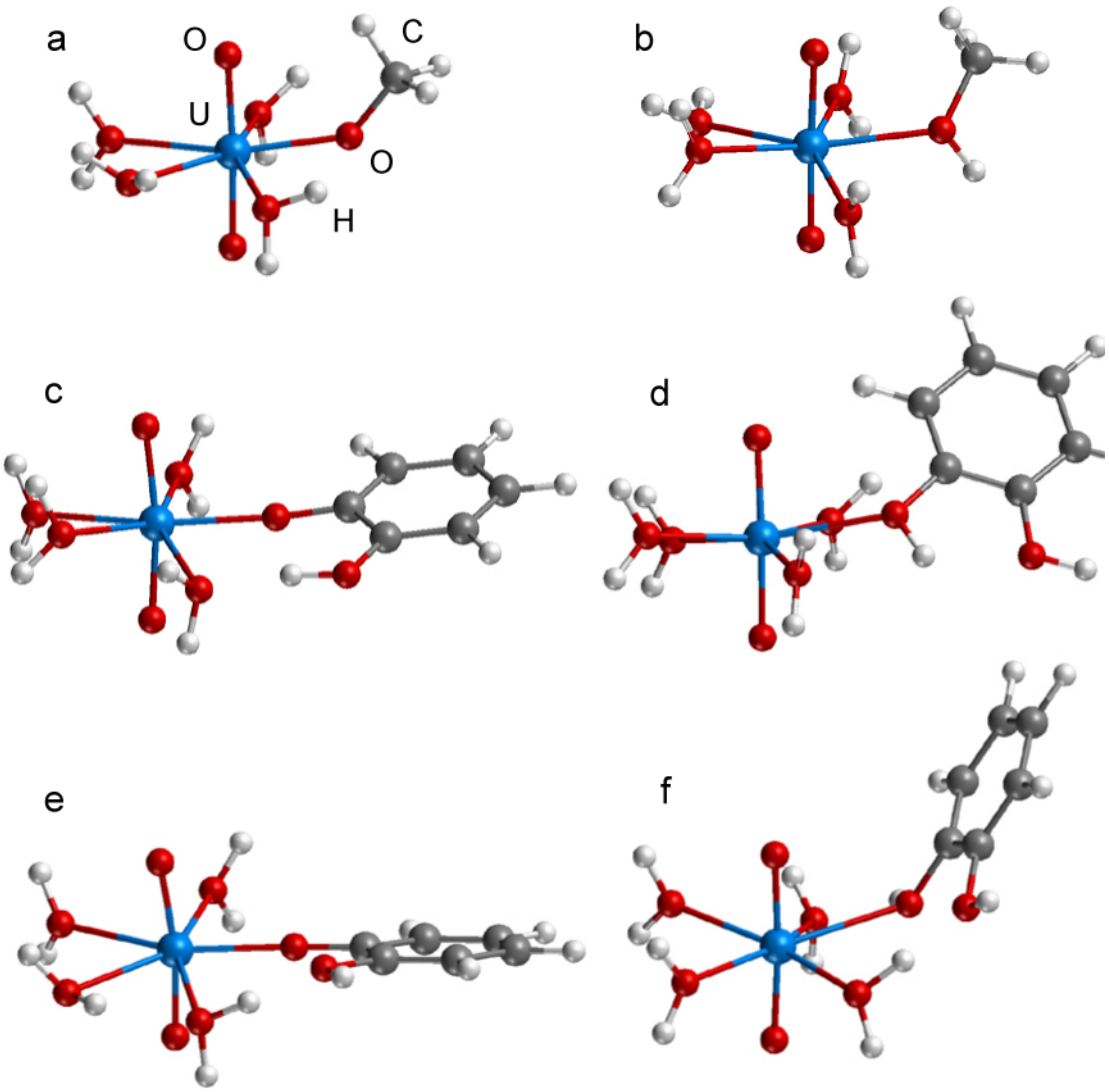

Figure 3.1. Optimized structures of uranyl complexes with methanol and ortho-OH-phenol in its neutral and deprotonated form: (a) MeO^-, (b) MeOH, (c) $oPhO^-$, in, (d) oPhOH, in2, (e) $oPhO^-$, out, (f) oPhOH, out isomer.

rather similar, 180–181 pm, whereas the bond distances U-O_c depend on the nature of the ligand: for aliphatic ligands it is 208–209 pm, for phenolic 213–217 pm. The shorter U-O_c values (213, 214 pm) belong to the complexes with $oPhO^-$ isomers, while the longest one (217 pm) was determined for the complex with PhO^-. That is in line with pK_a trends for the corresponding ligands: uranyl complexates stronger ligands with higher pK_a values. The uranyl moiety is slightly bent, up to 12° from the linear reference structure (angle O_t-U-O_t, Table 3.1), due to the asymmetry of the equatorial ligand shell.

Five-coordinated uranyl monohydroxide $[UO_2OH(H_2O)_4]^+$ (Fig. 3.2a) features a similar value of U-O_t, 180 pm, as uranyl complexes with alcoholate ligands; its U-O_H bond, 210 pm, is comparable to the distance U-O_c of aliphatic alcoholates (Table 3.1). Thus, a hydroxyl group may be regarded as a ligand that complexates uranyl as strongly as a deprotonated

alcohols. Note, however, that most probably five-fold coordinated uranyl monohydroxide is not the most stable isomer, as four-fold $[UO_2OH(H_2O)_3]^+$ was found to be preferred among several isomers examined.[103]

The bond distances to the four aqua ligands of the $[UO_2(H_2O)_4RO]^+$ complexes vary from 237 to 253 pm (Table 3.1); average distances from the U center to the aqua ligands are 242–245 pm, which is ~30 pm longer than the U-O_c bond. Thus, the first shell of equatorial U-O distances splits into a shorter bond to the alcoholate ligand and a set of longer bonds to the aqua ligands. Yet, the experimentally accessible average U-O_{eq} of all equatorial U-O distances is almost the same for all types of complexes, ~237 pm. This result is in accord with previous findings that the average U-O_{eq} depends mainly on the coordination number of uranyl (5 for the complexes examined) rather than on the ligand or the type of complexation.[76,72]

U-C distances, which vary with the type of ligand, do not characterize a chemical bond. Therefore, they depend on other parameters, like the bond length U-O_c, the angle U-O_c-C, the formation of hydrogen bonds with α-substituted ligands, etc. This distance is largest, ~345 pm, when the angle U-O_c-C is close to linear; see the complexes with the PrO^-, $iPrO^-$, and $oPhO^-$, and smallest for MeO^-, 324 pm, due to an U-O_c-C angle of 136 degree only (Table 3.1). Besides that there is no strongly pronounced trend.

The complexes with alcohol ligands, $[UO_2(H_2O)_4(ROH)]^{2+}$ (Table 3.1), show longer U-O_c bonds and shorter uranyl bonds than the alcoholate complexes, indicating a weaker interaction with the ligand. In the complexes with ROH ligands the U-O_t bond is notably shorter, by ~3 pm, hence less activated, than in complexes with negatively charged RO^- ligands. In fact, with ~178 pm, it is very similar to the terminal bond of a free uranyl cation.

The uranyl moiety is hardly bent, with O_t-U-O_t angles between 175° and 178°. The coordinative bond U-O_c is elongated compared to the corresponding alcoholate complexes, by ~25 pm for aliphatic ligands and by ~30 pm for ligands containing an aromatic ring. For

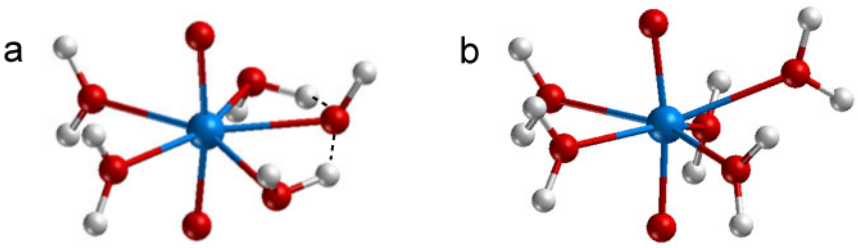

Figure 3.2. Optimized structures of (a) uranyl monohydroxide and (b) the free uranyl ion solvated by five aqua ligands. Hydrogen bonds are represented by dashed lines.

complexes with neutral ligands, U-O_c varies from 235 to 250 pm. In contrast to the alcoholate complexes, these values are comparable to distances U-O_w to the aqua ligands of 230 to 247 pm (Table 3.1). Again, aliphatic alcohols yield a shorter U-O_c bond of about 234 pm, while for aromatic alcohols a value of 245–250 pm is calculated. The differences between coordinative bonds to aliphatic and phenolic neutral ROH ligands are somewhat larger, ~10–15 pm, than for the corresponding complexes with deprotonated ligands, 8–9 pm. Apparently, the stronger interaction of a charged ligand (alcoholate) with the uranyl cation reduces differences between aliphatic and phenolic ligands. As for alcoholate ligands, U-C distances correlate with U-O_c-C angles; shorter U-C distances correspond to smaller angles. Because the oxygen center of ROH ligands is three-fold coordinated in the complexes with uranyl, the angle U-O_c-C is close to 120°, ranging from 123° to 132°. The complex with the "out" isomer of oPhOH (Fig. 3.1d) forms an exception, with U-O_c-O = 151° (Table 3.1), most probably because of the H-bond between the nearest aqua ligand and a neighboring OH group, specific to catechol. Besides, the U-C distances for complexes with aliphatic ROH ligands (335–343 pm) are on average shorter than for phenolic ligands (350–356 pm). Average U-O_{eq} distances are similar in the complexes with aliphatic ROH ligands, 236–237 pm, and almost the same as in the corresponding complexes with deprotonated RO^- ligands, 237–238 pm. These findings demonstrate once again that the distance U-O_{eq} is independent of the type of ligand.[72] Interestingly, in the complexes with phenolic ROH and RO^- ligands the U-O_{eq} distances are slightly longer, by 1–2 pm, compared to complexes with aliphatic ligands.

Finally, the optimized structure results will be compared to available experimental data for alcohol ligands as well as natural and modified humic acids. The lower part of Table 3.1 represents structural parameters for different types of ligands complexating uranyl.

Having uranyl complexation with HAs in mind, the results for alcohols are also compared to uranyl mono- and bi-acetate[72] as models for carboxylic groups of HAs (Table 3.1), which are considered to be the dominant functionalities of these compounds.[63,66] Differences between complexes with carboxyl and phenolic OH groups may be discernible, for example, when phenolic OH groups of HAs are blocked.[13]

The complexes of uranyl with CH_3COO^- in monodentate (Fig. 3.3a) or bidentate coordination feature shorter U-O_t bonds, 179 pm, than the complexes with aliphatic or phenolic alcoholate ligands, 180–181 pm. This points to a weaker interaction with the acetate ligand; this interpretation is corroborated by the longer U-O_c distance to the acetate, 229 pm for monodentate and 237 pm for bidentate coordination. The bonds U-O_t and U-O_c of the uranyl-monoacetate complex as well as other structure parameters are close to those of complexes with neutral ROH ligands, which are expected to co-exist at neutral and weakly acidic pH conditions. The bidentate complex of uranyl with an acetate ligand differs from

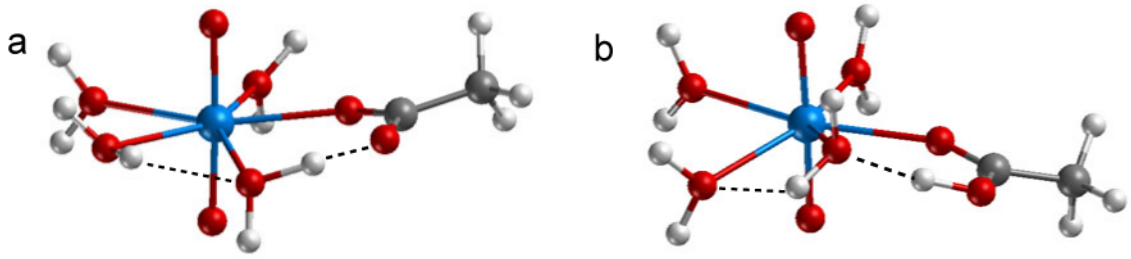

Figure 3.3. Optimized structures of uranyl complexes with: (a) acetate CH_3COO^- in mono coordinative form and (b) acetic acid CH_3COOH. Hydrogen bonds are represented by dashed lines.

other uranyl complexes by rather a short U-C distance, which was not observed in EXAFS experiment when uranyl complexation by HAs was inspected.[13] The structures of uranyl complexes with acetic acid (Fig. 3.3b), which might be present at low pH, and of monodentate coordinated acetate ligands differ somewhat: the terminal bond U-O_t as well as the U-O_c bond to the ligand by 1 pm, the average equatorial distance U-O_{eq} is 1–2 pm shorter in the acetate complex.

As essential result one can note that the distances measured in HAs by means of EXAFS,[13,16] U-O_t = 178 pm and U-O_{eq} = 237–240 pm, are very close to those calculated for the complexes with alcohols, acetate, and acetic acid (Table 3.1). For alcoholates, the value of U-O_{eq} falls in the same range; only U-O_t is up to 2 pm longer (Table 3.1). Therefore, the parameters U-O_t and U-O_{eq} alone do not suffice for distinguishing between alcoholic and carboxylic ligating groups of HAs that contribute to uranyl complexation. The calculated data for alcoholic as well as carboxylic complexes agree very well with experimental data for HA without or with blocked phenolic OH groups: for both probes U-O_t and U-O_{eq} have been determined to 178 and 239 pm, respectively.[13] The close similarity of these parameters, as calculated for uranyl complexes with alcoholic and acetate ligands, rationalizes why these parameters remained unchanged in EXAFS experiments on HAs with methyl-blocked phenolic OH groups.[13] Even the slight elongation, 2 pm, of U-O_t in alcoholate complexes may be regarded as too small to have an effect, as the experiments average over all complexing sites of HAs, and then the effect of blocked phenolic OH groups easily falls within the experimental uncertainty of U-O_t.[13] Thus, the close similarity of local structures of uranyl complexes of alcoholic and carboxylic groups allows one to rationalize why blocking of phenolic groups leads to a drop of the loading capacity for uranyl,[31] but has no apparent effect on structural characteristics like U-O_t and U-O_{eq} as determined by EXAFS.[13]

3.2 Energetics

From the above it has become clear that the structural parameters U-O_t and U-O_{eq} commonly measured by EXAFS are not sufficient to decide whether aliphatic and phenolic OH groups of HAs indeed coordinate uranyl because such complexes were calculated to be structurally similar to complexes with carboxyl groups which are always present in HAs. To shed further light onto this problem, various energetic characteristics were studied. The stability of the complexes was estimated from the formal ligand substitution reaction

$$[UO_2(H_2O)_5]^{2+} + ROH/RO^- \rightarrow [UO_2(H_2O)_4ROH/RO]^{2+/+} + H_2O \qquad (3.1)$$

The substitution free energies ΔG_{sub} are given in Table 3.2. Substitutions by aliphatic MeO^-, EtO^-, PrO^-, and $iPrO^-$ ligands are energetically most favorable (Table 3.2), with substitution energies of -226, -211, -189, and -190 kJ mol^{-1}, respectively. Substituting an aqua ligand of the first coordination shell of uranyl by phenolate or its derivatives is considerably less favorable: ΔG_{sub} is calculated as -105 and -112 kJ mol^{-1} for PhO^- and singly deprotonated $pPhO^-$, respectively, in line with the lower pK_a of these alcohols compared to aliphatic ones. When $oPhO^-$ forms a monodentate complex, then the second hydroxyl group undergoes a hydrogen bond with one of the aqua ligands of uranyl. Depending on the orientation of the second OH group, substitution energies, Eq. (3.1), of $oPhO^-$ differ by 36 kJ mol^{-1}. With the OH group in "out" position, the oxygen center of the ligand serves as electron donor of the H-bond with the neighboring aqua ligand (Fig. 3.1c). This ligand orientation yields the largest substitution energy, -139 kJ mol^{-1}, among all aromatic ligands examined. When the second

Table 3.2. Substitution free energies, including standard state corrections, calculated according to Eq. (3.1), for deprotonated RO^- (a) and neutral ROH (b) ligands. For the designations of the various alcohols, see Figs 2.2 and 2.3.

	RO^-	ROH
H_2O	-261	0
MeOH	-226	8
EtOH	-211	16
PrOH	-189	23
iPrOH	-190	24
PhOH	-105	57
oPhOH, in	-103	55
oPhOH, out	-139	38
pPhOH	-112	49
CH_3COOH, mono	-107	20
CH_3COOH, bi	-122	

OH group is in "in" position, then the oxygen center of a neighboring aqua ligand acts as electron donor of the hydrogen bond with the hydroxyl group. This complex is 12 kJ mol^{-1} less stable than the "out" isomer, the substitution energy being -103 kJ mol^{-1}. The substitution energy, of -122 kJ mol^{-1}, for acetate in bidentate coordination is calculated lower than that of phenolic ligands, but higher than for other aromatic alcoholates.

Substitution by neutral ligands is always much less favorable than by alcoholates: it is endothermic. MeOH, EtOH, PrOH, iPrOH, and acetic acid feature substitution energies of 8–24 kJ mol^{-1} (Table 3.2). Complexes with neutral oPhOH, pPhOH and phenol exhibit even more positive substitution energies, ~50 kJ mol^{-1}.

3.3 Alternative mechanism of complexation

Because alcoholate ions of aliphatic alcohols do not exist at neutral pH conditions, complexes of uranyl with these alcoholates are unlikely in a natural environment, despite of the large driving force for substitution of an aqua ligand. On the other hand, complexation of uranyl by neutral alcoholic ligands is accompanied by rather small energy changes (Table 3.2) and deprotonation of the ligand will be facilitated in the field of the uranyl dication. With all this in mind, two mechanisms of complexation were considered (Scheme 3.1).

Scheme 3.1

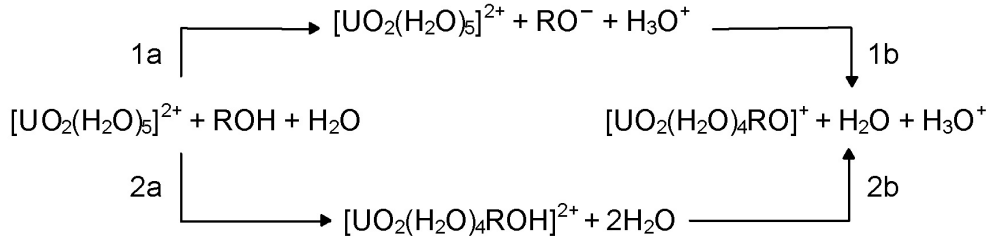

The first mechanism starts off with deprotonation of the ligand (1a), followed by complexation of uranyl (1b). Alternatively, a neutral ligand, containing a protonated reactive site, coordinates at uranyl (2a), followed by deprotonation (2b) which is facilitated in the vicinity of the uranyl ion. At experimental pH conditions, at which typically complexation by humic acids is studied,[13,31,32] most probably complexation by carboxylic groups occurs via the analogue of the first mechanism, whereas phenolic and aliphatic OH groups of HAs may (or may not) contribute to uranyl complexation via the second alternative that bypasses the deprotonation problem.

Scheme 3.1 depicts the elementary reaction steps involved in complexation and was used as a first approximation to model these reactions. Table 3.3 collects the resulting Gibbs free energies. Inspection of these results shows that deprotonation free energies (1a) of simple alcohols are too high compared to experiment. For example, water dissociation is known to require only ~90 kJ mol^{-1},[104] whereas the calculations yield a value of 307 kJ mol^{-1}. Sources

Table 3.3. Gibbs free energies ΔG, including standard state corrections, of reactions according to Scheme 3.1 (kJ mol^{-1}) from calculations with the PCM solvation model applied to monodentate complexes of uranyl with aliphatic or phenolic alcohols ROH. For the designations of the various alcohols ROH, see Figs. 2.2 and 2.3.

	ΔG				
	1a	1b	2a	2b	total
H_2O	307	-261	0	36	36
MeOH	254	-226	8	20	28
EtOH	250	-211	16	23	39
PrOH	248	-189	23	36	59
iPrOH	252	-190	24	38	62
PhOH	162	-105	57	0	57
oPhOH, in	139	-103	-	-	36
oPhOH, out	173	-139	38	-4	34
pPhOH	173	-112	49	12	61
CH_3COOH	140	-107	20	13	33

of inaccuracy may be the solvation model and the basis set superposition error for small ionic moieties. Although *differences* in total reaction free energies Δ*G*(total) (!) between various alcohols can be estimated reasonably well according to Eq. (3.1), free energies of intermediate steps and the overall absolute values suffer from the fact that the solvation of RO^- species and of the "proton" as H_3O^+ are poorly represented. For example, the solvation energy of the H_3O^+ species was calculated at -378 kJ mol^{-1}, i.e. 56 kJ mol^{-1} off the experimental value, -434 kJ mol^{-1},[105] which represents a deviation of ~ 15 %. The solvation energy of OH^- species was calculated at -370 kJ mol^{-1}, while the experimental value is -447 kJ mol^{-1}; a deviation of 77 kJ mol^{-1}. Calculating the accurate solvation energies of ions is known to be a challenging task. Continuum dielectric solvent models are inappropriate for ionic solutes which have concentrated charge with strong local solute-solvent interactions.[106] To overcome this limitation, explicit solvent molecules are added to the model ionic system.[107-110] For example, adding one explicit solvent molecule was shown to improve the accuracy of solvation energies[107] and the acid dissociation constants[108] when the SM6 continuum solvation model is used. A cluster-continuum solvent model with two or three explicit aqua ligands was reported to give pK_a values for 17 organic molecules in better agreement with experiment than those calculated with straightforward continuum solvation methods.[109] Therefore, to improve the model of solvation two further explicit aqua ligands were included. One water molecule was attached to the RO^- anion, resulting in the species $RO^-(H_2O)$; the other one was used in the complex $[H_5O_2]^+$ replacing $[H_3O]^+$ (Scheme 3.2) to achieve an improved representation of the

solvated proton. Species with uranyl were not changed because the first solvation shell of uranyl was already included in the quantum chemical model.

This more elaborate solvation model yields improved estimates of the solvation energies. For instance, the solvation energy of the ions was estimated via explicit consideration of one water molecules of the first solvation shell (n = 1):

$$A_{gas} + n\ H_2O_{aq} \rightarrow A\ (H_2O)_{n,\ aq} \qquad (3.2)$$

The free energy of the reaction 3.2 was calculated as described in Section 2.2 with the only exception of A_{gas}, which is always treated in the gas phase. Accordingly, the resulting solvation energy of H_3O^+ was calculated at -424 kJ mol^{-1}, when the solvated species is modeled as $H_3O(H_2O)^+$. It is improved by 54 kJ mol^{-1} compared to the simpler Scheme 3.1. Similarly, for methanolate, A = MeO^-, the calculated solvation energy changes from -289 kJ mol^{-1} to -333 kJ mol^{-1}, and, as a consequence, the deprotonation energy of methanol is improved from 254 kJ mol^{-1}to 164 kJ mol^{-1}. The corresponding experimental value is 89 kJ mol^{-1}.[111]

Another instructive check of the quality of the model reaction is the deprotonation of an aqua ligand of the first solvation shell of uranyl. This reaction yields uranyl monohydroxide:

$$[UO_2(H_2O)_5]^{2+} + \quad H_2O \ \rightarrow\ [UO_2(H_2O)_4OH]^+ + H_3O^+ \qquad (3.3a)$$

$$[UO_2(H_2O)_5]^{2+} + 2\ H_2O \ \rightarrow\ [UO_2(H_2O)_4OH]^+ + H_5O_2^+ \qquad (3.3b)$$

Eq. 3.3a corresponds to the first Scheme 3.1, while Eq. 3.3b includes the $H_5O_2^+$ species to represent the solvated proton. The resulting reaction free energy according to the simpler Scheme 3.1 (Eq. 3.3a) including standard state corrections is 36 kJ mol^{-1}, whereas the improved model (Eq. 3.3b) yields 9 kJ mol^{-1}. The experimental value for the first step of uranyl hydrolysis was estimated to 30 kJ mol^{-1}.[112] The calculated value of 36 kJ mol^{-1} from the Eq. 3.3a agrees very well with the experiment, but this agreement might be due to favorable error cancellation. Nevertheless, substitution of H_3O^+ by $H_5O_2^+$ changes free energy by 27 kJ mol^{-1} only. The resulting 9 kJ mol^{-1} is still in reasonable agreement with experiment. Using bigger clusters for the proton description and water clusters in the left part of the equation can further improve the free energy of the first hydrolysis step of uranyl. One should also take into account that in this work only five-fold coordinated uranyl was investigated, while uranyl monohydroxide was proved to be four-coordinated.[113]

Scheme 3.2

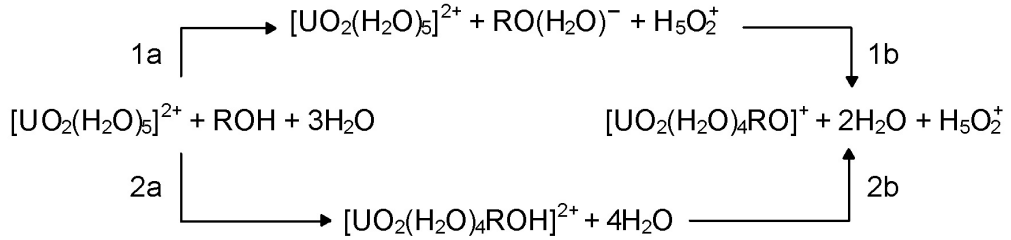

Table 3.4 collects Gibbs free energies determined according to Scheme 3.2. Also shown in Table 3.4 are the free energies ΔG(total) of the overall complexation reaction with reference to the protonated ligand:

$$[UO_2(H_2O)_5]^{2+} + ROH + H_2O \rightarrow [UO_2(H_2O)_4RO]^{+} + H_5O_2^{+} \qquad (3.4)$$

Comparison of Tables 3.3 and 3.4 shows that even the small improvement from Scheme 3.1 to Scheme 3.2 reduces the dissociation energies of the ligands (1a) by ~90 kJ mol^{-1} (~ 40 %) while the main trends of the energetic remain unchanged.

Adding more aqua ligands to the QM model may improve the energetics even further, but will also require a larger computational effort. The model of Scheme 3.2 turned out to be adequate for the purpose of the present study.

On Path 1, deprotonation (1a) of the ligands ROH is strongly endothermic, about 80 to 160 kJ mol^{-1}, while complexation of uranyl by the alcoholate (1b) is highly exothermic, about -70 to -160 kJ mol^{-1}. In line with the lower pK_a values of aromatic alcohols, both the free

Table 3.4. Gibbs free energies, with standard state corrections included, of reactions according to Scheme 3.2 (in kJ mol^{-1}) for monodentate complexes of uranyl with aliphatic and phenolic alcohols ROH[a] in comparison to aqua and acetic acid ligands.

	ΔG				
	1a	1b	2a	2b	total
H_2O	255	-236	0	9	9
MeOH	164	-163	8	-7	1
EtOH	168	-156	16	-4	12
PrOH	156	-124	23	9	32
iPrOH	161	-126	24	11	35
PhOH	126	-96	57	-27	30
oPhOH, in	83	-74	–	–	9
oPhOH, out	101	-94	38	-31	7
pPhOH	134	-100	49	-15	34
CH_3COOH	107	-101	20	-14	6

[a] For the designations of the various alcohols ROH, see Figs. 2.2 and 2.3.

energies of either partial reaction are notably lower (by absolute value) for the aromatic ligands than for the aliphatic alcohols (Table 3.4). On Path 2, substitution of the aqua ligand by a neutral ROH ligand (2a) is moderately endothermic, about 10 to 60 kJ mol^{-1} where the phenolic ligands are characterized by higher values, above about 40 kJ mol^{-1}. Acetic acid and aliphatic alcohols feature significantly lower substitution energies, at most 24 kJ mol^{-1} (Table 3.4). The largest substitution energy $\Delta G(2a)$ was calculated for phenol, 57 kJ mol^{-1}, while oPhOH and pPhOH yielded lower values, 38 and 49 kJ mol^{-1}, respectively. The latter two systems also feature smaller total free energies of complexation, because the OH groups in ortho and para positions donate electron density to the aromatic ring and thus stabilize the complex with the uranyl cation. Concomitant with the lower ligand substitution energies, also the deprotonation of the alcohol ligands in the vicinity of uranyl (2b) is associated with much smaller energy changes than along Path 1. Deprotonation is energetically favorable for aromatic alcohols (-31 to -15 kJ mol^{-1}) while it is energetically neutral (-7 to 11 kJ mol^{-1}) for the aliphatic alcohols (Table 3.4). Thus, the intermediates along Path 2 on the way from protonated alcohols to alcoholate complexes lie considerably lower in free energy, rendering this route significantly more probable at neutral or lower pH.

The free energy changes accompanying the overall complexation reaction, Eq. (3.4), for MeOH, EtOH, oPhOH, and acetic acid are small, ranging up to 12 kJ mol^{-1} (Table 3.4), while for PrOH, iPrOH, PhOH, and pPhOH higher complexation energies were determined, from 30 to 35 kJ mol^{-1} (Table 3.4). Comparing results for larger aliphatic with phenolic alcohols one can conclude that both types of alcoholic groups may well contribute in comparable way to the complexation of uranyl by HAs. At neutral or acidic pH alcohols in solution exist predominantly in protonated form. Under these conditions, the complexation energies are comparable to or lower than the formation of uranyl monohydroxide from solvated uranyl, $\Delta G \approx 10$ kJ mol^{-1} (Table 3.4). Therefore, one can expect complexation of uranyl by alcoholic groups to occur for pH values above ~4, in qualitative agreement with an earlier speciation calculation for oPhOH.[15]

3.4 Uranyl complexation by catechol

As mentioned above, oPhOH can complexate uranyl also in chelate fashion. Fig. 3.4 presents three model chelate structures of uranyl with protonated as well as singly and doubly deprotonated catechol.

The complexes shown in Figs. 3.4a and 3.4b can be formed only with isomer “out” of PhOH. Structural parameters of all possible monodentate and chelate structures (with C_s symmetry applied) of oPhOH with uranyl are collected in Table 3.5. Complexation energies

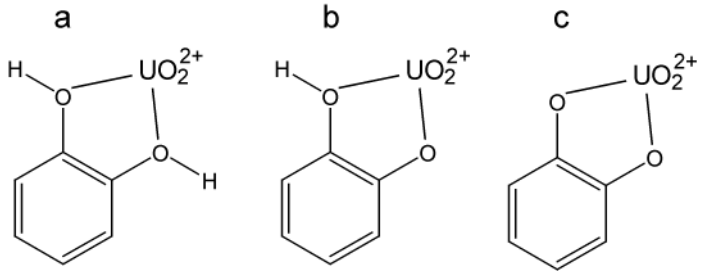

Figure 3.4. Schematic representation of chelate complexes of uranyl with oPhOH in (a) protonated form, (b) singly deprotonated form, and (c) doubly deprotonated form.

ΔE_1 were calculated according to the following formal reactions (m = 1, 2):

$$[UO_2(H_2O)_5]^{2+} + LH_2 \rightarrow [UO_2(H_2O)_{5-m}LH_2]^{2+} + m\,H_2O, \quad (3.5a)$$

$$[UO_2(H_2O)_5]^{2+} + LH^- \rightarrow [UO_2(H_2O)_{5-m}LH]^{+} + m\,H_2O, \quad (3.5b)$$

$$[UO_2(H_2O)_5]^{2+} + L^{2-} \rightarrow [UO_2(H_2O)_{5-m}L] + 2\,H_2O, \quad (3.5c)$$

In case of m = 2, the various reactions (3.5x) lead to chelate structures depicted in panel x of Fig. 3.4 (x = a, b, c) while for monodentate structures m = 1. $LH_n^{(2-n)-}$ represents the catechol species in various deprotonated forms; n can be 0, 1 and 2.

According to the calculations, the chelate complex with a doubly deprotonated catechol ligand is the most stable one among all inspected complexes because the complexation energy increases with the charge of the ligand. This complex also shows the longest U-O_t bond, 181 pm. The chelate form with the neutral oPhOH ligand is the least stable complex. It has the shortest U-O_t bond, 177 pm, and the most endothermic complexation energy, 55 kJ mol^{-1}. In

Table 3.5 Uranyl monodentate and chelate complexes with oPhOH in different deprotonation states: structure parameters in pm, and complexation energies corresponding to different reference ligands in kJ mol^{-1} (see text).

$LH_n^{(2-n)-}$	Complex	U-O_t	U-O_c	U-C	U-O_{eq}	ΔE_1	ΔE_2
C_6H_4OHOH	chelate	177	247	345	239	55	55
	mono, in2	178	245	350	237	42	42
	mono, out	178	251	356	239	27	27
$C_6H_4OOH^-$	chelate	180	220	323	237	-118	69
	mono, in	180	213	345	238	-122	25
	mono, out	180	214	345	237	-140	46
$C_6H_4OO^{2-}$	chelate	181	226	318	236	-268	143
exp., pH = 5[a]		178(2)			239(2)		
exp., pH = 10[a]		182(2)			237(2)		
exp., HAs[b]		178(2)			237–240(2)		

[a] Ref. 15. [b] Ref. 13.

contrast, corresponding monodentate complexes yield complexation energies that are 27 to 42 kJ mol^{-1} lower (Table 3.5). Thus, the second bond in chelate complexes is less stabilizing than the aqua ligand that is substituted. So far the main energy differences were associated with the charge of the ligand. To make the comparison uniform, ΔE_2 was estimated with isomer "out" of the oPhOH ligand chosen as common reference LH_2:

$$[UO_2(H_2O)_5]^{2+} + LH_2 \rightarrow [UO_2(H_2O)_{5-m}LH_2]^{2+} + m\ H_2O, \quad (3.6a)$$

$$[UO_2(H_2O)_5]^{2+} + LH_2 \rightarrow [UO_2(H_2O)_{5-m}LH]^{+} + (m\text{-}1)\ H_2O + H_3O^{+}, \quad (3.6b)$$

$$[UO_2(H_2O)_5]^{2+} + LH_2 \rightarrow [UO_2(H_2O)_{5-m}L] + 2\ H_3O^{+}, \quad (3.6c)$$

Using a neutral reference ligand, the complexation energies ΔE_2 for the formation of monodentate complexes with both neutral and singly deprotonated catechol ligands are comparable. Chelate formation is still not favorable compared to monodentate uranyl complexes. The chelate uranyl complex with neutral oPhOH is calculated to be more favorable than a chelate complex with deprotonated oPhO$^-$. For the uranyl chelate complex with doubly deprotonated catechol the highest complexation energy is determined as it requires two formal deprotonation steps of the ligand.

Nevertheless, these energy differences have to be discussed with due caution because thermodynamic corrections are missing. The trend that among all possible complexes with oPhOH and oPhO$^-$ the monodentate ones with "out" isomers are the most stable ones may change at the level of free energies. In Eqs. 3.5 and 3.6, the number of reactants stays the same when a monodentate complex with catechol is formed, whereas one extra H_2O species is generated when a chelate complex forms. Therefore, a favorable entropy contribution is expected in the latter cases. Analogously, entropy effects lead to a significant stabilization of the bidentate coordination of uranyl by carboxylic acids (~40 kJ mol^{-1})[73], while monodentate complexes are destabilized by ~10-15 kJ mol^{-1}.[73]

For catechol in aqueous solution at pH 5 and 10, U-O_t and U-O_{eq} distances are available from EXAFS.[15] U-O_t was determined at 178 pm for pH 5 and at 182 pm for pH 10. Concomitantly, U-O_{eq} drops slightly, from 239 to 237 pm, due to this change of pH (the concentrations of uranyl and catechol do not change, Table 3.5). However, these characteristics were assigned to chelate structures in 1:1 and 1:3 complexes, respectively.[15] On the other hand, the experimental results for pH 5 are in very good agreement with the calculated results for the more stable "out" isomer of the uranyl mono-oPhOH complex (U-O_t = 178 pm, U-O_{eq} = 239 pm), as well as with the chelate complex of protonated oPhOH (U-O_t = 177 pm, U-O_{eq} = 239 pm). Single deprotonation of the catechol ligand of these complexes resulted in longer U-O_t bonds, 180 pm, and a slightly reduced value of U-O_{eq}, 237 pm. For the chelate complex with doubly deprotonated catechol one calculates U-O_t = 181 pm and U-O_{eq}

= 236 pm. These latter values agree well with the experimental results at pH 10. Thus, also deprotonation of oPhOH with increasing pH is in line with the changes observed experimentally. On the other hand, one cannot exclude that oPhOH may be singly deprotonated at pH 5 when attached to the uranyl cation.

Comparing calculated results for complexes with catechol to EXAFS structural parameters for uranyl in solution with humic acids one finds best agreement for complexes with neutral catechol ligand. Nevertheless, taking into account an experimental inaccuracy of 2 pm, one can see that complexes with a singly deprotonated $oPhO^-$ ligand also agree with the experimental data. At higher pH levels uranyl is expected to form a chelate complex with $C_6H_4OO^{2-}$, when the doubly deprotonated ligand appears. As the EXAFS experiment on a solution with HAs was done at pH = 2, uranyl complexes of that type are not expected. This is confirmed by the calculations which yield different geometrical parameters: $U\text{-}O_t$ = 181 pm, $U\text{-}O_{eq}$ = 236 pm.

In summary, structures of uranyl catechol complexes are calculated in good agreement with EXAFS results. Due to relatively small deviations of $U\text{-}O_t$ and $U\text{-}O_{eq}$ the available experimental data do not allow a discrimination between monodentate and chelate complexes. Calculated energies yield a preference for monodentate coordination, but entropy effects stabilize chelate species which then are thermodynamically more probable.

4. Conclusions

The complexation of uranyl by ligands with phenolic and aliphatic OH groups was explored by means of an all-electron scalar relativistic density functional approach. Alcoholic ligands served as model systems for the corresponding functional groups of humic substances. Various characteristics were compared to those of acetate as model for carboxylic groups, which dominate uranyl complexation by humic acids. To account for environmental conditions, protonated as well as deprotonated forms of the ligands were considered.

Calculated structures feature short bonds between uranyl and alcoholate ligands, 210–220 pm, and longer bonds, ~230–250, to alcohol ligands. The calculated results agree well with the experimentally determined structure parameters of uranyl complexes with humic acids, the terminal uranyl bond $U\text{-}O_t$ (178 pm) and the average $U\text{-}O_{eq}$ to equatorial ligands (239 pm).[13] $U\text{-}O_t$ was calculated at 178 pm for alcohols and at ~180 pm for alcoholates. For both types of ligands $U\text{-}O_{eq}$ was determined at 236–239 pm. These results, with the exception of slightly elongated $U\text{-}O_t$ for alcoholates, are very similar to the corresponding calculated parameters for uranyl monoacetate. The elongation of $U\text{-}O_t$ for alcoholates is too small and the contribution of these groups to uranyl complexation may be too weak to be easily detected experimentally by EXAFS. Hence, the similarity of geometry parameters of uranyl complexes

with alcoholic and carboxylic groups permits one to rationalize why EXAFS experiments on uranyl complexation with HAs and HAs with blocked phenolic OH groups exhibit the same structural characteristics.[13] The calculated geometries also favorably agree with EXAFS results for ortho-hydroxy phenol (catechol).[15]

Complexation energies of alcohol or alcoholate ligands with uranyl reveal that at neutral and slightly acidic pH conditions complexation of uranyl by HAs to form alcoholate complexes is feasible via aliphatic and phenolic OH groups. Thus, this study corroborates experimental results which showed a reduced loading capacity of HAs with blocked phenolic groups at pH 4.[31]

Part II – Adsorption of uranyl on kaolinite

5. Clay minerals and their role in the environmental chemistry of actinides

Adsorption at minerals is one of the important and common processes which affect the actinide distribution in the environment. Adsorption of actinides by clay materials can take place everywhere in nature, in soils, aquifers, aquatic sediments and especially at uranium mining sites as well as repositories. Recently, scientific interest in this process increased in the context of the risk assessment of possible deep geological repositories for radioactive waste.[5,9] There, clay may act as either geological or technical barrier. The following introduction to this problem will provide a description of clays, clay minerals, and their interaction with actinides.

5.1 Clays and clay minerals

Clays are ubiquitous in the geosphere as rocks, also as sediments in rivers and lakes and in soils. Clays are naturally occurring materials composed primarily of fine-grained minerals of about 2 microns in size, which show plasticity through a variable range of water content, and which can be hardened when dried and/or burned.[114,115] Clays are typically formed over a long period of time by the products of weathering of rocks or by hydrothermal activity. Clays are typically associated with aqueous sedimentary depositional environments, e. g. lakes and the sea.. Firing in a kiln causes clay to convert into a ceramic material, hence the use of clays as material for manufacturing many objects, e.g. bricks, cooking pots, dishes, and even objects of art. In ancient times, clay tablets were used as the first writing medium, inscribed with the cuneiform script through the use of stylus. This usage likely is connected with the

main property of clays, namely to exhibit plasticity when mixed with water and to become firm when dried. Clays can exchange ions, adsorb organic materials or metal ions, store water (swelling), and represent the barriers for aquifers.[115] These properties allow clay to be used as a natural or technical barrier in repositories for toxic and radioactive waste. They provide isolation of waste material with respect to ground water on the one hand. On the other hand, they exhibit a rather low permeability for solvated waste material. The Jurasic opalinus clay in Switzerland is one of the host rocks under discussion.[5] Opalinus Clay was deposited 180 millions years ago by the sedimentation of fine clay, quartz, and carbonate particles in a shallow marine environment.[9] In the Zürcher Weinland in Switzerland the mesozoic sediments containing opalinus clay is of uniform thickness over several kilometers, almost flat-lying and little affected by faulting. About half of this formation consists of clay minerals, which is rather typical for a clay formation.

In general, clays are composed of clay minerals, calcite, quartz, and some other materials, which have very small content, less than 5 %.[9,115] Table 5.1 shows the average mineralogical composition of opalinus clay, as an example.[9]

Opalinus Clay was deposited 180 millions years ago by the sedimentation of fine clay, quartz and carbonate particles in a shallow marine environment.[9] In the Zürcher Weinland in Switzerland the mesozoic sediments containing opalinus clay are of uniform thickness over several kilometers, almost flat-lying and little affected by faulting. About half of this formation consists of clay minerals, which is rather typical for a clay formation.

On average opalinus clay contains mainly clay minerals (54 %, Table 5.1), of which 31 % correspond to kaolinite, 34 % to illite. Mixed illite/smectite layers take 26 % of the total clay content, and chlorite is present with the smallest contribution, 9 %.[9] Kaolinite forms a

Table 5.1. Average mineralogical composition of the Opalinus Clay, taken from Ref. 9.

Mineral	wt % (average)	Standard deviation wt %
Clay minerals	54	
Quartz	20	±5
Calcite	16	±10
Dolomite/ankerite	1	±0.4
Siderite	4	±2.4
Feldspar	3	±1.3
Pyrite	1.1	±1
Organic carbon	0.6	±0.3

significant part of the clay content of opalinus clay; it has a simple structure (see Section 5.2) which facilitates modeling. This was one of the reason for choosing it as an exemplary mineral to study uranyl adsorption.

5.2 Structure of clay minerals

Clay minerals are hydrous aluminium phyllosilicates which contain variable amounts of iron, magnesium, alkali metals, alkaline earths and other cations. Clay minerals are fundamentally built of Si tetrahedra and Al octahedra (Fig. 5.1), which each are connected to form sheet-like structures. Clay minerals are commonly classified as 1:1 or 2:1 structures. A 1:1 clay mineral consists of one tetrahedral Si sheet bonded to on octahedral Al sheet, like kaolinite (Fig.5.1). A 2:1 clay mineral consists of an octahedral sheet sandwiched between two tetrahedral sheets (Fig. 5.1).

Properties of clay minerals are varied because of the stacked layered structure and possible substitutions of Si^{4+} and Al^{3+} by Al^{3+} and Fe^{2+} or Mg^{2+} ions, respectively.[116] The simplest clay mineral group of kaolins results from combining a single silica sheet to one Al octahedral sheet, forming 1:1 phyllosilicates, among which kaolinite is the most simple one, since its basic composition is not varied by substitutions (Figs. 5.1, 5.2a). The simplest, neutral clay mineral in the 2:1 group is pyrophyllite (Figs. 5.1, 5.2b). Kaolinite and pyrophyllite do not include any substitutions and, therefore, afford simple models for facile studies of clay minerals. All other clay minerals are derived from these prototypes by substitutions, which create permanent charges. For example, in montmorillonite some Al^{3+} centers of octahedral sheets are substituted by Mg^{2+}.[115,116] As a result, a single layer of montmorillonite can have a permanent charge about -0.2 to -0.6 e per unit cell, which is

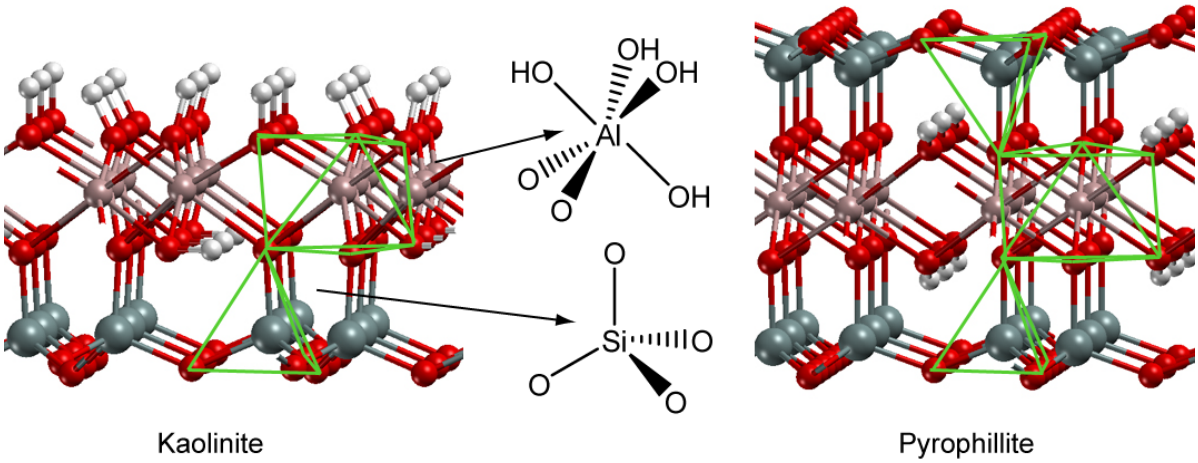

Figure 5.1. Structural building blocks SiO_4 and $Al(O,OH)_6$ of clay minerals, forming 1:1 kaolinite (left-hand panel) and 2:1 pyrophyllite clay minerals (right-hand panel).

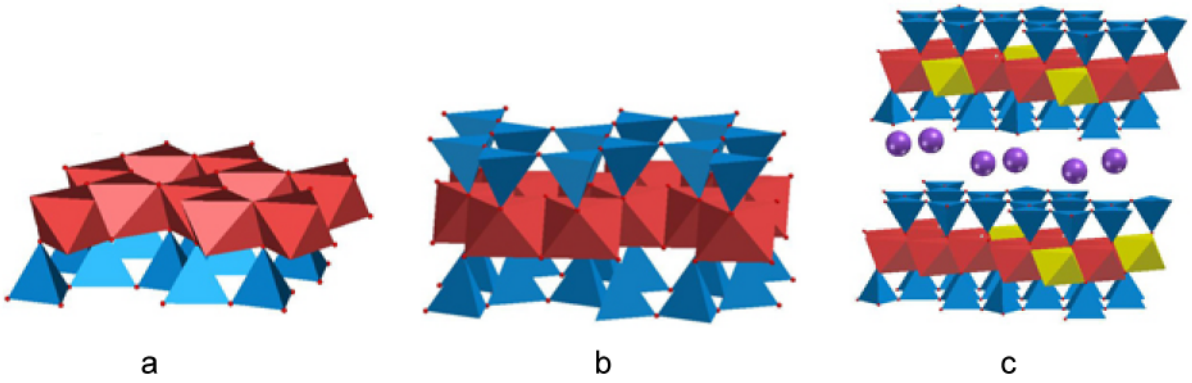

Figure 5.2. Polyhedra structures of (a) kaolinite, (b) pyrophyllite, (c) general 2:1 clay mineral.

neutralized by Na^+ or Ca^{2+} counterions placed between the layers (Fig. 5.2c). In the presence of water these cations tend to hydrate, forcing the clay layers apart; in consequence, clay increases strongly in volume. This property of the clays is called swelling.[116] The water content varies with the size and the charge of the counterions.

Illite has substitutions in both Al octahedral sheets (by Mg^{2+} or Fe^{2+}) and Si tetrahedral sheets (by Al^{3+}). Its charge is neutralized by K^+ counterions, which were found to prevent swelling.[115] Thus, illite is a non-expanding clay mineral. Kaolinite has been chosen as simple exemplary clay mineral in a collaborative project, where this thesis is also contributing. It has a relatively small unit cell, compared to other clay minerals, only two sheets, no counterions, and thus, is well suited for a computational study. On the other hand, it has both Al and Si terminated surfaces; therefore, the reactivity of these two types of surfaces can be compared.

5.3 Types of surfaces

In general clay minerals exhibit ideal (001) cleavage planes,[115,116] parallel to the plane of *a* and *b* vectors of the crystal structure, so-called basal plane (Fig. 5.3a). The (001) surfaces of kaolinite can be terminated by Al octahedra – Al(o), or Si tetrahedra – Si(t). A top view of both types of these surfaces is shown in Figs. 5.3b and 5.3c. Due to its composition in ideal kaolinite, an Al(o) planes is assumed to be more reactive than a Si(t) surface because the former is hydroxylated (Fig. 5.3b).[117] As a result, an Al(o) surface layer of kaolinite has a pH-dependent surface charge. At acidic pH, when there is an excess of protons, such a surface attaches protons at AlOH surface groups to form $AlOH_2^+$ groups.[117] Therefore, an Al(o) surface attracts negatively charged adsorbates. At higher pH, surface hydroxyl groups deprotonate and the surface acquires a negative charge, which attracts positive ions from the solution.

The (001) planes of 2:1 phyllosilicates, like pyrophyllite and montmorillonite, are siloxane surfaces, formed by Si(t) planes. Their reactivity depends on the nature of the local

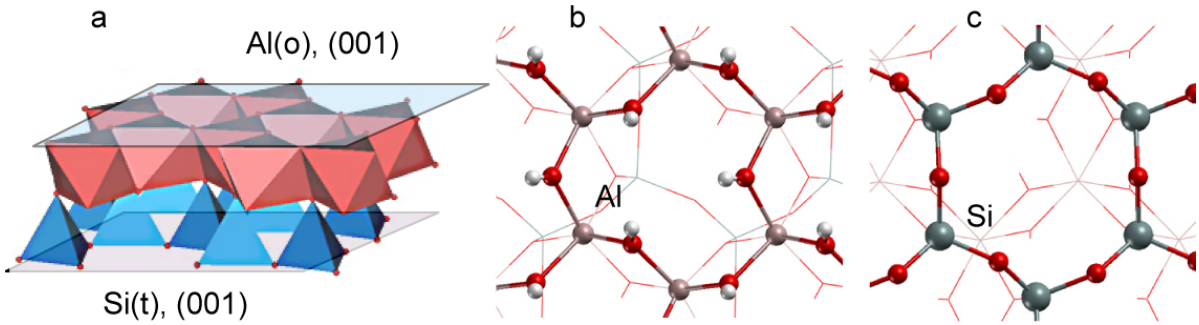

Figure 5.3. Structures of various basal planes of kaolinite: (a) side view; top views of (b) a hydroxylated Al(o) (001) surface, and (c) a Si(t) surface.

charge distribution in the clay layer.[117] In the absence of nearby isomorphic cation substitutions that create negative surface charges, a siloxane layer acts as a weak charge donor. If an Al^{3+} cation is substituted by Fe^{2+} or Mg^{2+} in the octahedral layer, the resulting excess negative charge makes rather strong adsorption of ions from solution possible. The substitution of Si^{4+} by Al^{3+} leads to a localization of an excess negative charge near to the siloxane layer, resulting in very strong adsorption complexes and strong hydrogen bonds with vicinal water molecules.[118]

Besides (001) planes, clay mineral particles are terminated by edge surfaces, which have been suggested to play a crucial role in the geochemistry of clay minerals.[119] Often up to 30% of the total mineral surface are observed to be edge surfaces, as demonstrated by atomic force microscopy (AFM) and scanning electron microscopy (SEM).[120] Fig. 5.4a shows a SEM

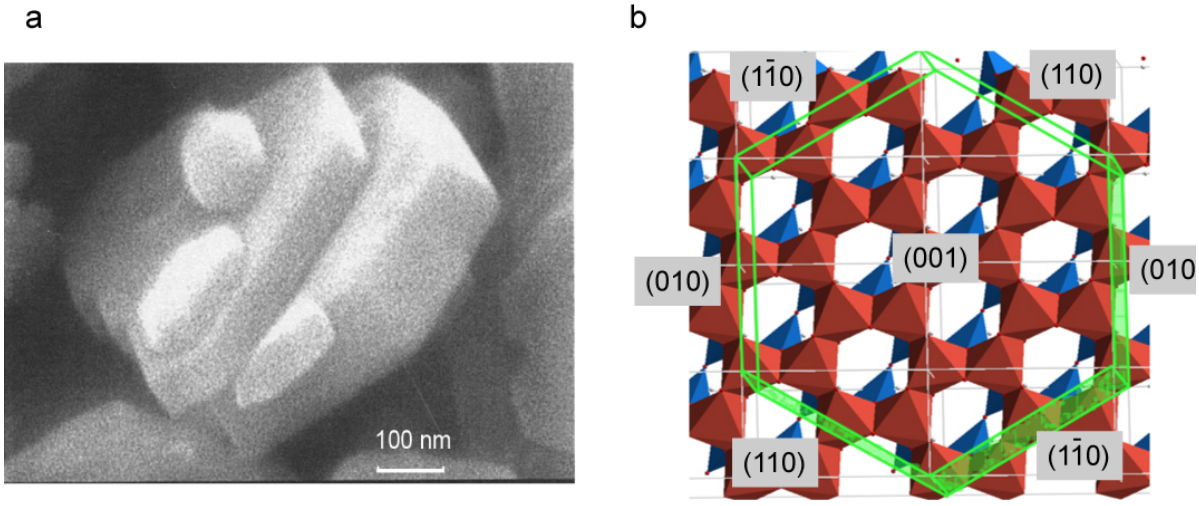

Figure 5.4. Structures of edge surfaces of kaolinite: (a) SEM micrograph (adapted from Ref. 120) showing well-developed crystals with a smooth basal plane and right angles between basal planes (001) and edge planes (110) and (010); (b) polyhedra representation of a kaolinite hexagonal crystallite viewed along the (001) direction exposing possible edge terminations.

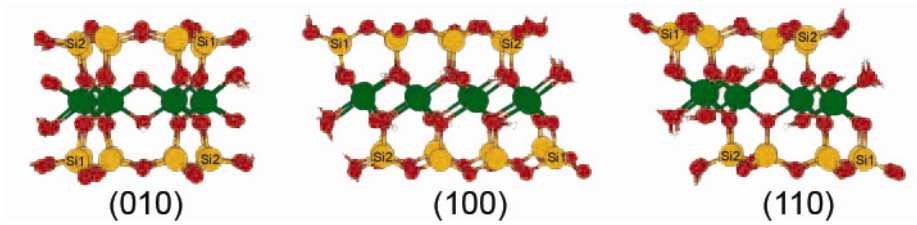

Figure 5.5. Structures of edge surfaces of pyrophyllite. Adapted from Ref. 124.

micrograph of Georgia kaolinite[120] with smooth basal planes and significant edge surface area. Edge and basal surfaces of clays can differ a lot in reactivity because of the anisotropy of the crystal structure. Edges are supposed to be more reactive. The dissolution of kaolinite, for example, takes place rather on edges, than on basal surface; also adsorption properties depend on the surface orientation.[121]

The exact atomic surface structure of edge surfaces is not known. Since most of the clay minerals exhibit a pseudohexagonal structure,[115] the edge surface orientations are predicted to be ±(010), ±(110) and ±(1-10).[122] These surfaces are parallel to the sides of hexagons (Fig. 5.4b). Pyrophyllite is the only mineral for which the atomic structures of different edge terminations were computationally characterized at the atomic scale (Fig. 5.5).[123,124] The structures of bare and solvated edge surfaces were modeled, but thus far no adsorption on them was simulated.

Edges are terminated by unsaturated oxygen atoms, which can attract protons and participate in pH-dependent surface charging.[119] For kaolinite, surface groups, like $AlOH^{-½}$, $AlOH_2^{+½}$, SiOH, are discussed in the literature.[125,126] The fractional charges of –½ and +½ are assigned to represent unsaturated or oversaturated oxygen atoms. They are derived from valence bond theory and will be described in detail later on (Section 8.1). Clay minerals with 2:1 morphology containing substitutions may exhibit MgOH, FeOH, etc. surface groups in addtion.

The important property of each surface is its net charge. Two chemical reactions defining the pH dependent surface charge are:[121]

$$S–OH + H^+ \rightarrow S–OH_2^+$$

$$S–OH \rightarrow S–O^- + H^+$$

The net charge of a surface is zero when the numbers of its positive and negative charges are equal. The pH of the solution at which the surface charge is 0 is called pH of zero-point charge, pH_{ZPC}.[121] For kaolinite it has been determined at ~5.5,[121] while for montmorillonite it is ~2.5.[121] This pH value is decisive for the adsorption properties. Below pH_{ZPC} anions are

attracted, above pH_{ZPC} cations can be adsorbed. Besides, pH_{ZPC} can be different for basal and edge surfaces of the same mineral. As an example, kaolinite was suggested to exhibit a pH_{ZPC} of 5.5 for the Al(o) basal surface, and about 7.5 for the edges.[127] In general, the point of zero charge is the result of a combined action of several types of surface groups. Aluminum hydroxides have Al_2OH groups on the basal surface, which can be protonated at very low pH ($\log K = -1.5$ for $Al(OH)_3$, gibbsite) and deprotonated at very high pH (12.3 for $Al(OH)_3$).[128] Edge planes of the aluminium hydroxides have $AlOH_2^{+½}$ groups which deprotonate starting from pH ~10.[128] Thus, in a wide pH range only Al_2OH and $AlOH_2^{+½}$ groups will coexist and the net charge of the total surface area will not change, if the ratio of edge and basal surface areas does not changed. As a result, the zero net charge of gibbsite can be in the pH range from 3 to 9.[128]

5.4 Adsorption of actinides by clay minerals

Adsorption of actinides by clay minerals is a critical process in the attenuation of chemical and radioactive contaminants in groundwater systems. The adsorption rate of actinides by clay minerals depends on many factors: oxidation state of the actinide,[129] pH level of the solution,[20,21,24,28,30,37,38] concentrations of actinides and mineral powder in batch experiments,[18,20,28,29,37] types of available surfaces,[17,19,20] and the presence of CO_2 as well as of other ligands in solution.[24,37]

Recently, the sorption of actinides by kaolinite has been widely studied. Results of batch experiment on sorption of important actinides with different oxidation states are summarized in Fig. 5.6.[129] The order of adsorption as a function of pH is mainly connected to the charge of the adsorbate: first highly charged Pu^{4+} is adsorbed, then Pu^{3+}, approximately at the same pH level as UO_2^{2+}, and finally NpO_2^{+}. As a result, tetravalent actinides are sorbed strongly over the pH range 1–9, while trivalent actinides adsorb in comparable amounts (> 80 %) only at pH larger than 6. Pu(III) is oxidized to Pu(IV) during the reaction with kaolinite; therefore sorption of Pu(III) at kaolinite starts to raise only after pH 5.[130] Only Np(V) is sorbed relatively weakly at micro molar concentrations and shows a maximum at about pH 9, but the adsorption is enhanced when the concentration of neptunyl ion decreased.[131] The common drop in the sorption diagram at high pH values is attributed to carbonate complexation, because the experiments were carried out under aerobic conditions. This effect vanishes in experiments under argon atmosphere and the sorption rate remains at the same high level as at about neutral pH.

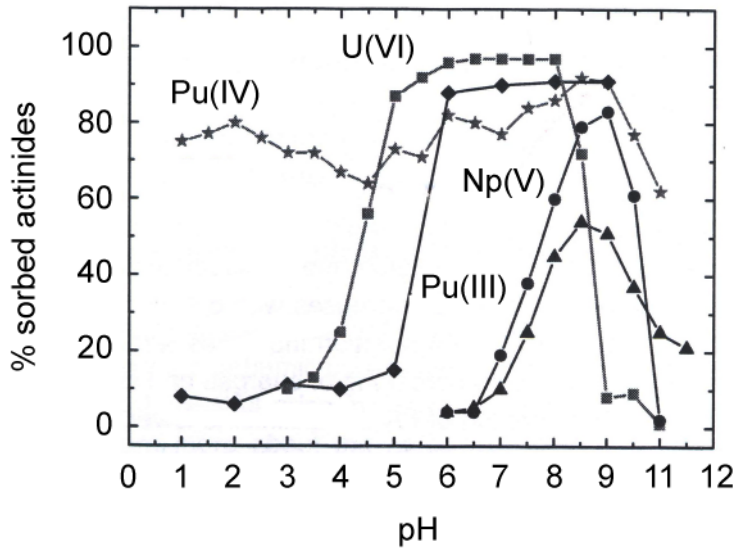

Figure 5.6. Sorption of actinide ions on kaolinite as a function of pH. The experiments have been performed under aerobic conditions, the sorption curve of Np is shown for two concentrations: triangles – $1 \cdot 10^{-6}$ M, dots – $7 \cdot 10^{-12}$ M. Adapted from Ref. 129.

Some aspects of the dependence of adsorption on the pH level were discussed in Section 5.3. Positively charged actinides are adsorbed at pH higher than some certain value. This value varies for different actinides and clay minerals.[121] For example, Np(V) sorption at montmorillonite starts from pH ~7.5, while uranyl adsorbs already at pH ~5.5.[132] The concentration of the clay mineral affects its adsorption capacity.[131] The amount of uranyl sorbed at montmorillonite relative to its initial amount in solution increases with increasing concentration of the clay mineral.[132] Ligands present in solution can enhance or block the adsorption process. For instance, as mentioned above, CO_2 in solution has a dramatic effects.[37,129] Due to the formation of actinide-carbonato complexes, adsorption is suppressed at a high pH values; see the adsorption of Np and U in Fig. 5.6.[37,129] This has been attributed to the failure of negatively charged metal-CO_3 complexes to adsorb. As an example, uranyl fully adsorbs on kaolinite at pH values above ~6.5 in N_2 atmosphere, whereas with air in the system the sorption drops to almost zero at pH above ~8.[37] In contrast, the presence of phosphate ligands in solution enhances uranyl adsorption on kaolinite, shifting the adsorption edge to lower pH values by 1 unit.[133] However, phosphate alone does not adsorb on kaolinite.

Inner- and outer-sphere complexes of actinide adsorption at mineral surfaces exhibit different structures (Fig. 5.7).[20,22,25] An inner-sphere complex is defined by the presence of direct bonds between the actinide and the surface; in other words, the surface participates in the first coordination shell of the actinide.[121] An outer-sphere complex can have one or more aqua ligands between the surface and the adsorbate.[121] EXAFS shows that Np(V) sorbs as inner-sphere complex at kaolinite in CO_2-free systems.[24] The adsorption of uranyl on

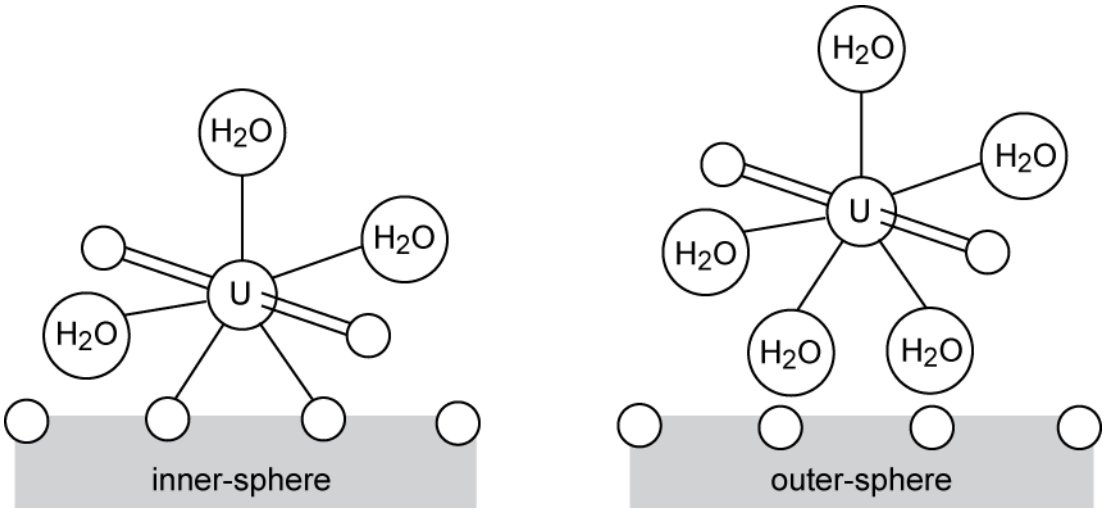

Figure 5.7. Schematic view of inner- and outer-sphere complexes of uranyl adsorbed at a mineral surface.

montmorillonite depends on the pH.[20] At montmorillonite uranyl adsorbs as an outer-sphere complex for low pH values, while at a higher pH inner-sphere complexes of uranyl are formed, most probably at edge sites.[20]

Thus far, the structure of adsorption complexes of actinyls and the mechanisms of adsorption on mineral surfaces are not well understood at the atomic level. While experimentally inner- and outer-sphere complexation or mono- and polynuclear adsorption species are distinguished,[20,22,24,28] several questions arise with respect to experiments on uranyl sorption at clay minerals. (*i*) Which adsorption sites are involved, aluminol (AlOH), silanol (SiOH), or other groups? (*ii*) Which surface orientations are preferred for adsorption, basal or edge surfaces? (*iii*) Is there a single preferred adsorption complex or is there an equilibrium between several of them?

While different experimental techniques were applied to explore actinide adsorption, only EXAFS provides structural parameters at the molecular level. Nevertheless, the composition and the structure of adsorbed complexes is difficult to determine unequivocally by means of XAFS, as these techniques average over all species present.[11,23] Quantum chemistry calculations may help to interpret experimental data and to improve our understanding of structures and mechanisms of the adsorption at the atomic level. Only few computational studies of actinide adsorption at mineral surfaces have been published. Quantum chemical methods were applied for studying uranyl adsorption at surfaces of TiO_2,[134] and α-Al_2O_3 (0001),[135] but the solvation of the surfaces was not taken into account. The study on TiO_2 investigated inner-sphere complexes adsorbed at (110) face of TiO_2, two of three examined complexes were found in a good agreement with experimental data. A

study of uranyl adsorption at the α-Al_2O_3 hydroxilated surface determined the outer-sphere complex to be more favorable than the inner-sphere complex at pH level close to pH_{ZPC} of corundum, which is ~9.1.[121]

Empirical force field calculations allow the inspection of more complex model systems even at the dynamical level. Molecular dynamics was applied for the uranyl adsorption at basal surfaces of different 2:1 phyllosilicates.[136,137] No adsorption was found at neutral pyrophyllite basal surfaces, while uranyl was calculated to adsorb at two other clay minerals, beidellite and montmorillonite, depending on the modeled concentrations of uranyl and CO_2 in solution.[137] The simulations confirmed the formation of outer-sphere uranyl complexes at these latter minerals. Computational studies can complement experimental investigations and help to achieve a better understanding of adsorption process on the atomic scale. Therefore, more detailed and systematic studies are worthwhile.

5.5 Adsorption of uranyl on kaolinite

As mentioned, this present thesis explores computationally uranyl adsorption on kaolinite. From experiment it is known that uranyl adsorption on kaolinite starts at pH ~6.[24,37,129] At lower pH levels uranyl prefers to stay as a free ion in solution. The crucial effect of the presence of CO_2 in solution was discussed before (Section 5.4). Fig. 5.8a shows adsorption curves for uranyl on kaolinite under aerobic and anaerobic conditions.[24,37] Also the presence of HA significantly influences uranyl sorption by kaolinite. It enhances the U(VI) uptake in the acidic pH range due to the formation of additional binding sites for uranyl resulting from HA adsorbed on kaolinite (Fig. 5.8b).[37] The formation of dissolved uranyl-humate complexes decreases the sorption rate to 60 % at near-neutral pH, at sufficiently high HA concentration. CO_2 and HA in solution at pH > 8 increase U(VI) sorption, while the presence of CO_2 alone results in almost full desorption of uranyl from kaolinite in this pH interval.[37] Thus far, reasons for this complex behavior are unclear. Nevertheless, it is obvious that HAs play an important role for the sorption behavior of uranyl under environmental conditions.

To elucidate the binding mechanism TRLFS[30] and EXAFS[22,24,25] were applied to uranyl-surface complexes. The TRLFS study yielded two life times for the uranyl-kaolinite system at a CO_2 pressure of $10^{-3.5}$ atm.[30] From this result, two complexes of adsorbed uranyl are postulated, which differ by the coordination number of uranyl.[30] Nevertheless, it is not clear whether there is one specific adsorbed complex with two different solvent coordination shells or whether there exists an equilibrium of several complexes at different sites.

At about neutral pH conditions (pH ~5–8.5), inner-sphere complexation of uranyl was determined by EXAFS.[22,24,25] An earlier study at pH ~7 in both air and Ar atmosphere showed two shorter U-O_{eq} values of about 228 pm and three longer ones of ~ 248 pm.[22] In addition an

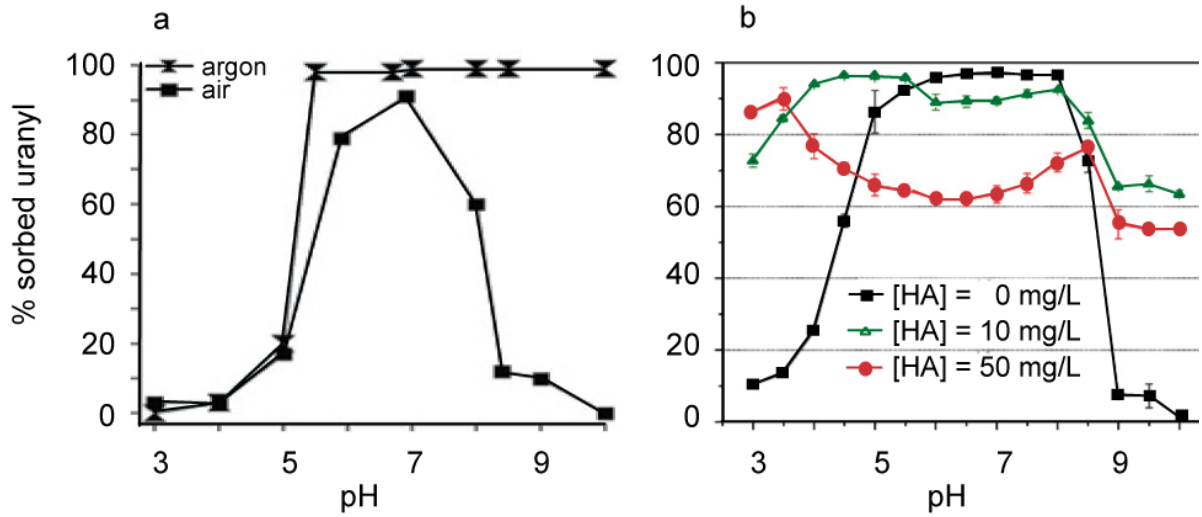

Figure 5.8. Sorption of actinide ions on kaolinite as a function of pH. (a) Sorption of 10 µM of uranyl in the presence and absence of ambient CO_2. Adapted from Ref. 24. (b) Sorption of uranyl in the presence and absence of humic acids. Adapted from Ref. 37.

U-Al/Si distance was measured at 330 pm.[22] Since Al and Si atoms can not be differentiated by EXAFS, it was not clear, whether aluminol or silanol groups contribute to the complexation, although the authors preferred the former because of the similarity with U-Al distances for uranyl adsorbed on gibbsite $Al(OH)_3$.[22] A recent study showed two U-Al/Si distances of 310 and 330 pm, and a range of average U-O_{eq} distances from 236 to 240 pm increasing with the pH of the solution.[24,25] In both studies the authors advanced the hypothesis that silanol groups most probably do not contribute to uranyl adsorption.[22,24,25] Nevertheless, they cannot be excluded from the adsorption process.

In this thesis, the computational investigation of uranyl sorption at kaolinite was started by examining the bare (001) basal surfaces of kaolinite and then varying the protonation of adsorption sites to model different pH conditions. This study was then extended to the adsorption at the (010) surface as a representative of edge surfaces of kaolinite with a larger variety of adsorption sites.

6 Computational treatment

6.1 Challenges and different approaches of computational treatment

A computational approach for investigating actinides adsorption at water-mineral interfaces requires an accurate method to model electronic structure and suitable computational power. In addition, knowledge of physical and chemical properties of the systems treated and some guided imagination is necessary. One needs to find a suitable compromise between the sophistication of the methods applied and the computational effort. Establishing an adequate

model of realistic environmental conditions, including solvation, counterions and other ligands, which can affect the adsorption (Section 5.4), is another challenge for a computational treatment. A clear difficulty for modeling actinide adsorption in solution is the size of the simulated system, which may include hundreds of atoms. Furthermore, relativistic effects of heavy elements like actinides have to be be accounted for;[41] they do increase the computational effort. Another complication is a proper treatment of solvation which can be modeled by different approaches,[47] each with its own advantages and shortcomings.

The first computational studies of the structure of clay minerals were done at the HF level using a cluster model.[138,139] Later on, DFT methods with periodic boundary conditions were used to investigate the bulk structure and bare clay mineral surfaces.[140] The solvation of clays as well as interaction of single aqua ligands with clays were studied computationally[141,142] by cluster models at the DFT level,[143] and by periodic DFT methods.[144,145] In this way one may determine the most stable configuration of isolated adsorbed water molecules, but not the solvation of a mineral surface, which needs a full coverage by water. More effective methods for that purpose, like *ab initio* MD and classical MD, became popular recently and were used in several investigations of clay solvation and clay swelling processes.[146-149] The Vienna *ab initio* simulation package (VASP)[150] as well as Car-Parinello molecular dynamics (CPMD)[123,124] codes were used in these studies. Both methods apply periodic boundary conditions. Methods with periodicity often are limited to neutral unit cells and face restrictions as the structure of water may not be compatible with periodic boundary conditions in case of too small unit cells. Corrections for charged unit cells are estimated fully in VASP only for cubic unit cells, for example.[151] Therefore, a model approach is needed if one wants to investigate charged systems with other types of unit cells with such a computer code. Note that in nature materials are locally neutralized by counterions. Therefore, neutralization can be modeled by counterions, which normally are present in solution or as defects in clay structures. Artifacts due to translational symmetry can be avoided by rather large unit cells, which prevent the interaction between adsorbed ions or, more importantly, an artificially ordered structure of the solvent.

In this thesis, the adsorption of UO_2^{2+} on kaolinite was studied keeping these limitations in mind. To control the computational effort, a density function (DF) procedure with periodic boundary conditions was selected. To overcome charge problem a neutralization model approach was introduced. Solvation effects were estimated by various approaches.

6.2 Computational details

First principles DF calculations on supercell models of kaolinite surfaces were carried out, using the plane-wave based Vienna *ab initio* simulation package (VASP).[150] The structures of

uranyl complexes adsorbed at the bare (001) kaolinite surfaces were optimized with the local density approximation (LDA-VWN),[152] which is known to furnish more accurate results for molecular geometries, whereas calculations with the generalized gradient approximation (GGA)[153,154] yield improved adsorption energies. Thus, energies were evaluated with the gradient-corrected exchange-correlation functional PW91.[155] This strategy was used in the first part of this thesis for uranyl complexes in solution as well.[76,84] Subsequently, when surface solvation effects were studied, the GGA approximation was applied for the optimization as well, as LDA is unable to describe weak interactions (hydrogen bonds) in a reliable way.[156] LDA and GGA results will be compared later on (Section 9.1). In a plane-wave based periodic slab model approach, one needs to invoke an effective Hamiltonian where the effect of the core electrons is represented in an approximate fashion. Here, the full-potential projector augmented wave (PAW) method was used as implemented in VASP.[157,158] Scalar relativistic effects are incorporated in the PAW potential via mass-velocity and Darwin corrections.[159] A plane-wave energy cut-off of 400 eV was adopted for surface models and of 520 eV for kaolinite bulk to reduce the effect of Pulay forces when the unit cell is optimized. This cut-off value was found sufficient in optimizations of a bare kaolinite (001) slab model; test calculations with an energy cut-off of 520 eV lead to negligible changes in structural parameters of surface models (< 0.1 pm). Brillouin zone integration was carried out with a (2×2×1) *k*-point grid,[160] applying a generalized Gaussian smearing method[161] with the smearing width set to 0.15 eV. The choice of such a small grid is justified by the rather large unit cells of about 1000 × 1800 pm. In geometry optimizations, the total energy was converged to 10^{-4} eV, and forces acting on ions were required to be less than 10^{-2} eV/Å.

All adsorption energies derived from VASP calculations formally refer to systems in the gas phase. Solvation effects on adsorption energies were estimated by applying corrections for molecular species $[UO_2(H_2O)_5]^{2+}$, H_2O, and H_3O^+ as obtained with a polarizable continuum model (PCM).[94-96] These solvation energies of molecular species were calculated with the linear combination of Gaussian-type orbitals fitting-functions density functional method (LCGTO-FF-DF)[78] as implemented in the program PARAGAUSS (Section 2.1). Calculations with a scalar relativistic version of the Kohn-Sham method were carried out (Section 2.1). For consistency the same choice of exchange-correlation functionals was adopted in these calculations on molecular species: the VWN variant[85] of LDA for geometry optimizations and the gradient-corrected PW91 functional[155] for energetics and for geometry optimization where appropriate. The corresponding basis set and convergence parameters were chosen as described in Section 2.1. The compatibility of both computational strategies, VASP and PARAGAUSS, was checked on the gas phase structure of the complex $[UO_2(H_2O)_5]^{2+}$. Both structures were found to agree very well: bond lengths differed by less

than 1 pm, bond angles at most by 2 degrees.

7. Kaolinite bulk and surfaces structures

7.1 Bulk structure of kaolinite

To examine the accuracy of the computational approach chosen, bulk and surface structures of kaolinite were first optimized without adsorbates. As mentioned, kaolinite belongs to the class of layered two-sheet aluminosilicates (Section 5.2).[162] The chemical composition of one such layer can be represented by a triclinic unit cell of composition $Al_4Si_4O_{10}(OH)_8$, which is overall neutral (Fig. 7.1). Two adjacent layers are connected via hydrogen bonds. In the beginning, space group *C*1 was assumed for the monoclinic bulk structure of kaolinite, which implies a *C*-faced centering[1] of the structure. Nevertheless, Young et al.[162] suggested the space group *P*1 (no symmetry), which requires twice the number of atoms in the asymmetric unit by allowing crystallographically identical atoms in *C*1 to occupy non-equivalent sites. Bish[163] found out that the coordinates of Al, Si, and O atoms of bulk kaolinite, refined assuming *P*1 symmetry, are very similar to the published *C*1 structures, but the positions of H atoms are distinct.

In this work bulk kaolinite was optimized without *C*-centering, applying space group *P*1. The resulting optimized triclinic primitive unit cell of bulk kaolinite is characterized by the parameters *a*, *b*, and *c*, representing the lengths of unit cell vectors, and the angles *α*, *β*,

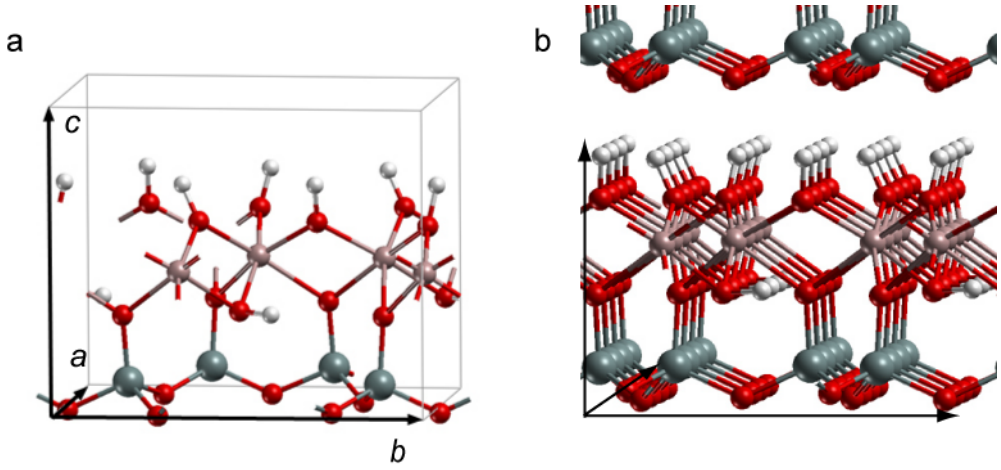

Figure 7.1. Kaolinite structure: (a) primitive unit cell; (b) bulk kaolinite.

[1] The symmetry center is in the plane perpendicular to lattice vector *c*. Coordinates of lattice points are designated as follow: (0, 0, 0), (½, ½, 0). Thus, for every unique atom with the coordinates (*x*, *y*, *z*) there is symmetry-equivalent one with coordinates (*x*+½, *y*+½, 0).

Table 7.1. Optimized unit cell parameters of bulk kaolinite, calculated with different exchange-correlation functionals: *a*, *b*, *c* in pm, angles in degrees. Experimental parameters from Ref. 162 are given for comparison.

	a	*b*	*c*	*α*	*β*	*γ*
LDA	512	888	719	92.0	105.1	89.9
PW91	521	905	745	92.2	105.2	89.8
exp.	515	893	738	91.9	105.0	89.8

and *γ* between them. Results of the optimizations at the LDA and GGA levels as well as experimental data obtained by means of neutron diffraction[162] for bulk kaolinite are compared in Table 7.1. LDA results compare very well with the experimental ones. The present LDA optimization slightly underestimates the lattice parameters *a* and *b*, by 3 and 5 pm, respectively, while the length of vector *c* is underestimated by ~20 pm. These findings may be attributed to the trend that LDA calculations overestimate nonbonding interactions (between the layers).[156] Computational results at the GGA-PW91 level agree better with experiment for the vector *c* (deviation 7 pm), but overestimated vectors *a* and *b* by 6 and 12 pm, respectively. Thus, the GGA values for the lattice parameters agree within about 1% with experiment, a very satisfactory result. Agreement of calculated and experimental angular parameters can be considered as rather accurate with either of the two computational approaches.

The optimized unit cells parameters from these calculations with different exchange-correlation functionals were used in subsequent slab calculations.

7.2 Models of (001) basal kaolinite surfaces

In the following, models of basal kaolinite surfaces were used that comprised only a single two-sheet layer. Structure optimizations of the uranyl adsorption on the bare surface were done at the LDA-VWN level. As mentioned in Section 5.3, kaolinite exhibits two basal (001) surfaces: the tetrahedral Si(t) and the hydroxylated octahedral Al(o) surfaces (Fig. 5.3). The latter is assumed to be more reactive due to the possibility to create negatively charged surface sites by deprotonation of hydroxyl groups. Each layer consists of six atomic "sublayers", H-O-Al-O-Si-O, exposing the (001) basal surface.

To test the quality of the one-layer model one-layer to two-layer models as well as models with different numbers of relaxed and fixed sublayers were compared. Various surface models are labeled as (*n*-*m*), where *n* is the number of relaxed sublayers and *m* the total number of sublayers in the slab model. Thus, *m* = 6 corresponds to a one-layer and *m* = 12 to a two-layer model. Optimized geometries for different surface models are collected in Table

7.2. This table also shows the averaged characteristic bond lengths of the optimized bulk structure of kaolinite (Fig. 7.2): bonds Si-O_{basal} between Si and O atoms of the basal plane, bonds Si-O_{inner} from Si to inner O atoms, Al-hydroxyl groups Al-OH_{surf} from the Al(o) surface, bonds Al-OH_{inner} from Al atoms to inner OH groups, and Al-O_{inner} to inner vertex oxygens, and bond lengths O-H_{inner} and O-H_{surf} for inner and surface OH groups, respectively. For simplicity, in Table 7.2 only changes in geometrical parameters with respect to the bulk are given for the various optimized surface slab models of the (001) Al(o) surface. For one-layer models 2, 4, and 6 "sublayers" were relaxed. The changes between slabs with 4 and 6 relaxed sublayers are marginal, at most 0.7 pm. Geometry parameters of the (4-6) model applied subsequently agree up to 1 pm with those of a two-layer model with all six "sublayers" of the surface slab relaxed, which is in turn very similar to the (8-12) slab model (Table 7.2). Overall, the surface relaxation effects for the largest slab model, (8-12), amount to 5 pm at most. The latter deviation is calculated for Al-OH_{surf} bonds. As can be seen from the data in Table 7.2 relaxation effects are more pronounced for the Al(o) than for the Si(t) surface. The (4-6) slab model represents surface relaxation effects to about 90% (Table 7.2). Thus, a one-layer slab model with four upper sublayers relaxed and two bottom sublayers fixed to the bulk structure was found to be a reasonable model of the (001) Al(o) surface.

The optimized surface structure of the chosen one-layer slab model of the Al(o)-KL (001) surface is shown in Fig. 7.3a. The surface unit cell contains four cyrstallographically different Al atoms and six OH groups, which can be grouped into three pairs of essentially equivalent centers because the space group *C*1 of the unit cell is only very weakly perturbed,

Table 7.2. Geometry parameters of bulk kaolinite (in pm), optimized at the LDA-VWN level, and average changes due to surface relaxation of the (001) Al(o) surface relative to the ideal bulk termination. Various surface models are labeled as (*n*-*m*), where *n* is the number of relaxed sublayers and *m* the total number of sublayers in the slab model. For labels of bonds see Fig. 7.2.

	bulk	Δ(2-6)	Δ(4-6)	Δ(6-6)	Δ(6-12)	Δ(8-12)
Si-O_{inner}	159.8		2.7	2.9	2.4	2.7
Si-O_{basal}	162.4			-1.4	-0.9	-1.0
Al-OH_{surf}	183.6	4.8	5.1	5.4	4.6	4.8
Al-OH_{inner}	192.1		-4.3	-4.5	-3.9	-3.9
Al-O_{inner}	195.6		-3.7	-4.4	-3.2	-3.2
O-H_{surf}	98.1	-0.5	-0.5	-0.6	-0.5	-0.5
O-H_{inner}	98.4		-0.6	-0.5	-0.5	-0.5
H-bond[a]	183.0				27.9	24.8

[a] Hydrogen bonds between layers.

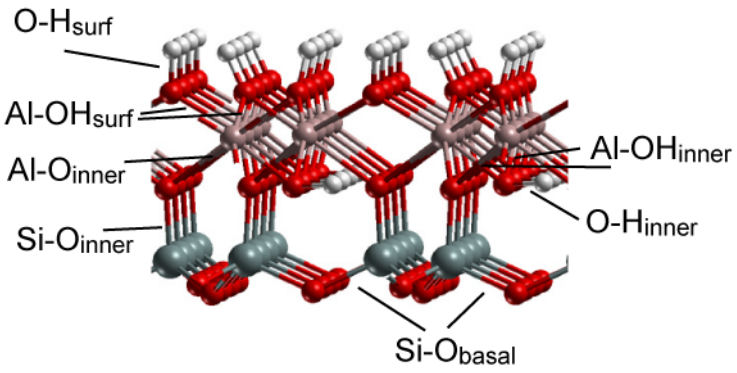

Figure 7.2. Definition of the main structural parameters of kaolinite.

showing *P*1 symmetry (Section 7.1).[162,163] Thus, there are essentially three different surface sites for monodentate adsorption and six pairs of close lying OH groups (OH groups attached to the same Al atom) which can form sites for bidentate adsorption (Fig. 7.3a). The distance between OH groups coordinated to different Al atoms amounts to more than 330 pm.

Pairs of non-neighboring OH groups are not considered as adsorption sites in this thesis. The main effect of relaxation of the Al(o) kaolinite surface is that one third of the surface hydroxyl groups is oriented parallel to the surface (Fig. 7.3a). The same effect was observed in an *ab initio* molecular dynamics study of the bare and solvated kaolinite surfaces by Tunega et al.[146] As a result, the Al(o) surface exhibits two types of hydroxyl groups: two thirds are "upright" OH groups (uOH), oriented largely perpendicular to the surface plane, and one third are "lying" OH groups (lOH), which are oriented essentially parallel to the surface.[140] The latter type of hydroxyl groups is bent to the surface since it forms two hydrogen bonds (O···H ~ 250 pm) to O atoms of upright OH groups. Each Al atom of the top layer is coordinated by three surface hydroxyl groups, two uOH and one lOH. The two types

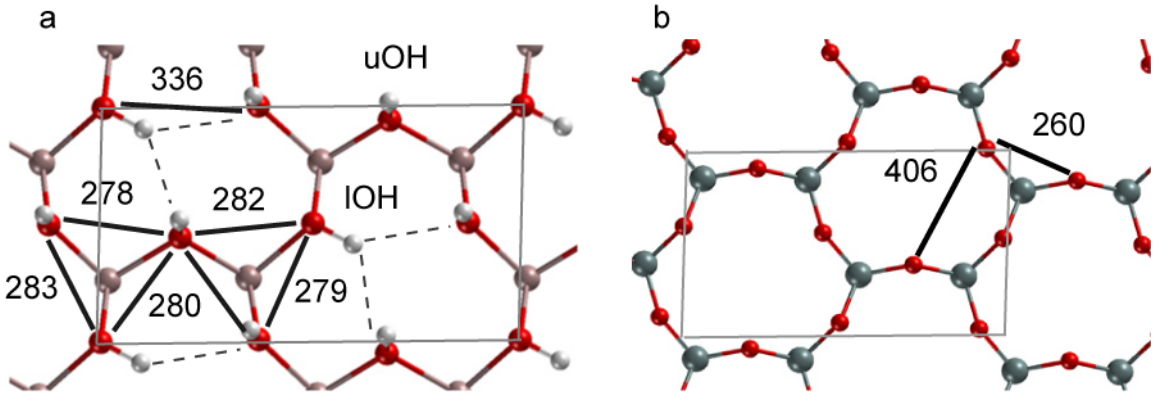

Figure 7.3. Top view of (a) Al(o) and (b) Si(t) (001) kaolinite surfaces. Numbers give distances of neighboring surface O atoms in pm.

Table 7.3. Geometry parameters of the Si(t) basal kaolinite surface: bulk termination and one-layer slab model with 2, 4, and 6 sublayers relaxed. Average changes of main characteristic bond lengths due to surface relaxation relative to the ideal bulk termination are given in pm.

	bulk	Δ(2-6)	Δ(4-6)	Δ(6-6)
Si-O_{inner}	159.8	3.3	3.0	2.9
Si-O_{basal}	162.4	-1.9	-1.4	-1.4
Al-OH_{surf}	183.6		3.5	5.4
Al-OH_{inner}	192.1		-4.8	-4.5
Al-O_{inner}	195.6		-4.6	-4.4
O-H_{inner}	98.4		-0.4	-0.5

of hydroxyl groups present qualitatively different coordination sites for uranyl.

For consistency, the Si(t) (001) surface of kaolinite was modeled in a similar manner as the Al(o) surface: a one-layer slab model with four relaxed surface sublayers and the "bottom" OH groups fixed to their bulk positions was invoked. For comparison, a one-layer model with only two "sublayers" relaxed was also studied and both can be compared to the (6-6) model. Table 7.3 shows the average changes in the main geometrical parameters of the Si(t) surface due to relaxation. The Si(t) basal surface of kaolinite was found to be rather rigid. The relaxation effect of the Si-O_{basal} bonds does not exceed 2 pm, while relaxation of all types of Al-O bonds of the Al(o) surface amounts to 3–5 pm (Tables 7.2 and 7.3). A top view of the Si(t)-KL surface is shown in Fig. 7.3b. Since the distance between oxygen atoms connected to the different Si is more than 400 pm, only neighboring surface oxygens (O-O = 260 pm), bound to the same Si atom, are considered as a bidentate adsorption sites for uranyl.

Different sizes of unit cells were compared to find an appropriate one for studying the adsorption of uranyl: (2×1), (2×2), and (3×2). For an exemplary inner-sphere complex, adsorbed at the Al(o) surface, these three unit cell sizes of approximately 1×0.9, 1×1.8,

Table 7.4. Geometry parameters of an inner-sphere bidentate uranyl complex $UO_2(H_2O)_3$-Al(o) adsorbed at a doubly deprotonated site of the Al(o) kaolinite surface, modeled with a single-layer slab and (2×1), (2×2), and (3×2) unit cells. Approximate sizes of the unit cells are in nm^2. The optimization was done at the LDA level. Geometry parameters in pm, adsorption energies ΔE (see Section 8.1) in kJ mol^{-1}.

Cell	Size	U=O	U-O_{surf}	U-Al	U-O_w	U-O_{eq}	ΔE
(2×1)	1×0.9	184, 186	210, 223	307	249, 251, 255	238	244
(2×2)	1×1.8	184, 187	209, 221	307	250, 253, 253	237	256
(3×2)	1.5×1.8	184, 186	209, 221	308	250, 252, 253	237	265

1.5×1.8 nm^2, respectively, were tested (Table 7.4). The resulting geometry parameters differ by ~2 pm for uranyl adsorbed at (2×1) and (2×2) unit cells, the adsorption energy difference amounts to 12 kJ mol^{-1}. Geometry changes from a (2×2) to a (3×2) unit cell do not exceed 1pm, while the adsorption energy again increases slightly by 9 kJ mol^{-1} (Table 7.4). The test result for the Al(o) surface can be transferred to the Si(t) surface since only weak adsorption is expected there (see below).

As a result, the (2×2) surface unit cell was regarded to be sufficiently accurate for modeling uranyl adsorption on both basal (001) surfaces. It has an area of ~1000 pm × 1800 pm. The (2×2) unit cell of a single-layer (001) slab model contains 136 atoms: 16 Al, 16 Si, 72 O, and 32 H centers. All slab models were repeated periodically with a vacuum spacing normal to the surface of ~1.5 nm.

7.3 Models of adsorption complexes at (001) kaolinite surfaces

The two principal types of species postulated for metal sorption at mineral surfaces in contact with an aqueous solution are inner-sphere and outer-sphere complexes (Section 5.4, Fig. 5.7). Characteristic features of inner-sphere complexes, as described according to experimental results, are a split first coordination shell of the adsorbed ion with short bonds to the surface and longer ones to aqua ligands, as well as the presence of rather short U-Al/Si distances (300–400 pm).[22] In the case of outer-sphere adsorption, the distance between the adsorbed metal ion and surface Al or Si centers is too large (more than 400 pm) to be detectable by EXAFS;[164] for uranyl, the geometric characteristics of an outer-sphere adsorption complex, by definition,[121] are indistinguishable from those of a free hydrated ion according to experiment.[20,21] One may classify the interaction of inner-sphere complexes with the support as chemisorption, while outer-sphere complexes are bound to the surface essentially electrostatically. Thus, it is natural to expect inner-sphere complexes to be stronger bound to the surface than outer-sphere ones. Then inner-sphere should be the predominant adsorption mode, provided appropriate sites are available.

In the present work, various adsorption complexes with different coordination modes were explored. On the Al(o) surface, different types of complexation can be imagined, depending on the degree of deprotonation of the surface hydroxyl groups (Fig. 7.4). There can be three different bidentate inner-sphere complexes: uranyl bound to the Al(o) surface via (*i*) two O^- centers (AlOO), (*ii*) one O^- center and one OH group (AlOOH), or (*iii*) two OH groups (AlOHOH). In all three cases only surface oxygen atoms connected to the same Al center of kaolinite are considered as approximate sites. As already mentioned (Section 7.2), the Al(o) surface of kaolinite comprises “upright” and “lying” surface hydroxyl groups.

Hence, uOH-uOH and uOH-lOH pairs of hydroxyl groups, bound to the same Al center, are considered as essentially different sites for bidentate uranyl adsorption. Deprotonated surface sites correspond preferentially to a pH regime above the point of zero charge, which for kaolinite is at a pH of ~5.5.[127] Correspondingly, two monodentate adsorption complexes can be distinguished (Fig. 7.4): (*iv*) uranyl bound either to an O^- center (AlO) or (*v*) via an OH group (AlOH) of the surface. Since uOH or lOH surface groups may be involved, four monodentate adsorption complexes of uranyl were considered. Finally, (*vi*) a model of an outer-sphere complex is constructed, where aqua ligands of the first solvation shell of uranyl interact with the surface via hydrogen bonds.

The Si(t) surface exhibits only coordinatively saturated oxygen centers and therefore is expected to be less reactive. The structures of two exemplary uranyl complexes on (001) Si(t) were optimized: a bidentate inner-sphere complex (SiOO), and an outer-sphere complex, constructed in analogy to the outer-sphere species at the Al(o) surface. Other positions of the adsorbate on this surface were not examined, as only a weak adsorption of uranyl on the Si(t) surface is expected.

7.4 Models of the bare (010) edge surface of kaolinite

The (010) plane of kaolinite was chosen as representative edge surface. The exact structure and termination of edge surfaces of kaolinite are unknown. Nevertheless, reactive groups at the edges, their distribution and density, estimated with different models, are discussed.[125,126]

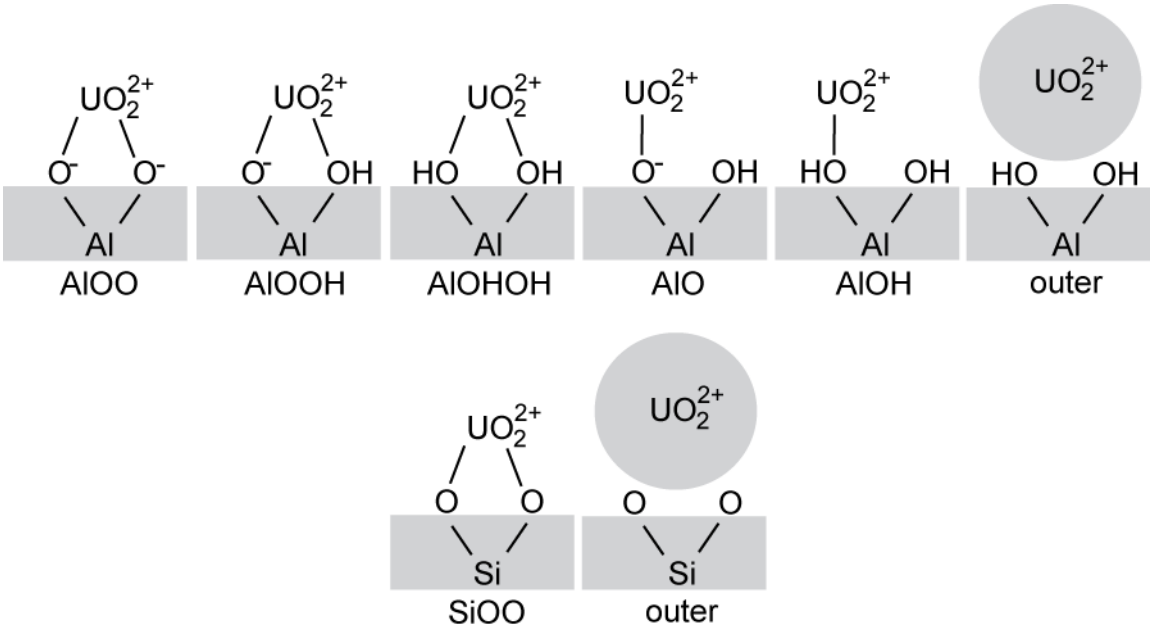

Figure 7.4. Schematic representation of studied model adsorption complexes on the basal Al octahedral and Si tetrahedral (001) surfaces of kaolinite: bidentate inner-sphere, monodentate inner-sphere, and outer-sphere complexes.

These groups for kaolinite are AlOH, $AlOH_2$, and SiOH. Some of the reactive groups are assigned an effective charge on the oxygen atom. Oxygen centers bound to Al atoms in the kaolinite crystal are threefold coordinated. They exhibit two bonds to Al atoms and one bond to hydrogen or a Si atom from the tetrahedral sheet. Formally the valence of a bridging surface OH group is determined as follows.

According to Pauling[165] an ionic structure will be stable to the extent that the sum of the strengths of the electrostatic bonds that reach an anion equal the charge on that anion, i.e. a stable ionic structure must be arranged to preserve local electroneutrality. As a Al cation (+3) in the bulk of kaolinite has a valence of +3 and six neighboring oxygen atoms of valence -2 which therefore translates into a strength of 1/2 per Al-O according to Pauling. Oxygen centers (formal charge -2) in the bulk of kaolinite share their valence with one Si and two Al centers (Fig, 7.2). Thus, all Si-O bonds exhibit a strength of 1, as do O-H bonds at Si centers of a basal surface. Recall the formal charge of H, +1. According to this view, the oxygen center of an AlOH group at an edge surface features a valence of 3/2 (1/2 from the Al-O bond and 1 from the H-O bond) instead of 2. Consequently, such a center is undercoordinated compared to oxygen centers of the bulk and the group is assigned an overall charge of -1/2 according to the formal counting of valence strength. The oxygen center of an $AlOH_2$ group in turn acquires a valence of 5/2 (1/2 from the Al-O bond, 2 from two H-O bonds); therefore, a formal charge of +1/2 is assigned to such a group (Fig. 7.5).

Possible terminations of the edge surface can be constructed by cutting the crystal parallel to the surface of interest, breaking the weakest bonds, and preserving the stoichiometry.[166] Bonds with lower valence (strength) values are considered to be weaker. The same result can be reached by cutting the crystal along the periodic bond chains (PBCs), defined by the Hartmann-Perdock PBC theory.[167,168] Nevertheless, thus far, there is no unique protonation scheme to saturate formally the bonds broken by constructing various terminations of the (010) surface. For example, a computational study of (010) edge surfaces of pyrophyllite suggested a termination mode of the edge surfaces, and proposed various

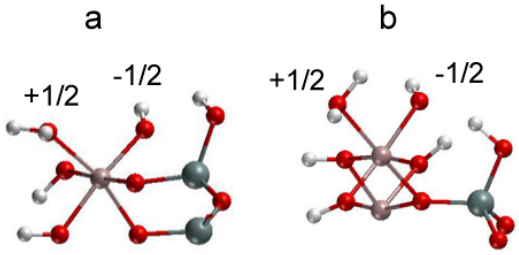

Figure 7.5. Charge assignment of surface aluminol groups for two different terminations of the (010) kaolinite surface.

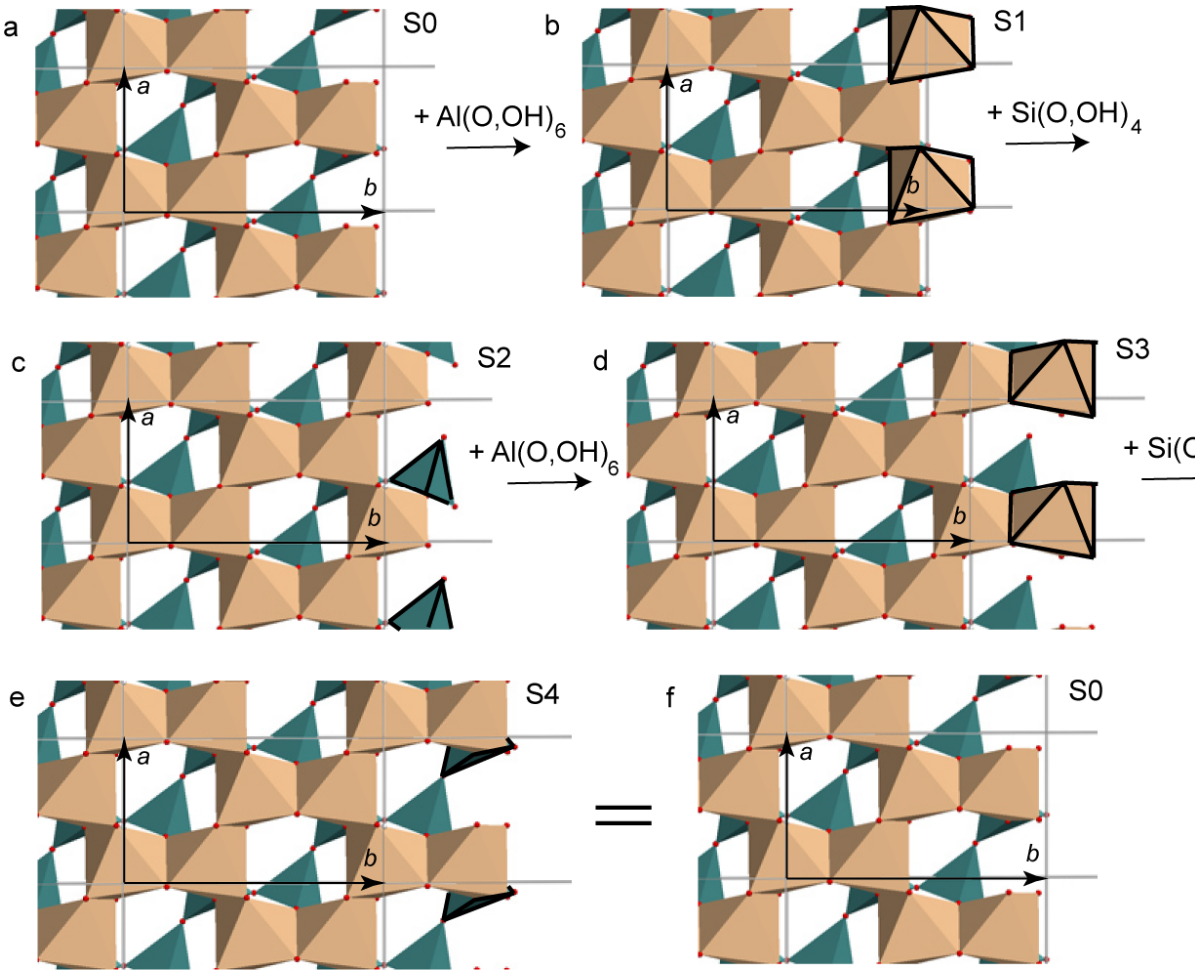

Figure 7.6. Polyhedron top view on the plane spanned by lattice vectors *a* and *b* of the kaolinite bulk structure. Several terminations of the (010) surface normal to *b* are shown: (a) S0 termination, (b) S1, (c) S2, (d) S3, and (e) S4, which is identical to S0 (f). Polyhedra distinguishing the various terminations are marked with bold edges.

protonation schemes.[126] A molecular dynamics study of the solvated (010) pyrophyllite surface suggested that protons hop along the surface, from one reactive site to another. Thus, the atomistic structure of hydroxylated solvated edge clay mineral surfaces can be even dynamic.

In this work, several possible terminations of (010) kaolinite surface were inspected. According to Bleam the crystal should be cut parallel to the (010) surface in such a way that the sum of bond valences of broken bonds is minimized.[166] Since the strength (valence) of a bond is associated with its length, an empirical model of the "actual" bond strength, correlated with the bond length, has been constructed.[169] Accordingly, a favorable edge termination is reached at the minimum of the empirical energy expression:

$$X = \sum S_{ij} = \sum_{ij} e^{(r_{ij}-r)/B}, \qquad (7.1)$$

Table 7.5. Characteristics of different terminations of the (010) surface of kaolinite: broken bonds, created reactive surface sites, and sum *X* of bond strengths, according to Eq. 7.1.

	Broken bonds	Reactive groups	*X*
S0	Si-O, 3 Al-O	2 $AlOH_2^{+½}$, $AlOH^{-½}$, SiOH, $(Al)O(Si)^{-½}$	3.14
S1	2 Si-O, 2 Al-O	SiOH, $AlOH^{-½}$, $AlOH_2^{+½}$	3.12
S2	2 Si-O, 2 Al-O	2 SiOH, $AlOH_2^{+½}$, $(Al)O(Si)^{-½}$	3.07
S3	3 Si-O, 4 Al-O	2 SiOH, 2 $AlOH_2^{+½}$, 2 $AlOH^{-½}$,	5.23

where S_{ij} is the strength of the bond between atoms *i* and *j*, and r_{ij} is the corresponding fitted reference bond length. *B* is a parameter, which usually is taken to be 0.37.[169] The second approximation used during the modeling of edge surfaces is that the Al and Si atoms should preserve their coordination number, and all the dangling bonds have to be hydroxylated. Several cuts of the (010) surface of bulk kaolinite are shown in Figure 7.6. If one cuts exactly through the plane of *a* and *c* cell vectors, then one obtains termination S0 of the (010) surface (Figure 7.6a). All further terminations are constructed by adding one polyhedron per unit cell – an $Al(O,OH)_6$ octahedron or a $Si(O,OH)_4$ tetrahedron (Fig. 7.6). Termination S1 contains one Al octahedron more than termination S0. Termination S2 contains one Si tetrahedron in addition, etc. After two Al octahedra and two Si tetrahedra have been added, one reaches termination S4 which is identical to termination S0. Thus, the cycle is closed. Taking into account that reference bond lengths Al-O and Si-O, obtained from a systematic analysis of the inorganic crystal structure database,[169] are 165 and 162 pm, respectively, one can estimate the sum of broken bond strengths for creating terminations S0, S1, S2, and S3, see Table 7.5. Creation of these terminations requires 3.14, 3.12, 3.07 and 5.23 units, respectively. Since the model is empirical and the fitted reference bond lengths induce uncertainties, the values 3.12, 3.14 and 3.07 have to be considered as essentially the same. Therefore, from this model one can not determine the most stable termination safely, except that termination S3, which needs 5.23 units to be created, can certainly be disregarded as thermodynamically unstable and hence excluded from further considerations.

Experimental investigations of dissolution of kaolinite show that the detachment of Al cations from edge facets of kaolinite is the rate-determining step (Fig. 7.7).[127] Therefore, termination S2, which can be transformed to termination S1 by dissolution of a $Si(OH)_4$ fragment, can be regarded as kinetically unstable.

In an earlier molecular dynamics study on Cs adsorption on different facets of kaolinite termination S0 was explored as an exemplary structure of the (010) kaolinite surface and

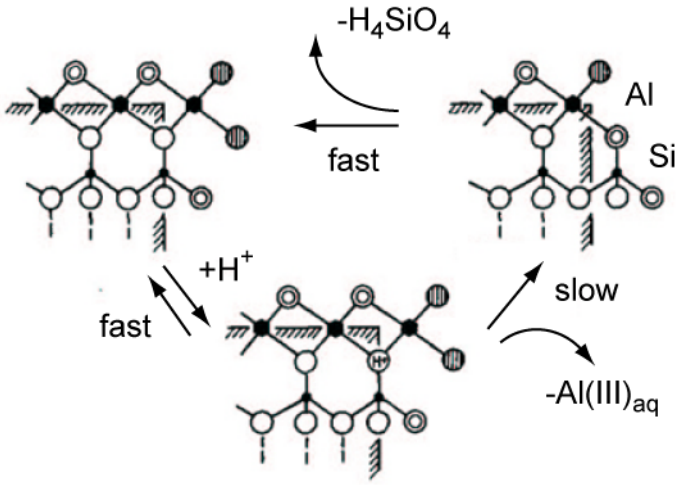

Figure 7.7. Kinetics of dissolution of kaolinite, adapted from Ref.127.

inner-sphere adsorption on aluminol sites was found to be most favorable.[170] In the following, both terminations S0 and S1 and uranyl adsorption on them will be explored.

The two preferred terminations S0 and S1 were modeled to represent the (010) surface of kaolinite (Fig. 7.8). Since slabs modeling the (010) surface hardly show pronounced geometrical sublayers, it is useful to distinguish different models by their numbers of Si tetrahedra SiO_4 and Al octahedra $Al(O,OH)_6$ per unit cell. Test calculations were carried out for "thinner" and "thicker" slab models, as well as for different choices of the fixed part of the slab. A smaller slab model of the S0 surface was constructed from four Si tetrahedra and three Al octahedral (Fig. 7.8). A more extensive model included in addition two tetrahedra and two octahedra. Finally it exhibits six SiO_4 and five $Al(O,OH)_6$ structural units. Accordingly, the second termination S1 incorporates one extra Al octahedron in the slab models. Dangling bonds at both sides of the slabs were hydroxylated. Figure 7.9 shows the two slab models of termination S0 (8 and 12 formal "sublayers"). Horizontal lines schematically indicate how

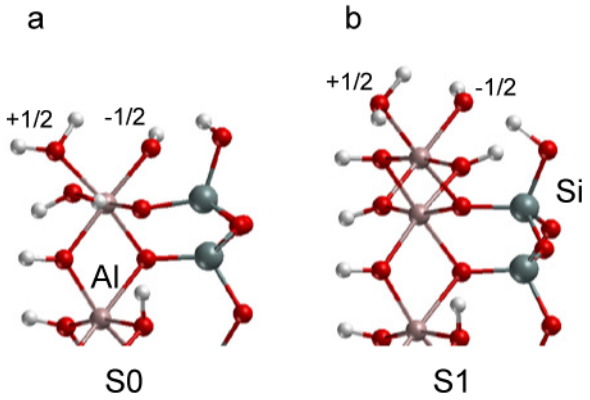

Figure 7.8. Two most probable terminations of the (010) surface of kaolinite (at the top of the sketches), including surface protonation: (a) termination S0, (b) termination S1.

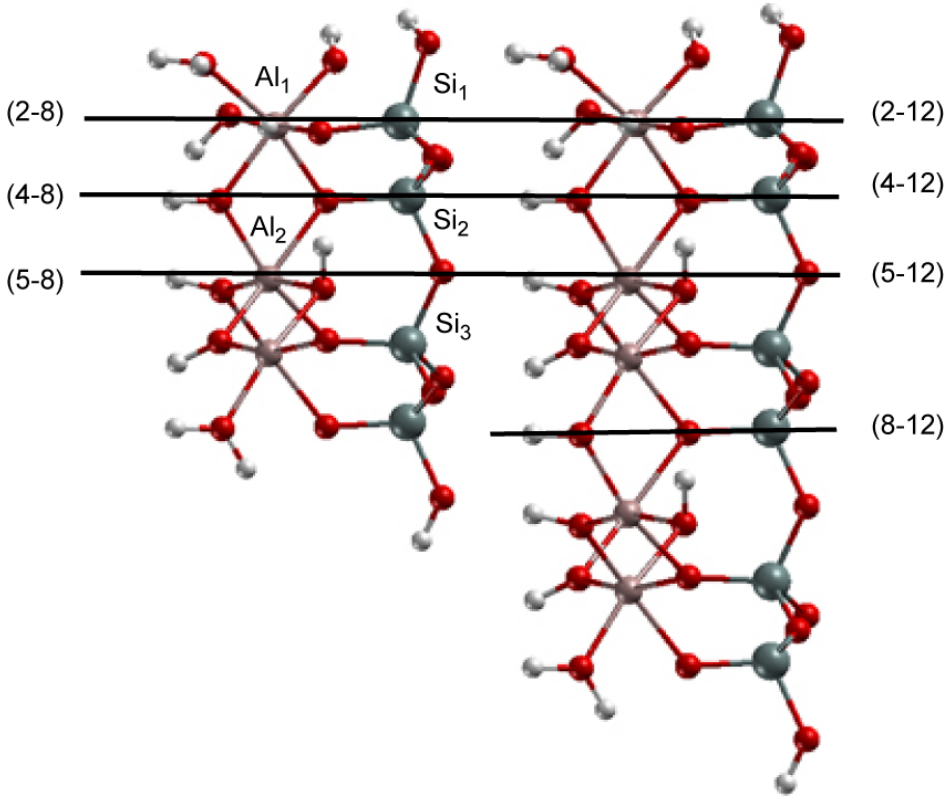

Figure 7.9. Two slab models (thinner and thicker) of termination S0 of the (010) kaolinite surface. Horizontal lines separate relaxed (top) and fixed parts (bottom) of various surface models sublayers.

many "sublayers" were relaxed. The main structural parameters and their changes due to surface relaxation are given in Tables 7.6 and 7.7. Test calculations for slab models with 2 (13 atoms: Al, Si, 5O, 6H), 4 (19 atoms: Al, 2Si, 9O, 7H), and 5 (25 atoms: 2Al, 2Si, 12O, 9H) relaxed formal "sublayers" were performed for both thin and thick models. Table 7.6 collects structural parameters for the thin slab model (8 sublayers) and their changes, when the thicker slab (12 sublayers) is considered.

As on can see from Table 7.6, surface relaxation is essentially independent of the thickness of the slab model, as long as a sufficient number of surface sublayers is relaxed. The surface relaxation effects are rather large due to formation of new surface reactive groups, like $AlOH_2$, which are not available in the bulk. The strongest elongation is calculated for the Al_1-OH_{2surf} bond, which amounts to 197–198 pm on the surface. The corresponding Al-OH bond in the bulk is 184 pm only. Nevertheless, both thin and thick slab models described surface relaxation similarly. Differences between (x-8) and (x-12) models are well below 1 pm, when more than two surface layers are relaxed. Therefore, the slab model with 8 sublayers was chosen for further calculations. Since termination S1 differs from termination S0 only by an additional Al octahedron, all tests were carried out for the smaller models of the S0 terminated surface. The chosen slab model of S0 was then extended to S1 by adding an Al

Table 7.6. Main relaxation effects of bonds at the (010) surface of kaolinite with respect to the bulk for different surface models. Δ denotes the difference between (x-8) and (x-12) models. (*n*-*m*) labels the models by means of the number of relaxed "sublayers" *n* and the total number of sublayers *m*. Distances in pm.

	bulk	(2-8)	Δ	(4-8)	Δ	(5-8)	Δ
Al_1-OH_{basal}	184.2	183.2	-0.7	183.0	-0.1	182.7	0.0
Al_1-OH_{2surf}	184.2	196.7	-0.6	197.3	0.0	197.7	-0.3
Si_1-OH_{surf}	162.4	164.9	0.2	164.4	0.0	164.4	-0.2
Al_2-OH_{basal}	184.0					188.5	-0.6

octahedron, which extends the relaxed part of the surface model.

The number of relaxed sublayers was tested as well. The main geometry parameters and their changes with respect to the bulk geometry are given in Table 7.7. The biggest effect of relaxation is obtained for the surface Al-O bonds, since they are involved in surface $AlOH_2^{+½}$ and $AlOH^{-½}$ groups, which are not present in the bulk structure. Bonds from an Al_1 center to surface OH_2 groups are 6–13 pm elongated, compared to the bulk, while bonds from Al_1 to surface OH group are shrunk by ~8 pm. Also the Al_1-OSi_1 bond is reduced by ~10 pm. These calculated changes can be related to the effective charges on O atoms. Oxygen centers of $AlOH_2^{+½}$ groups exhibit a formal partial positive charge (see beginning of this section), which leads to its repulsion from the Al cation. While $AlOH^{-½}$ and $(Al)O(Si)^{-½}$ groups show undercoordinated oxygen centers, which exhibit partial negative charges, and thus are stronger bound to the Al center. The remaining geometry changes due to the surface relaxation are limited to 4–5 pm. Nevertheless, two relaxed sublayers were found to be not enough to represent properly the surface relaxation; for instance, such a limited model does not reflect the relaxation of deeper lying Al_2-O bonds, which is up to 4 pm (Table 7.7). The (4-8) slab model exhibits 50 % of the slab relaxed and 50 % fixed; differences from the results of the (2-8) slab are ~1 pm. In addition, it features relaxation of deeper layers. In turn, the (5-8) model shows differences to the (4-8) results of up to 0.4 pm, which indeed are very small. Just to compare with the more extended model, (8-12) results of the thicker slab model with 8 sublayers relaxed are also shown. Differences to the (4-8) model are even smaller than in the case of (5-8) model. Thus, the model (4-8) is appropriate to represent termination S0 of (010) kaolinite.

As a result, the slab model of 8 sublayers with 4 of them relaxed, was regarded to be trustworthy enough for the further calculations. Correspondingly, termination S1 will be modeled by a similar slab with the same number of fixed sublayers, but with Al octahedron in "upper" part in addition. The corresponding (2 × 2) slab models of terminations S0 and S1 of

Table 7.7. Main relaxation effects of the (010) surface atoms of kaolinite for different depths of relaxation of the models (Fig. 7.8): differences Δ from bulk values and second differences Δ^2 between specific models. Relative relaxation energies ΔE_{total} are also given, in kJ/mol. The first part of the table contains mainly bonds at the surface. The second part shows bonds between 4 and 6 sublayers, representing relaxation of deeper layers. Al and Si polyhedra are numbered consecutively from the surface to the bulk side of the models (Fig. 7.8). Differences between the chosen (4-8) and bigger slab models are shaded. Distances in pm.

	bulk	Δ(2-8)	Δ(4-8)	Δ(5-8)	Δ(5-12)	Δ^2 [(5-8)-(4-8)]	Δ^2 [(5-12)-(4-8)]
Al_1-OSi_1	199.7	-10.8	-9.8	-9.5	-9.6	0.3	0.2
Si_1-OAl_1	159.9	-0.1	0.4	0.4	0.4	0.0	0.0
Al_1-OSi_2	193.4	-3.3	-2.8	-3.0	-2.8	-0.2	0.0
Al_1-OH_{basal}	184.2	-1.0	-1.2	-1.5	-1.5	-0.3	-0.3
Al_1-OH_{surf}	191.8	-8.2	-7.5	-7.4	-7.6	0.1	-0.1
Al_1-OH_{2surf}	183.8	12.9	13.5	13.9	13.5	0.4	0.0
Al_1-OH_{2surf}	183.6	6.4	6.3	6.2	6.2	-0.1	-0.1
Si_1-OH_{surf}	162.4	2.5	2.0	2.0	1.8	0.0	-0.2
Al_2-OSi_2	200.7		-1.3	0.9	-0.1	2.2	1.2
Al_2-OH_{basal}	184.0		3.7	4.5	3.9	0.8	0.2
Si_2-OAl_2	159.6		0.5	0.5	0.4	0.0	-0.1
Al_2-OH_{inner}	192.3			-2.4	-1.4		
Al_2-OSi_3	195.1			-1.5	-0.6		
Al_2-$OH_{basal, low}$	183.2			0.9	0.1		
	183.0			-1.3	-1.3		
ΔE_{total}		0	-6	-8		-2	

the (010) surface comprise 156 and 172 atoms per unit cell; 12 Al, 16 Si, 76 O, and 52 H, and 16 Al, 16 Si, 84 O, and 56 H centers, respectively.

7.5 Models of adsorption complexes on (010) kaolinite

Since in EXAFS experiments on uranyl adsorption on kaolinite only U-Al/Si distances were resolved that were interpreted as characteristic for bidentate inner-sphere surface complexes,[20,24,25] the present study focuses on bidentate uranyl complexes on (010) kaolinite. Experiments show uranyl adsorption to take place at higher pH (starting from pH 6),[24] the surface models should offer deprotonated sites. Thus, the surfaces are expected to be partially deprotonated under such conditions. Therefore, uranyl adsorbed at singly and doubly deprotonated surface sites was examined in this work.

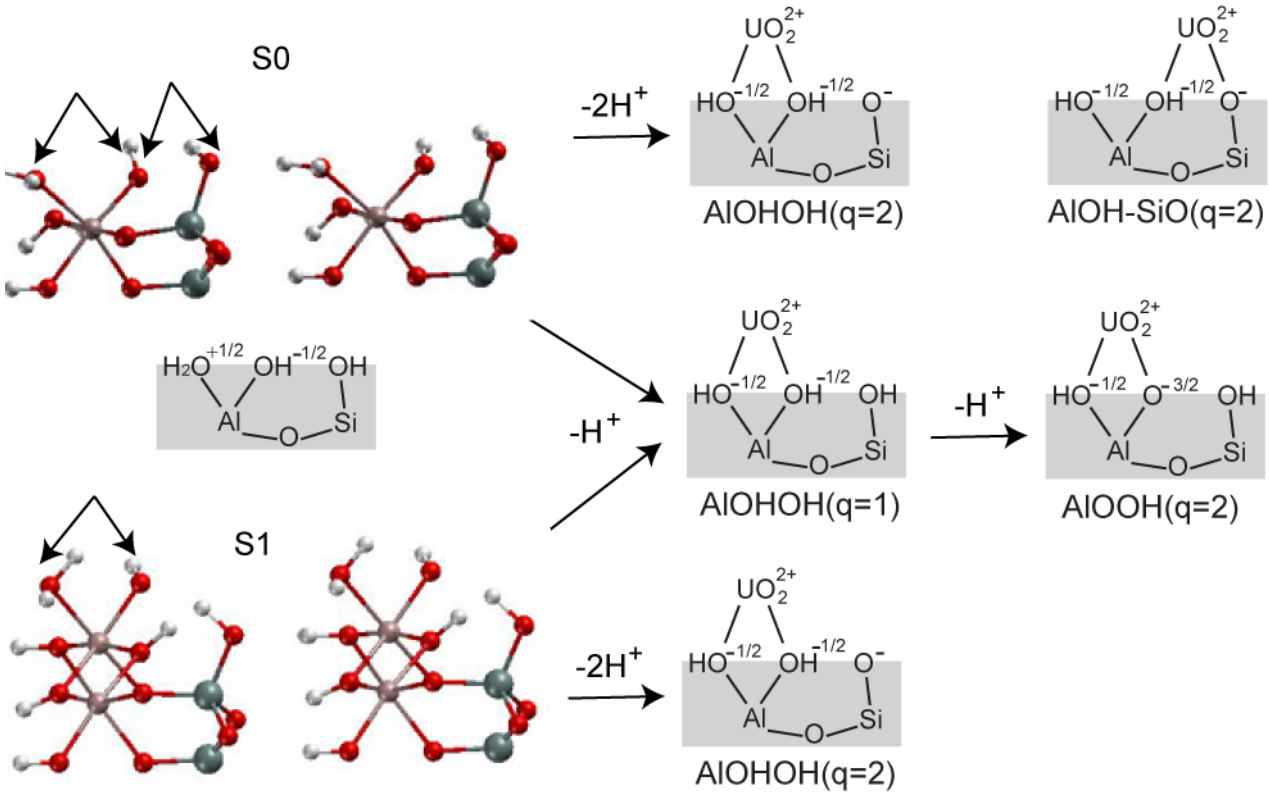

Figure 7.10. Schematic representation of possible bidentate complexes of uranyl adsorbed at S0 and S1 terminated (010) kaolinite surfaces. AlOOH, AlOHOH, AOH-SiO – models of doubly deprotonated (q=2) sites, AlOHOH – models of singly deprotonated (q=1) sites. The mixed site AlOH-SiO exists only for the S0 termination.

The (010) edge surface in the gas phase exhibits $AlOH^{-½}$, $AlOH_2^{+½}$, and SiOH groups, which can contribute to the adsorption when they are at least partially deprotonated. Terminations S0 and S1 of the (010) surface offer rather similar, though not identical types of complexation sites for uranyl. All examined adsorption sites for bidentate complexation at the terminations S0 and S1 are shown in Figure 7.10. Several adsorption sites were modeled on both terminations S0 and S1: (*i*) uranyl bound to $AlO^{-3/2}$ and $AlOH^{-½}$ surface groups, connected to the same Al atom and corresponding to the site charge of q=2 (AlOOH), (*ii*) uranyl bound to two $AlOH^{-½}$ groups corresponding to a singly deprotonated site, q=1, and representing the lower pH regime (AlOHOH), and (*iii*) uranyl bound to two $AlOH^{-½}$ groups corresponding to q=2, when a neighboring SiOH group is deprotonated; (*iv*) uranyl bound to $AlOH^{-½}$ and SiO^- groups (AlOH-SiO) with the site charge of q=2 which was created only for termination S0. Termination S1 does not exhibit an easily accessible mixed AlOH-SiO site, since the silanol group is not close enough to the surface for uranyl adsorption. Those sites which are singly deprotonated, need a neutralization of the surface model unit cell.

Since (010) terminations show always one $AlOH_2^{+½}$ group with threefold coordinated oxygen one proton was always removed from this group to construct an adsorption site for

uranyl since deprotonation of the $AlOH_2^{+½}$ group is assumed to occur first according to empirical model estimates.[171]

8. Adsorption of uranyl on bare surfaces of kaolinite

8.1 A simple model of uranyl adsorption on the Al(o) surface

The discussion of uranyl adsorption on the Al(o) surface was started with a comparison to the adsorption on the (0001) surface of corundum, α-Al_2O_3. The same modeling strategy was applied as used by Moskaleva et al.[135] for corundum. A bidentate inner-sphere complex and an outer-sphere complex were modeled so that a neutral unit cell is achieved. As in the inner-sphere complex uranyl is attached to two deprotonated surface oxygen centers bound to the same Al atom, a neutral unit cell results (AlOO site of the Section 7.3). For the outer-sphere complex, a neutral unit cell was constructed by replacing solvated uranyl by the corresponding neutral dihydroxide complex. Thus, the neutral unit cell results from the double deprotonation of the surface site in the former case, or of the adsorbate complex in the latter. One should keep in mind that the substitution of the uranyl ion by its dihydroxide yields a neutral unit cell, which allow an estimate of the formation energy of the adsorbed complex, but the geometry belongs to a different surface species.

Table 8.1 compares geometry parameters and formation energies, calculated for these model complexes on (001) Al(o) kaolinite and (0001) α-Al_2O_3. For these "gas phase" models, the energy of uranyl adsorption as inner-sphere complex at the Al(o) (001) surface was calculated at 209 kJ mol^{-1} according to the reaction

$$S(OH)_2 + [UO_2(H_2O)_5]^{2+} \rightarrow S(O)_2{-}UO_2(H_2O)_3 + 2\ H_3O^+ \qquad (8.1)$$

where S represents the surface of the substrate. Then corrections were applied to estimate the corresponding formation energy of the complex at the water-mineral interface. As a first approximation the solvation energy of the clean surface was assumed to be identical to that of the surface with adsorbed uranyl; then the corresponding solvation corrections cancel in Eq. (8.1). With calculated solvation energies for the molecular species, -382 kJ mol^{-1} for H_3O^+ and -811 kJ mol^{-1} for the solvated uranyl ion, the sum of the solvation corrections for Eq. (8.1) was estimated at 47 kJ mol^{-1}; hence, the energy of adsorption at the water-Al(o) interface, including the estimated effect of solvation, is 256 kJ mol^{-1}. Using the same procedure, uranyl adsorption on the neutral α-Al_2O_3(0001) surface from aqueous solution had been estimated as more endothermic, with an energy change of 328 kJ mol^{-1}.[135]

The outer-sphere complex of uranyl, modeled as doubly hydroxylated neutral species, binds to the surface via hydrogen bonds between surface hydroxyl groups and aqua ligands of

the first solvation shell of uranyl. To estimate the formation energy of adsorbed solvated uranyl,

$$S + [UO_2(H_2O)_5]^{2+} \rightarrow [S\cdots UO_2(H_2O)_5]^{2+}, \quad (8.2)$$

the analogous adsorption of uranyl dihydroxide was invoked to circumvent a charged unit cell:

$$S + UO_2(H_2O)_3(OH)_2 \rightarrow S\cdots UO_2(H_2O)_3(OH)_2 . \quad (8.3)$$

If one assumes the deprotonation energy of two aqua ligands of the first solvation shell to be similar for free and weekly adsorbed uranyl when these ligands are directed away from the surface, one can estimate the energy of reaction (Eq. 8.2). As an implicit approximation, this model replacement of charged uranyl by neutral uranyl dihydroxide also neglects the electrostatic attraction between the uranyl ion and the surface dipole (~6 au per unit cell), which essentially vanishes for uranyl dihydroxide.

The solvation energy correction from Eq. (8.2) is expected to be small and is neglected, because, due to weak adsorption, hydration energies of reactants and products should be similar. From these considerations an approximate formation energy of -105 kJ mol^{-1} results for the outer-sphere complex of uranyl on Al(o) kaolinite. Thus, outer-sphere adsorption of uranyl is 80 kJ mol^{-1} more favorable on Al(o) than on corundum (ΔE_{ads} = -25 kJ mol^{-1}). In summary, outer-sphere adsorption is expected to be favored compared to inner-sphere adsorption at AlOO sites when in both cases the reference is the hydroxylated surface. These conditions are fulfilled for a pH around zero-point charge conditions of the surface, which is estimated to about 5.5 for basal (001) kaolinite, but at 9.1 for (0001) corundum.[121]

The optimized inner-sphere complex of uranyl at the (001) Al(o) surface of kaolinite is shown in Fig. 8.1a. The structures of the inner-sphere complexes at Al(o) kaolinite and (0001) corundum surfaces are qualitative similar (Table 8.1): they show rather long U-O_t bonds, two shorter U-O_{surf} and three longer U-O_w bond lengths. Nevertheless, one notes that although U-O_{surf} distances are shorter for uranyl adsorbed at kaolinite (209 and 221 pm), the U-Al distance is 16 pm shorter for uranyl adsorbed on corundum. This difference is mainly due to the structure of the mineral surfaces: Al-O_{surf} bonds of corundum are ~20 pm shorter than those of kaolinite. Hence, on α-Al_2O_3 Al atoms are closer to the actual surface than on Al(o) kaolinite. On the other hand, U-O_{surf} bonds are slightly shorter for kaolinite, in line with a tendency to longer terminal U-O_t bonds and a higher adsorption energy of uranyl, i.e. reaction Eq. (8.1) is less endothermic (Table 8.1). For both surfaces, the U-O_t bonds elongate compared to a free solvated uranyl ion (from 177 up to 186 pm) due to the strong interaction of uranyl with the surface AlO^- groups and the hydrogen bonds of 166–180 pm between terminal oxygen centers of uranyl and protons at either surface.

The main distinction between outer-sphere complexes of $UO_2(H_2O)_3(OH)_2$ adsorbed on Al(o)-KL (Fig. 8.1b) and α-Al_2O_3 is the coordination number 4 in the former case (see below), but 5 in the latter case (Table 8.1). As the U-OH bonds are rather short and strong, 210–225 pm, the bonds to equatorial aqua ligands not directed to the surface, are weakened compared to solvated uranyl (Table 8.1). Note that uranyl dihydroxide does not yield a faithful representation of the uranyl ion; therefore, the geometry parameters of the outer-sphere uranyl complex adsorbed at the Al(o) kaolinite surface are different from those of $UO_2(H_2O)_3(OH)_2$, although this model should give a reasonable estimate for the adsorption energy of the uranyl outer-sphere complex according to the model considerations discussed above. One of the water ligands of the first solvation shell of uranyl on the Al(o) surface tends to be attracted by the surface and therefore the bond to uranyl is considerably elongated. From Fig. 8.1b one notes that uranyl has only two short bonds to aqua ligands and two shorter bonds to OH groups, while the third water molecule exhibits a U-O_w distance of 348 pm and thus can not be considered as an aqua ligand of the first solvation shell. This water molecule forms a hydrogen bond (O···H = 180 pm) to a surface OH group. Thus, this complex effectively shows a coordination number of 4. Adding a water molecule at the kaolinite surface at the position, to which one of the aqua ligands of uranyl is attracted, does not change the arrangement of the water molecules around uranyl in a major way (Fig. 8.1c). The

Table 8.1. Calculated characteristics of an uranyl inner-sphere complex and an uranyl dihydroxide outer-sphere complex on neutral hydroxylated mineral surfaces α-Al_2O_3 (0001) and octahedral (001) kaolinite (KL). Structures from LDA calculations (distances in pm), energies (in kJ mol^{-1}) from GGA calculations. Data for solvated uranyl are given for comparison.

Complex	N	U-O_t		U-O_w	U-O_{eq}	U-Al	ΔE^a
$[UO_2(H_2O)_5]^{2+}$	5	177		238, 238, 240, 241, 243	240		
inner-sphere			U-O_{surf}				
α-Al_2O_3[b]	5	184, 185	211, 232	245, 260, 263	242	291	328
Al(o)-KL	5	184, 186	209, 221	249, 251, 256	237	307	256
outer-sphere			U-OH				
α-Al_2O_3[b]	5	180, 181	221, 225	230,[c] 259, 268	241		-25
Al(o)-KL	4	181, 181	210, 222	233,[c] 257, 348	231		-105
+ H_2O[d]	4	180, 183	209, 227	243, 245, 298	231		

[a] For inner-sphere complexes estimated according to Eq. (8.1), for outer-sphere complexes according to Eq. (8.3). Value includes an estimate of long-range solvation effects, see text.
[b] Ref. 135. [c] Distance from U to the aqua ligand oriented to the support. [d] Outer-sphere with additional water molecule adsorbed at the surface nearby.

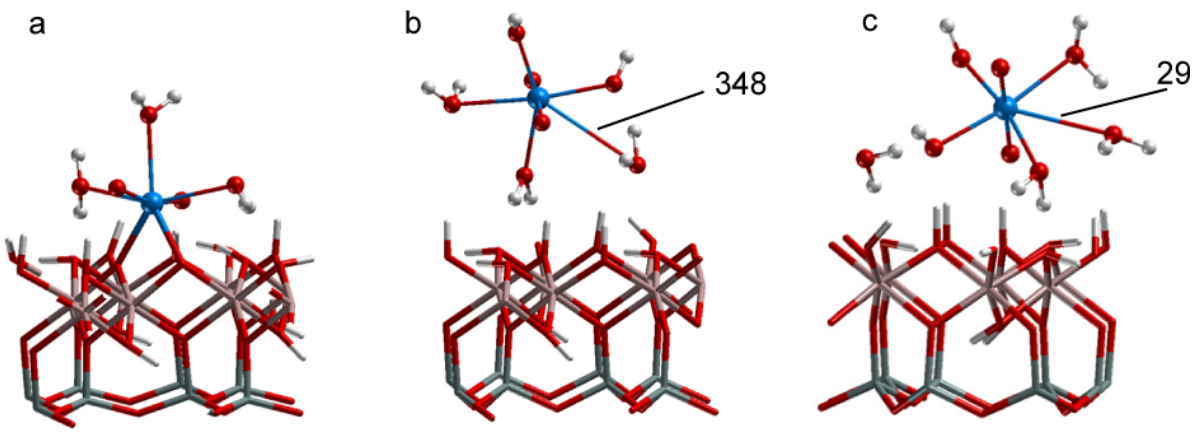

Figure 8.1. Optimized geometries of neutral model adsorption complexes of uranyl on Al(o) (001) kaolinite. Inner-sphere complex (a); outer-sphere complex of $UO_2(OH)_2(H_2O)_3$ (b) and of $UO_2(OH)_2(H_2O)_3 \cdot H_2O$ (c).

resulting complex again shows one rather long U-O_w distance, 298 pm, which is now directed away from the surface of the substrate. Thus, the coordination number of uranyl has to be regarded as 4 also in this model of the outer-sphere complex of $UO_2(H_2O)_3(OH)_2$ on Al(o) kaolinite. As a result, the U-O_{eq} bond is rather short, 231 pm, which is typical for uranyl complexes with coordination number 4.[172] The terminal bonds U-O_t of both outer-sphere complexes, ~181 pm, are longer than the corresponding bonds of solvated uranyl $[UO_2(H_2O)_5]^{2+}$, 177 pm (Table 8.1), which points even for the outer-sphere complex to a non-negligible surface interaction of the uranyl moiety.

8.2 Improved neutralization model

The program VASP provides accurate compensating corrections for charged unit cells only for cubic lattices.[151] This strategy was applied when optimizing the structures of the molecular species $[UO_2(H_2O)_5]^{2+}$ and H_3O^+ in simple cubic unit cells of size 1000×1000×1000 pm.

In nature one can assume local charge compensation in the case of a charged defect. Similarly, one can aim a charge neturalization by various compensation strategies. One of the possibilities to construct a neutral unit cell is deprotonation of surface hydroxyl groups. An inner-sphere complex of uranyl adsorbed at two O^- surface groups of the Al(o) (001) surface of kaolinite leads to a neutral unit cell, since the surface charge of -2 e and the adsorbate charge of +2 e compensate (see above, Section 8.1). The disadvantages of this method is that an uranyl complex adsorbed at partially deprotonated sites or adsorbed as monodentate species can not be neutralized easily in the same manner.

Models with neutral unit cells can be also created by invoking silanol surface defects which are formally created by hydrolysis.[173] This strategy leads to a more widely applicable

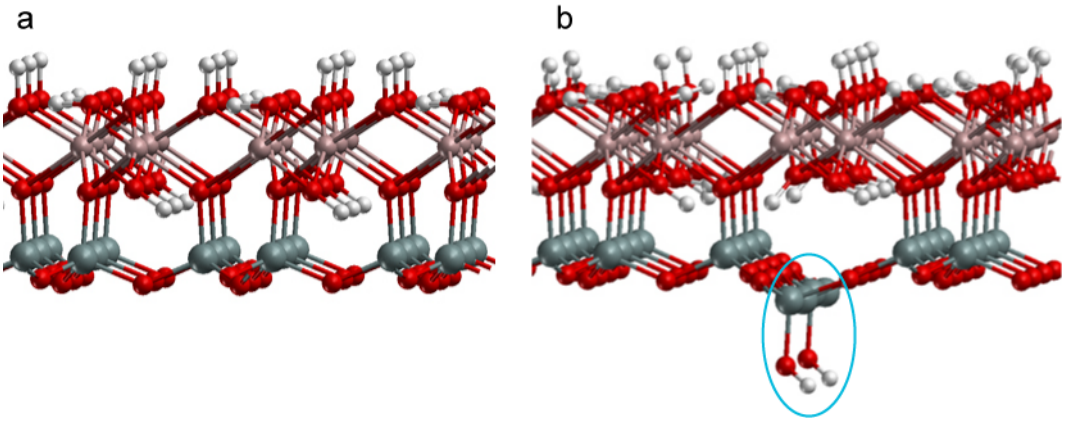

Figure 8.2. Ideal kaolinite surface slab model (a) and the slab with silanol defects (b) after hydrolysis of a Si-O bond.

concept. When modeling uranyl adsorption at the Si(t) kaolinite surface, two silanol groups are deprotonated at the side of the slab model opposite to the Al(o) surface to compensate for the charge of uranyl. To test this approach, protons were removed from different positions on the opposite side of the slab for a model of an inner-sphere bidentate complex of uranyl adsorbed at Si(t) kaolinite, which did not affect neither structural parameters, nor complex formation energies. Similarly, to compensate the charge of adsorption complexes at the (010) edge surface, protons are removed from SiOH groups present at the opposite side of the slab. AlOH and $AlOH_2$ groups, which are also present, were not used for these purposes. Thus, one and the same model cluster $[(HO)_3SiOH]^{50}$ can be used for the estimate of reprotonation energies. In this way the introduction of another cluster model to account for reprotonation energies of Al related edge face groups can be avoided.

For modeling uranyl adsorption at the Al(o) kaolinite surface, two silanol defects per (2 × 2) unit cell were introduced at the opposite Si(t) side of the slab model, which may be deprotonated when necessary for charge compensation. Such defects are formally constructed as follows. First, an inner-vertex O-Si bond is broken and the oxygen center is artificially saturated by hydrogen, to form an "inner" hydroxyl group. The Si center is moved outward to the surface and saturated by an OH group, which after deprotonation forms a silanolate moiety (Fig. 8.2). As indicated above, this results in a structure that is the result of a formal hydrolysis reaction.

Uranyl adsorbed as inner-sphere complex at the AlOO site of the basal Al(o) kaolinite surface was chosen to test the effect of the neutral silanol defect on adsorption. This complex was first optimized without defects present, then with two defects per (2 × 2) unit cell in different positions with respect to uranyl. Schematically these positions are shown in Fig. 8.3.

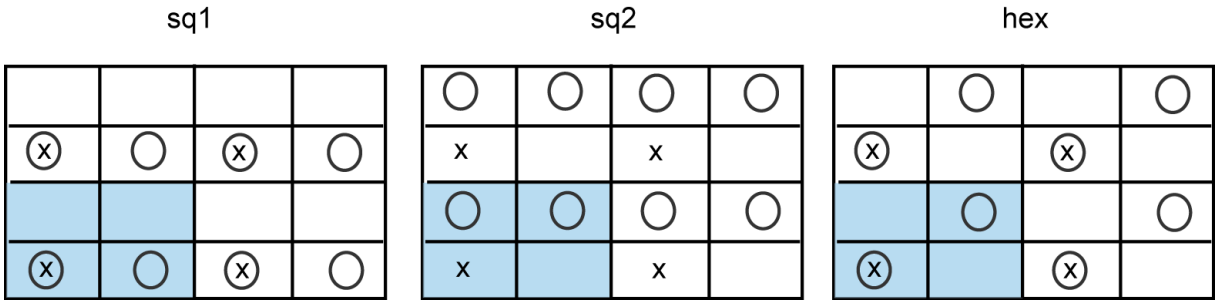

Figure 8.3. Schematic representation of positions of two silanol defects in the (2 × 2) unit cell (shaded) of a kaolinite slab. Adsorption complexes of uranyl at an AlOO site are indicated by a crosses, circles represent the positions of the defect groups: sq1 – square lattice of defect positions below the surface (uranyl is adsorbed directly above one of them); sq2 – square lattice of defect positions below the surface. Uranyl is adsorbed between two defects; hex – defects of a hexagonal lattice (uranyl adsorption above the defects).

The geometry details and formation energies of this complex for different positions of the silanol defects are given in Table 8.2. From the table one can see, that the defects affect the adsorption only marginally: uranyl bond distances U-O_t were changed by 1 pm at most; U-O_{surf} distances vary by up to 2 pm, while the U-Al distance changes only by 1 pm. The average equatorial U-O distance is not affected. The complex formation energies vary between 239 and 256 kJ mol^{-1}. This is only 6 % of the absolute value. Nevertheless, one should take into account, that this test was done for a neutral defect. Therefore, it gives only a lower estimate of effects to be expected due to introduction of charged defects. The defect positions according sq1 model (Fig. 8.3) was chosen for all subsequent simulations.

One more test was done for a monodentate adsorption complex of uranyl at the AlO site of the octahedral (001) surface of kaolinite. Since this complex needs only one deprotonated silanolate group for the unit cell neutralization, different defect SiOH groups, present on the opposite side of the slab, were deprotonated and optimization results are compared in the Table 8.3. All obtained geometry parameters differ by 2 pm at most, and the complex

Table 8.2. Main geometry parameters and formation energies (in kJ mol^{-1}) for an inner-sphere uranyl complex adsorbed at an AlOO site of Al(o) kaolinite with different positions of two silanol defects in the (2×2) unit cell in comparison to the ideal surface free of defects. For model designators see Fig. 8.3. Distances in pm.

Surface	U-O_t	U-O_{surf}	U-Al	U-O_{eq}	ΔE
ideal	184, 187	209, 221	307	237	256
sq1	184, 187	208, 223	308	237	248
sq2	184, 187	209, 222	308	237	239
hex	184, 186	210, 221	307	237	252

formation energy changes by 2 kJ mol^{-1} only, confirming the test with neutral SiOH defects (see above). Therefore, it does not play a crucial role, which defect group in the (2 × 2) unit cell is deprotonated: directly below the adsorbed uranyl or more distant (sq1, Fig. 8.3).

To check the stability of the defect charge after deprotonation, a charge distribution analysis was done for the surface with neutral SiOH defects and some models with deprotonated defects SiO^-. The charge distribution was characterized by means of a Bader charge analysis.[174] However, similar qualitative trends are expected when another charge analysis would be used. The definition of an atom in the Bader analysis is based purely on the electronic charge density. Bader uses zero flux surfaces between atoms to divide a cell around each atom. A zero flux surface is a two-dimensional surface on which the charge density is a minimum in the direction perpendicular to that surface. Typically, in molecular systems the charge density reaches a minimum between atoms and this is a natural way to define atoms in compounds. The Bader analysis is a rather an intuitive scheme for visualizing atoms in molecules, therefore, one should take the absolute numbers with care, and compare only similar systems.

The simplest model with a deprotonated SiO^- group was constructed by moving the proton from the silanol defect group to one of the surface AlOH groups to form an $AlOH_2^+$ surface group, which should be present in solution at acidic pH. The same model was also treated with one water ligand in the vicinity of SiO^- to simulate the effect of solvation, and therefore, screening of the negative charge. A two-layer surface model including the simple SiO^- defect was chosen for comparison. In all models applied the defect was frozen, while the water molecule, modeling "solvation", was relaxed. From the calculated atomic charges in Table 8.4 one can see that solvation–screening is not necessary to stabilize the charge on oxygen since the charge of the silanolate oxygen is hardly affected due by the presence of an aqua ligand. The two layer model looks worse, as the negative charge on oxygen decreases from 1.3 e for the one-layer model to 0.9 e for the two layer model. Thus, the charge analysis corroborates the stability of the neutralization defect, but shows that for more accurate studies a two-layer model should be applied.

Table 8.3. Main geometry parameters and formation energies (in kJ mol^{-1}) for an inner-sphere monodentate uranyl complex adsorbed at the AlO site with different positions of the deprotonated SiO^- defect group in the (2 × 2) unit cell. Distances in pm.

defect SiO^-	U-O_t	U-O_{surf}	U-Al	U-O_w	U-O_{eq}	ΔE
below UO_2^{2+}	181, 184	216	361	238, 250, 250, 260	237	46
far from UO_2^{2+}	181, 184	216	360	237, 248, 250, 260	237	44

Table 8.4. Bader charge analysis of the defect atoms for neutral (SiOH) and deprotonated (SiO^-) defects (in e) for one and two layer slab models of kaolinite, as well as for the defect solvated by one aqua ligand ($SiO^-{\cdot}H_2O$).

	Si	O	H
SiOH	+2.9	-1.9	+0.3
SiO^-	+2.7	-1.3	
$SiO^-{\cdot}H_2O$	+2.7	-1.2	
SiO^-, 2 layers	+2.8	-0.9	

In summary, when adsorption of UO_2^{2+} on the Si(t) (001) surface is studied, two protons from AlOH groups on the opposite side of the slab are removed for neutralization. When uranyl adsorption on the Al(o) (001) surface of kaolinite is studied, protons are removed from SiOH defects, introduced by formal hydrolysis, account for charge neutralization. In analogy, to neutralize the unit cell with adsorbed uranyl at the (010) edge kaolinite surface, protons are removed from SiOH groups on the opposite side of the slab.

8.3 Energy cycle

The following strategy was invoked to estimate the complex formation energy of uranyl at bare octahedral (001) and edge (010) kaolinite surfaces. One starts with the formal reaction of interest

$$S(OH)_2 + [UO_2(H_2O)_5]^{2+} \rightarrow [S(OH)_{2-n}(O)_n\text{–}UO_2(H_2O)_m]^{(2-n)+} + n\ H_3O^+ + (5\text{-}n\text{-}m)\ H_2O, \quad (8.4)$$

where $S(OH)_2$ denotes the substrate, with two hydroxyl groups explicitly indicated. These can be either surface OH groups or OH groups at silanol defects. n is the number of deprotonated surface OH groups and m counts the aqua ligands of the adsorbed uranyl. To achieve a strategy which demands only the calculation of systems with neutral unit cells, Eq. (8.4) was separated formally into two consecutive reactions:

$$S(OH)_2 + [UO_2(H_2O)_5]^{2+} \rightarrow S(O)_2\text{–}UO_2(H_2O)_m + 2\ H_3O^+ + (3\text{-}m)\ H_2O \quad (8.5)$$

$$S(O)_2\text{–}UO_2(H_2O)_m + (2\text{-}n)\ H_3O^+ \rightarrow [S(OH)_{2-n}(O)_n\text{–}UO_2(H_2O)_m]^{(2-n)+} + (2\text{-}n)\ H_2O \quad (8.6)$$

Eq. (8.5) represents the surface complexation of uranyl and implies the simultaneous charge compensating deprotonation of SiOH groups when appropriate. The corresponding reaction energy ΔE (8.5) can be calculated directly. Eq. (8.6) represents an eventual reprotonation of SiO^- groups on the "opposite" side of the slab. The corresponding reaction energy ΔE (8.6) is

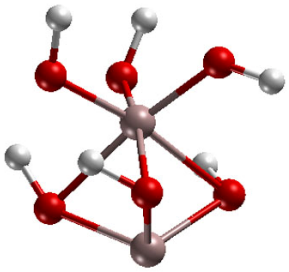

Figure 8.4. Cluster model $Al_2(OH)_6$ used to estimate deprotonation energies of aluminol groups.

proposed to be estimated as the energy ΔE (8.7) of reprotonation of a SiO^- moiety of a finite molecular model,

$$[Si(OH)_3O]^- + H_3O^+ \rightarrow Si(OH)_4 + H_2O, \qquad (8.7)$$

which can be determined from a molecular model by means of a VASP calculation. Thus, neglecting long-range solvation effects, the overall energy of complex formation of uranyl can be estimated as:

$$\Delta E\ (8.4) = \Delta E\ (8.5) + \Delta E\ (8.6) \approx \Delta E\ (8.5) + (2\text{-}n)\ \Delta E\ (8.7)\ . \qquad (8.8)$$

Solvation corrections to Eq. (8.4) change ΔE (8.4) into the corresponding complexation energy in solution, ΔE_{form}. These corrections are estimated as suggested previously[135] by assuming that the solvation energy of the clean surface equals that of a surface with adsorbate; this seems reasonable at low adsorbate concentrations. The solvation corrections for the molecular species in Eq. (8.4) were calculated by applying the COSMO solvation model as implemented in the program ParaGauss (Section 2.1) at -29 kJ mol^{-1} for H_2O, -382 kJ mol^{-1} for H_3O^+, and -811 kJ mol^{-1} for $[UO_2(H_2O)_5]^{2+}$.

To estimate the formation energy of adsorbed complexes of uranyl at the Si(t) kaolinite surface, the same type of model approach was applied, invoking where necessary deprotonation of hydroxyl groups of the Al(o) surface for charge compensation. Formally, analogous equations can be invoked, with the modification that the adsorption site does not comprise any surface OH groups. The reprotonation energy of Al(OH) groups, ΔE (8.9) = -1000 kJ mol^{-1} at the LDA level, is again estimated with a molecular model:

$$[Al_2(OH)_5O]^- + H_3O^+ \rightarrow Al_2(OH)_6 + H_2O \qquad (8.9)$$

The $Al_2(OH)_6$ cluster was modeled by an octahedrally coordinated Al atom, surrounded by three surface OH groups and three O atoms, fixed at their positions in the kaolinite slab model (Fig. 8.4). Then an Al atom and three protons were added to saturate dangling bonds of undercoordinated oxygens. The positions of these latter atoms were optimized. Thus, the rigid

part (cut out from the optimized Al(o) kaolinite slab) represents the surface, while the lower part of the cluster model is introduced for bond saturation, to preserve the coordination number of the surface Al atom, and to neutralize the cluster.

Then the formation energy of adsorption complex of uranyl on the Si(t) surface can be calculated as

$$\Delta E\ (8.4) \approx \Delta E\ (8.5) + 2\ \Delta E\ (8.9). \qquad (8.10)$$

Adding solvation corrections as before, one obtains ΔE_{form}.

The reprotonation energy of the silanol cluster ΔE (8.7) was estimated with different approaches. First, both clusters $Si(OH)_4$ and $Si(OH)_3O^-$ were relaxed at the LDA level and their total energies were determined from single point calculations at the PW91-GGA level. Second, optimization of both clusters was done at the PW91 level. As a third variant, single point PW91-GGA calculation of ΔE (8.7) without geometry relaxation of the cluster was done. The bond saturating protons of the cluster were fixed in the same direction as nearest Si neighbors in bulk kaolinite with the O-H bond lengths at 97 pm. The reprotonation energies calculated for all models are collected in Table 8.5. The choice of ΔE (8.7) will determine the absolute values of complex formation energies ΔE_{form} later on. Therefore, it is important to find arguments in favor of one or another cluster model. The deprotonation of the cluster leads to stabilization of $Si(OH)_3O^-$ species due to relaxation, which is not present in surface slab models, where Si and bottom O atoms are rigid. Thus, the concept of rigid cluster is reasonable to keep the models consistent.

The strategy of invoking defect deprotonation to construct a neutral unit cell can be compared to the one mentioned above (Section 8.1), which uses the deprotonation of the adsorbate for neutralization of the unit cell. The uranyl outer-sphere complex adsorbed at the Al(o) basal kaolinite surface was modeled in two different ways. The first way is to adsorb $[UO_2(H_2O)_3(OH)_2]^0$ instead of penta-aqua uranyl (Section 8.1). The second way is to adsorb $[UO_2(H_2O)_5]^{2+}$ and to neutralize the unit cell with the help of two deprotonated SiO^- defects on the opposite side of the slab. The energy required for adsorption in the former case was approximated as described in Section 8.1, in the latter case it was estimated according to

Table 8.5. Reprotonation energies of the silanol cluster estimated with different approaches. PW91-LDA(opt): optimization at the LDA level and single point calculation of the total energies with PW91. PW91(opt): optimization at the PW91 level. PW91(sp): single point calculations of rigid clusters. See text for details. Energies in kJ mol^{-1}.

	PW91-LDA(opt)	PW91(opt)	PW91(sp)
ΔE (8.7)	-764	-775	-848

Table 8.6. Structural and energetic parameters of outer-sphere complexes of uranyl on Al(o) (001) kaolinite, modeled by adsorption of $[UO_2(H_2O)_3(OH)_2]^0$ or $[UO_2(H_2O)_5]^{2+}$ in the presence of two silanolate defects. Distances in pm, energies in kJ mol^{-1}.

Complex	N	U-O_t	U-O_w	U-O_{OH}	U-O_{eq}	ΔE_{form}
$[UO_2(H_2O)_3(OH)_2]^0$	4	181, 181	233,[a] 257, 348	210, 222	247	-105
$[UO_2(H_2O)_5]^{2+}$	4	181, 182	229,[a] 241,[a] 250, 267, 280		247	-42[b] (-210)[c]

[a] Distance to aqua ligand between uranyl and the surface. [b] A relaxed cluster was used as molecular model for estimating the energy of reprotonation of the SiOH defect, ΔE (8.7) = -764 kJ mol^{-1}. [c] A rigid cluster was used as molecular model for estimating the energy of reprotonation of the SiOH defect, ΔE (8.7) = -848 kJ mol^{-1}.

model reaction Eq. 8.8. The geometry parameters and complex formation energies for these two models are collected in the Table 8.6. Both optimized structures are shown in Fig. 8.5.

Both models exhibit uranyl ions with effective coordination numbers 4, both yield rather short bonds to the aqua ligand directed to the kaolinite surface, and both show the same U-O_t and U-O_{eq} distances. Such an accordance in geometry is accidental because different adsorbate models are used, the free uranyl ion and uranyl dihydroxide, which can not be compared directly. The calculated formation energies for an outer-sphere adsorption complex of uranyl yield a remarkable difference. Adsorption of neutral dihydroxide of uranyl releases 105 kJ mol^{-1} of energy, while the model with charge compensating defects yields only 42 kJ mol^{-1}, when the relaxed silanol and silanolate clusters were used as molecular models to estimate the reprotonation energy of the defect (Eq. 8.7), but the formation energy of this complex is estimated at 210 kJ mol^{-1}, when rigid clusters are used. Compared to the more

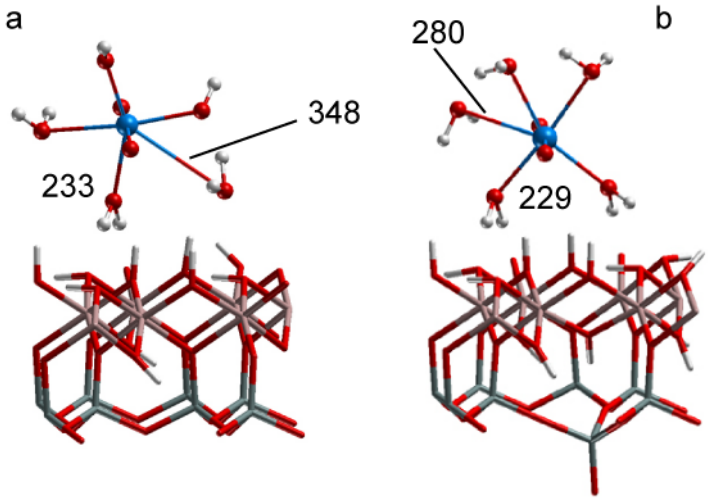

Figure 8.5. Adsorbed $[UO_2(H_2O)_3(OH)_2]^0$ at the Al(o) kaolinite surface (a) and the outer-sphere model of uranyl adsorbed at Al(o), modeled with the help of two silanolate defects (b).

approximate model employing uranyl dihydroxide, relaxation of the clusters underestimates the complex formation energy, while the rigid cluster approach seems to overestimate it. In contrast, the simpler model of dihydroxide adsorption misses the electrostatic attraction and thus should underestimate the formation energy as well, which makes the value of ΔE_{form} estimated with rigid cluster approach more reasonable. All three energies are exothermic, though they were calculated with rather different procedures and approximations. One has to accept that a trustworthy reference is difficult to achieve. In the following, rigid cluster models will be used to determine the reprotonation energy which implies a value ΔE (8.7) = -848 kJ mol^{-1} for estimating energies of the formation of adsorption complexes.

8.4 Improved models of uranyl adsorption at Al(o) kaolinite

To extend the study of uranyl adsorption at kaolinite surfaces the improved model approach with defects for charge neutralization of the unit cell was invoked as described in the preceding section. The introduction of defects allows one to investigate a variety of adsorption sites and their different deprotonation modes, as described in Section 7.3. All models for studying adsorption complexes of the Al octahedral (001) kaolinite surface are shown schematically in Fig. 7.4.

Geometry

Table 8.7 collects optimized geometry parameters as well as estimated formation energies ΔE_{form} for the various adsorption complexes studied. The main characteristics given in the table are (*i*) the uranyl U-O_t bond length, (*ii*) bond distance from U to surface oxygens U-O_{surf}, (*iii*) bond lengths to aqua ligands U-O_w, (*iv*) distances from U to Al or Si and (*v*) the average equatorial uranyl-ligand bond U-O_{eq}. The latter parameter is commonly available from EXAFS experiments. In the following, all uranyl adsorption complexes at uu sites of the Al(o) surface will be discussed fist; then differences between uu and ul sites will be addressed (see Section 7.3).

All but one adsorption complexes kept their chemical identity. The exception is a complex where uranyl is adsorbed at the lying AlOH group, which after convergence featured adsorbed uranyl monohydroxide. The proton of one of the aqua ligand of the first solvation shell of uranyl was adsorbed at the surface, forming an $AlOH_2^+$ surface group (see below for a detailed description).

As expected, the bidentate complex at two surface O^- groups is most strongly bound (Fig. 8.6a), as judged by geometrical features. It exhibits the longest U-O_t bond, 185 pm, and two short U-O_{surf} bonds, 208 and 223 pm, as well as the tightest shell of ligand bonds, with U-

Table 8.7. Calculated characteristic structural parameters and formation energies ΔE_{form} of inner-sphere and outer-sphere models of adsorption complexes of uranyl on basal (001) Al(o) surfaces of kaolinite. Experimental results are given for comparison. *m* = number of aqua ligands, *n* = number of deprotonated surface OH groups. N is the coordination number. Distances in pm, energies in kJ mol^{-1}.

	Site	(*m*,*n*)	site	N	U-O_t	U-O_{surf}	U-O_w	U-O_{eq}	U-Al	ΔE_{form}
bi	AlOO	(3,2)	uu	5	185	208, 223	251, 253, 253	237	308	248
	AlOOH	(3,1)	uu	5	184	210, 260	247, 248, 248	243	327	-46
	AlOHOH	(3,0)	uu	5	183	235, 259	242, 245, 251	246	346	-256
mono	AlO	(4,1)	u	5	183	216	238, 250, 250, 260	242	361	-42
	AlOH	(4,0)	u	5	183	244	236, 246, 248, 255	246	384	-323
bi	AlOO	(3,2)	ul	5	185	212, 217	253, 254, 254	238	305	248
	AlOOH	(3,1)	ul	5	184	212, 253	248, 248, 251	242	322	-50
	AlOHOH	(3,0)	ul	5	184	244, 250	244, 245, 247	246	337	-273
mono	AlO	(4,1)	l	5	183	217	239, 246, 251, 251	241	362	-63
	AlOH	(4,0)	l	5	183	240	240, 241, 253, 253	245	381	-218
outer		(5,0)		4	182	229, 241[a]	250, 267, 280	247		-210
outer,	H_2O	(5,0)		5	181	228[a]	241, 253, 254, 256	246		-223
	exp.[b]			5	180	228(×2)	248(×3)	240	330	
	exp.[c]			5	180			236-240	310 330	

[a] Bond lengths from U to aqua ligands oriented to the substrate surface.
[b] Ref. 22. [c] Ref. 25.

O_{eq} of 237 pm. One observes that the first coordination shell of uranyl splits, with two shorter bonds to the surface and three longer ones (252 pm on average) to the aqua ligands (Table 8.7). This complex also features the shortest U-Al distance, 308 pm, among all complexes examined. In comparison to the complexes adsorbed at AlOO, complexes representing uranyl adsorption at AlOOH or AlOHOH sites reflect in their geometry weaker adsorption bonds to the Al(o) surface. The U-O_t bond lengths decrease by 2 pm while the average length of ligand and surface U-O bonds, U-O_{eq}, increases by 9 pm (for adsorption at AlOHOH, Table 8.7). Also the U-Al distance increases from 308 pm for adsorption at AlOO to 327 pm for AlOOH and to 346 pm for AlOHOH. This trend is in line with the decreasing charge of the complexation site (-2 *e* for AlOO, -1 *e* for AlOOH, and 0 *e* for AlOHOH). The complex adsorbed at AlOOH still exhibits a rather short U-O_{surf} bond of 210 pm to the O^- group of the adsorption site. The second bond to the OH group at that site, 260 pm, is longer than the average distance U-O_w, 248 pm, to the aqua ligands. Bidentate complexation at two OH groups of the Al(o)-KL surface yields two relatively long U-O_{surf} bonds, 235 and 259 pm. Because of these long bond to the surface oxygen centers, adsorption at AlOOH and

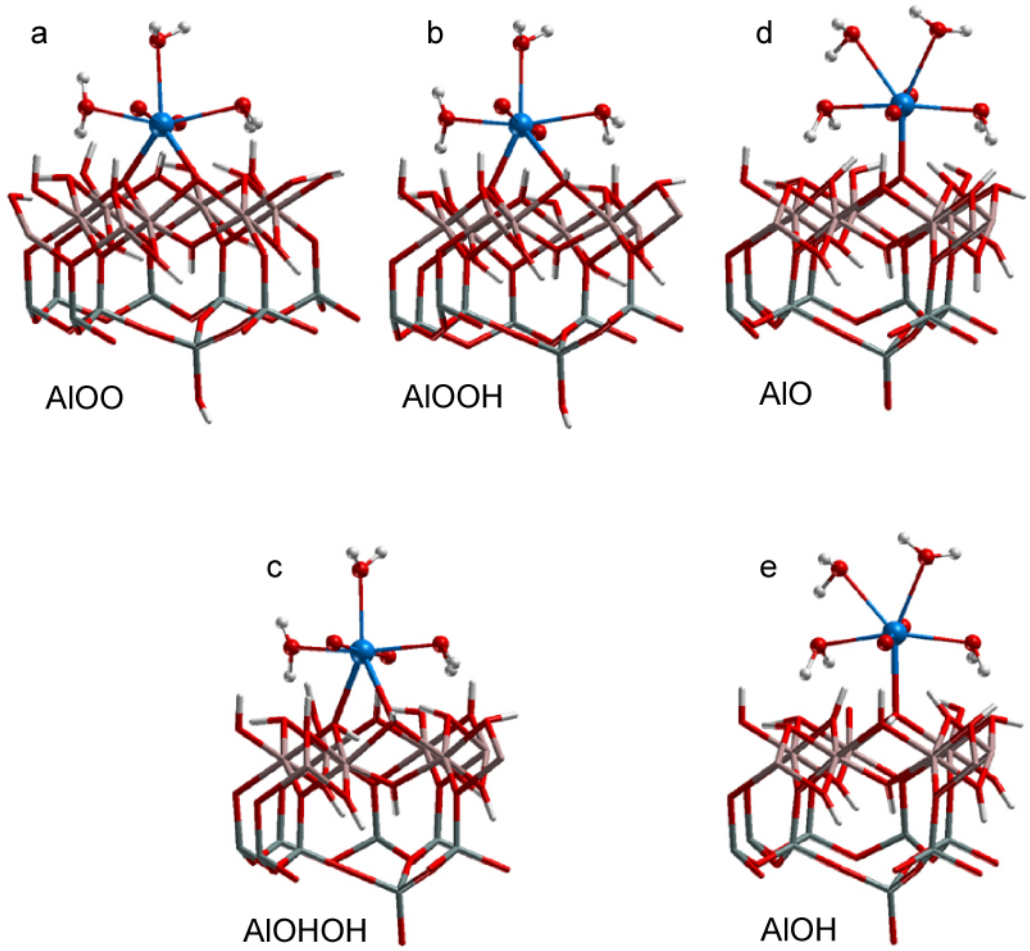

Figure 8.6. Optimized geometries of uranyl adsorption complexes on the Al(o) (001) surface of kaolinite: bidentate inner-sphere complexes adsorbed at (a) AlOO, (b) AlOOH, and (c) AlOHOH sites; monodentate inner-sphere complexes at (d) AlO and (e) AlOH sites.

AlOHOH may both be assigned as essentially monodentate complexes; the bonds U-O_{surf} of 260 pm length can already be regarded as rather weak. This interpretation is corroborated by the agreement with the U-O_{surf} bond lengths of monodentate complexes at AlO and AlOH sites, 216 and 244 pm, respectively, which are roughly similar in length to the shorter U-O_{surf} bonds of the bidentate complexes at AlOOH and AlOHOH sites (210 and 235 pm, respectively; Table 8.7).

The geometries of monodentate complexes differ from those of the corresponding bidentate complexes mainly by the U-Al distance, which amounts to 361 pm for uranyl adsorbed at AlO and 384 pm for AlOH. These values, at the limit of distances detectable by EXAFS, are about 35 pm longer than those for the corresponding bidentate adsorbed complexes at AlOOH and AlOHOH (327 pm and 346 pm, respectively) with the same type of deprotonation of the adsorption site. As for bidentate complexes, longer U-Al distances are obtained for adsorption at protonated sites (AlOHOH and AlOOH). Other characteristic

structural parameters vary mainly with the number of deprotonated surface hydroxyl groups that participate in the complex. The monodentate complex adsorbed at AlO and the bidentate complex adsorbed at AlOOH show similar values for U-O_t (AlO: 183 pm, AlOOH: 184 pm), the shortest U-O_{surf} distances (AlO: 216 pm, AlOOH: 210 pm), and somewhat longer U-O_{eq} values (AlO: 242 pm, AlOOH: 243 pm, Table 8.7). The same similarity is obtained for the bidentate complex adsorbed at AlOHOH and the corresponding monodentate complex adsorbed at AlOH: U-O_t calculated at 183 pm, U-O_{surf} at 235 and 244 pm, respectively, and U-O_{eq} at 246 pm.

The main difference between uranyl bidentate adsorption at uu and ul sites is that the two U-O_{surf} distances at the ul-sites are a bit closer to each other (uu AlOO: 208, 223 pm; ul AlOO: 212, 217 pm; uu AlOOH: 210, 260 pm; ul AlOOH: 212, 253 pm; uu AlOHOH: 235, 259 pm; ul AlOHOH: 244, 250 pm; Table 8.7). The bidentate complexes adsorbed at uu sites exhibit slightly longer U-Al distances (AlOO: 308 and 305 pm; AlOOH: 327 and 322 pm; AlOHOH: 346 and 337 pm, for uu and ul sites, respectively). The main geometrical parameters of the monodentate uranyl complexes adsorbed at "uOH" and "lOH" sites are very similar, differing at most 5 pm.

A model of an outer-sphere complex has been set up so that the solvated uranyl ion is in direct contact with the Al(o) surface via one of the aqua ligands of its first coordination sphere (Fig. 8.7a). As a result of optimization, one of the aqua ligands is loosely bound to the U center, with U-O_w = 280 pm, while two aqua ligands interact strongly with the surface (Fig. 8.7a). Due to bond competition between uranyl and the reactive (unsolvated) Al(o) surface, a "bidentate" outer-sphere complex is formed to which one can tentatively assign coordination number 4, because U-O_w of 280 pm is too long to be considered in the first solvation shell. To

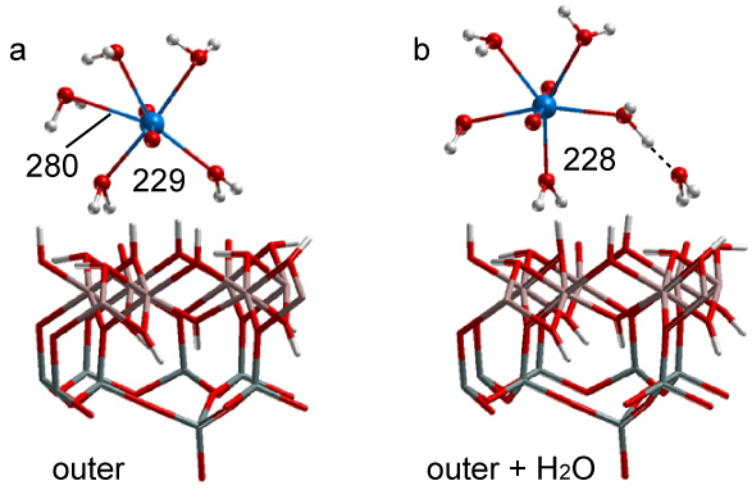

Figure 8.7. Optimized geometries of uranyl outer-sphere adsorption complexes on the Al(o) (001) surface of kaolinite.

further probe this bond competition, an additional water molecule was introduced in this model and positioned close to the uranyl adsorption site with the intent to reduce the (artificial) attraction of one of the aqua ligands of uranyl by the non-solvated surface OH-groups (Fig. 8.7b). Optimization of that model resulted in a five-coordinate "monodentate" outer-sphere complex of uranyl. Both models of outer-sphere complexes yield rather similar structure parameters, with the exception of a single long U-O_w contact of the "bidentate" outer-sphere complex, as discussed above. Compared to inner-sphere complexes, these models of outer-sphere complexes exhibit rather large U-O_{eq} values (bi: 247 pm, mono: 246 pm) and the shortest U-O_t bonds (bi: 182 pm, mono: 181 pm) which are still longer than for the solvated uranyl ion. U-Al distances are above 480 pm and thus outside the range detectable with EXAFS.[164] In contrast to common expectation,[121] both outer-sphere complexes exhibit a short U-O_w bond of about 230 pm to one aqua ligand oriented to the surface, while the other U-O_w bonds are in the range of 240–250 pm. Thus, the outer-sphere complexes examined exhibit a split first coordination shell; this also holds at the Si(t) surface (Section 8.5). From these results one can conclude that experimentally detected adsorbed species with geometric characteristics of solvated uranyl, classified as outer-sphere complexes,[121] should involve more than a single layer of water molecules between uranyl and the surface.

When evaluating all these results, one has to be aware of the fact that the surface model used overestimates the reactivity of the surface because screening due to solvation is lacking. Nevertheless, the qualitative structural differences between the two outer-sphere models examined and the experimental characterization of outer-sphere complexes as essentially identical to uranyl in aqueous medium may suggest to refer to species similar to these outer-sphere models with a separate terminology, perhaps as "semi-outer-sphere" complexes. Although their first solvation shell comprises the same *number* of solvent molecules, the *structure of the shell* reflects a surface interaction that exceeds mere electrostatic attraction.

Energetics

The energy needed for forming inner-sphere uranyl complexes at the neutral Al(o) surface reflects mainly the number of deprotonated surface groups of the adsorption site: AlOO > AlOOH ≈ AlO > AlOHOH ≈ AlOH (Table 8.7). Adsorption reaction of an uranyl dication at a doubly deprotonated site (AlOO) was calculated to be endothermic, by 248 kJ mol^{-1}, because that reaction energy includes the deprotonation of two surface OH groups. Note that the neutral Al(o) surface is used as a reference, which corresponds to a pH value of about 5.5.[127] The resulting complex formation energy is rather close to the value for uranyl adsorption at the Si(t) surface (239 kJ mol^{-1}, see Section 8.5) and in good agreement with the value ΔE_{form} = 256 kJ mol^{-1}, estimated for the same complex with the simpler adsorption model that does not

rely on silanol defects (Table 8.1, Section 8.1). This complex formation energy also does not depend on the reprotonation energy of the defect. All the others do. Thus, when the rigid cluster model is used, mono- or bidentate complexation at a singly deprotonated site (AlOOH, AlO) is exothermic, by ~ -48 kJ mol^{-1}.

For inner-sphere adsorption at AlOHOH and AlOH sites as well as outer-sphere complexation, uranyl adsorption was determined highly exothermic at the neutral Al(o) surface (Table 8.7), -323, -256, and -210 kJ mol^{-1} for monodentate (AlOH), bidentate (AlOHOH), and outer-sphere structures, respectively. Nevertheless, at higher pH, the Al(o) surface will be partially deprotonated, facilitating uranyl adsorption due to electrostatic attraction. Thus, the complex formation energy and thermodynamically accessible surface complexes will change with the change of reference and the formation of bidentate complexes bound to O^- surface groups will be preferred at sufficiently high pH conditions.

As for different adsorption sites (lying and upright surface hydroxyl groups), l sites should be more favorable than u sites since the OH group of the latter has to be bent to allow a direct U-OH bond. For example, uranyl bidentate adsorption at the AlOHOH site is preferred at the ul site, rather than at uu (-273 kJ mol^{-1} vs -256 kJ mol^{-1}), because during the optimization of the former only one OH group is bent parallel to the surface, while the latter needs two OH groups to be rotated. Adsorption at AlOO at both uu and ul sites is equally endothermic, at 248 kJ mol^{-1}, although in case of the uu AlOO site the deprotonation of two "upright" OH groups is involved. This should need less energy than the deprotonation of one "uOH" and one "lOH" group, since the latter is stabilized by hydrogen bonds (see Section 7.2). The formal reaction energies for the formation of adsorption complexes used in this thesis consist of the energy required to create the appropriate site and the adsorption energy of uranyl. The energy needed to create the site is the deprotonation energy of various surface groups involved. The deprotonation of lying OH groups seems to be more endothermic, due to the stabilization by two hydrogen bonds with neighboring surface groups, than the deprotonation of uOH which is not stabilized (Section 7.2, Figure 7.3). Therefore uu sites should be slightly more favorable than the corresponding ul sites. The only exception for this general trend is found for monodentate uranyl adsorption at u AlOH and l AlOH groups (Table 8.7). According to the above considerations, adsorption at the "lying" hydroxyl group should be more favorable. Nevertheless, adsorption at l AlOH releases 218 kJ mol^{-1} only, while adsorption at u AlOH is exothermic by 323 kJ mol^{-1}. The reason for this strong difference is found in chemically different adsorbed complexes. At the l AlOH site one of the aqua ligands of the first solvation shell of uranyl deprotonates during the optimization and the proton is attached to a surface hydroxyl group, probably due to the high reactivity of the

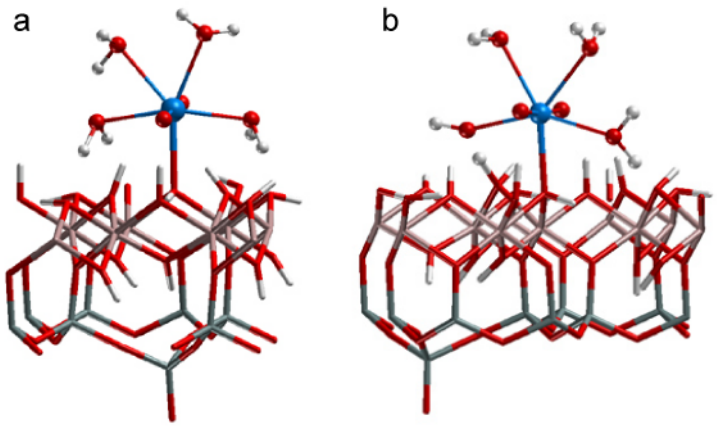

Figure 8.8. Optimized structures of uranyl monodentate inner-sphere complexes at AlOH sites of (001) kaolinite: (a) "upright" AlOH groups, (b) "lying" AlOH – one of the aqua ligands deprotonated.

surface and the lack of solvation, which could prevent such artificial hydrolysis reactions (Fig. 8.8).

The majority of experimental results on uranyl adsorption at mineral surfaces are interpreted as outer-sphere (at low pH)[20,21] or inner-sphere bidentate complexes (at higher pH).[20,25] In contrast to these assignments, the present model study yielded a monodentate uranyl complex adsorbed at AlOH on (001) Al(o) kaolinite as preferred adsorption complex at moderate pH values. As formation energies of adsorption complexes are always calculated with respect to the neutral surface of kaolinite, this result refers to a pH level of about pH_{ZPC} ~ 5.5.[127] At higher pH the Al(o) surface will be partially deprotonated, thus the reference surface will be changed. More deprotonated sites will be available, resulting in preferred adsorption of uranyl at the O^- surface groups at sufficiently high pH conditions. Also recall that in experiments edge surfaces (see below, Section 8.6) may play a crucial role in uranyl adsorption on kaolinite, while only basal surfaces have been investigated so far.

Charge distribution

Comparison of calculated uranyl adsorption complexes with experimental data shows a major discrepancy with respect to the U-O_t bond length (Table 8.7). While EXAFS yields the uranyl bonds of 180 pm for complexes assigned as inner-sphere, the calculations provide 183-185 pm for inner-sphere and 181-182 pm for outer-sphere complexes. Such an elongation can not be the consequence of incomplete solvation, since non-solvated uranyl complexes exhibit shorter uranyl bonds than solvated ones (see Section 9.4). One of the reasons may be strong charge transfer from the surface to uranyl. On the other hand, a redox reaction may occur at the surface, resulting in adsorbed U(V) instead of U(VI). To inspect these topics a charge analysis was carried out for several adsorbed uranyl complexes: two bidentate species

adsorbed at AlOO and AlOOH sites, a monodentate complex adsorbed at the AlO site, and the outer-sphere complexes of UO_2^{2+} and UO_2^{+} for comparison. The results obtained are shown in Table 8.8.

The uranyl moiety of the solvated uranyl (VI) ion exhibits the charge of 1.54 e, while solvated uranyl (V) shows the significantly lower charge of 0.39 e. The uranyl bond length changes from 177 pm for solvated U(VI) to 181 pm for U(V), which agrees with the decreasing charge of the uranyl dication. The outer-sphere complexes of uranyl (VI) and (V) adsorbed at the Al(o) kaolinite surface exhibit charges of 0.95 e and 0.17 e, respectively, of the UO_2 moiety. The charge of uranyl (VI) in the outer-sphere complex is reduced compared to the solvated ion by ~ 0.5 e, which results in an elongation of the uranyl bond of 5 pm (to 182 pm). Nevertheless, the calculated uranyl charge is still too high to be comparable to the characteristics of U(V). The outer-sphere complex of uranyl (V) also shows a reduced charge of UO_2, but the change is smaller than for U(VI), by ~0.2 e only. This complex also exhibits an elongated U-O_t bond length, 185 pm, which is 4 pm longer than in the solvated UO_2^{+} ion. However, the estimated charges may be affected by Kohn-Sham artifacts due to a remaining self-interaction which disfavors charge localization. To assess the effect of a potential artifact, the charge distribution of the outer-sphere complex of UO_2^{2+} as obtained with the DFT+U approach[175] was analyzed; the difference between effective on-site Coulomb and exchange interaction parameters was set to 1 eV.[176] The calculated charges are very similar to those shown in Table 8.8; differences amount to less than 0.02 e. Thus, charge transfer from the surface is present already for the outer-sphere uranyl complexes, although they do not have direct contact to the surface. The splitting of the first solvation shell of uranyl in the outer-sphere complex supports this idea (see above) as it demonstrates that the U-O_w bonds are

Table 8.8. Calculated Bader charges of inner-sphere and outer-sphere models of adsorption complexes of uranyl on basal (001) Al(o) surfaces of kaolinite. Results for free uranyl (VI) and (V) ions are given for comparison. In addition uranyl bond lengths as well as H-bonds to terminal uranyl oxygen atoms are given. Charge in e, distances in pm.

	Site	Charge					U-O_t	H-bonds
		U	O_t	O_{surf}	UO_2	SiO^-		
	UO_2^{2+}	3.17	-0.82, -0.81		1.54		177	
	UO_2^{+}	2.15	-0.93, -0.83		0.39		181	
outer	U(VI)	2.70	-0.88, -0.87		0.95	-1.07(×2)	182	-
	U(V)	1.46	-0.66, -0.63		0.17	-1.41	185	-
bi	AlOO	2.84	-0.96, -0.90	-1.48,-1.58	0.98		185	173(×3)
	AlOOH	2.80	-0.97, -0.93	-1.50	0.90	-1.58	184	182(×3)
mono	AlO	2.81	-0.96, -0.93	-1.58	0.92	-1.55	183	199(×2)

strongly affected by the substrate.

The adsorbed inner-sphere mono- and bidentate uranyl complexes of U(VI) yield a charge of uranyl of about 0.9 e, which is rather close to the uranyl charge of the outer-sphere complex of U(VI). Although the uranyl charges of the inner- and outer-sphere complexes of U(VI) are rather similar, the U-O_t bond lengths differ significantly. One observes from Table 8.8 that the overall positive charge on the uranium center is reduced for the complexes compared to the free uranyl ion (VI) and the outer-sphere complex; terminal oxygen centers gain slightly more negative charge. This may be traced back to hydrogen bonds formed with surface hydroxyl groups by the terminal oxygen centers of uranyl, adsorbed as inner-sphere complex at the Al(o) surface. These hydrogen bonds might be the second effect which contributes to the elongation of uranyl bonds. The average distances of hydrogen bonds between uranyl terminal oxygens and surface OH groups and their number are given in Table 8.8. As one can see, the bidentate complex at the AlOO site of (001) kaolinite exhibits three rather short hydrogen bonds of 173 pm and a uranyl bond length of 185 pm. The bidentate complex of uranyl at the partially deprotonated AlOOH site also shows three hydrogen bonds which are a little longer, 182 pm on average. This complex also exhibits a slightly shorter uranyl bond length of 184 pm. The monodentate complex includes only two weaker hydrogen bonds (O···H = 199 pm) of terminal uranyl oxygen atoms with surface OH groups, and concomitantly yields a shorter U-O_t bond of 183 pm. The outer-sphere complex does not show any hydrogen bonds of O_t atoms because they are situated too far from the surface OH groups (~ 300 pm).

As result of the charge analysis, adsorption of U(VI) is corroborated. A comparable amount of charge transfer from the surface is observed for all types of adsorption modes. Caused by the charge transfer, an elongation of the uranyl bond is calculated in case of outer-sphere adsorption. For the inner-sphere complexes H-bonds between surface hydroxyl groups and oxygen atoms of uranyl enhance this elongation.

8.5 Adsorption on Si(t) kaolinite

Uranyl adsorption on the Si(t) tetrahedral surface of kaolinite was modeled by two complexes: a bidentate inner- and an outer-sphere complex. To neutralize the unit cell, two protons were removed from the opposite side of the slab model. The results calculated for uranyl adsorption on the Si(t) surface are shown in Table 8.9. The U-O_t distance of both inner- and outer-sphere complexes is about the same, 178–179 pm, and close to the U-O_t bond length of the solvated uranyl ion, 177 pm. This result is in contrast to the Al(o) surface, where considerably longer U-O_t bonds of 181–185 pm have been calculated (Section 8.4). The shorter uranyl bonds at the Si(t) surface indicate a much weaker charge transfer for that

surface. In the bidentate inner-sphere complex adsorbed at the SiOO site of the Si(t) surface, the distance U-O_{eq}, calculated at 246 pm, is longer than U-O_{eq} obtained for a free uranyl aqua complex, 240 pm (Table 8.9). Bond distances to surface oxygen centers are similar, 246 and 249 pm. Interestingly, no appreciable "splitting" of the first coordination shell is obtained when uranyl adsorbs as inner-sphere complex: U-O distances vary between 241 and 249 pm, including those to surface O centers. The calculated results for the inner-sphere model complex A do not show a short equatorial U-O bond as determined in Ref. 22 (Table 8.9). Moreover, the calculated U-O_t bond is somewhat shorter than the experimental one of 180 pm, while U-O_{eq} at 246 pm is larger than the available distance from EXAFS measurements, 236–240 pm.[22,25] At variance, the optimized geometry of the inner-sphere complexes adsorbed at the SiOO site exhibits U-O_t and U-O_{eq} values that are very similar to those of the solvated uranyl ion (Table 8.9).

The outer-sphere complex exhibits an average value U-O_{eq} of 243 pm which is only 3 pm longer than calculated for a free uranyl aqua complex. On the other hand, the uranyl-oxygen distances U-O_w of different aqua ligands vary considerably, from 224 pm to 252 pm; curiously, the shortest distance was obtained for the ligand between uranyl and the support, just as for outer-sphere complexes at the Al(o) surface (Section 8.4). This aqua ligand of the outer-sphere complex is in direct contact with both the uranyl ion and the Si(t) surface. Due to moderately strong hydrogen bonds between this water molecule and surface oxygen centers (O···H = 157 and 148 pm) O-H bond distances are elongated from 98 pm in $[UO_2(H_2O)_5]^{2+}$ to 102 and 104 pm. As a rationalization, weak charge transfer from the surface to this water ligand may be invoked, which would strengthen the interaction with uranyl and lead to a

Table 8.9. Calculated characteristics of inner-sphere and outer-sphere models of adsorption complexes of uranyl on the basal Si(t) tetrahedral (001) surface of kaolinite. Results for the optimized solvated uranyl ion and experimental results are given for comparison. *M* = number of aqua ligands, *n* = number of deprotonated surface OH groups. Distances in pm, energies in kJ mol^{-1}.

Site	(*m*,*n*)	N	U-O_t	U-O_{surf}	U-O_w	U-O_{eq}	U-Al/Si	ΔE_{form}[a]
UO_2^{2+}		5	177			242		
SiOO	(3,0)	5	178	246, 249	241, 243, 249	246	320	239
outer	(5,0)	5	179	224[b]	243, 249, 251, 252	243		206
exp.[c]		5	180	228(×2)	248(×3)	240	330	
exp.[d]		5	180			236–240	310, 330	

[a] Formation energies for the adsorption complex, calculated according to the mechanism described in Section 8.3. [b] Bond length from U to aqua ligands oriented to the substrate surface. [c] Ref. 22. [d] Ref. 25.

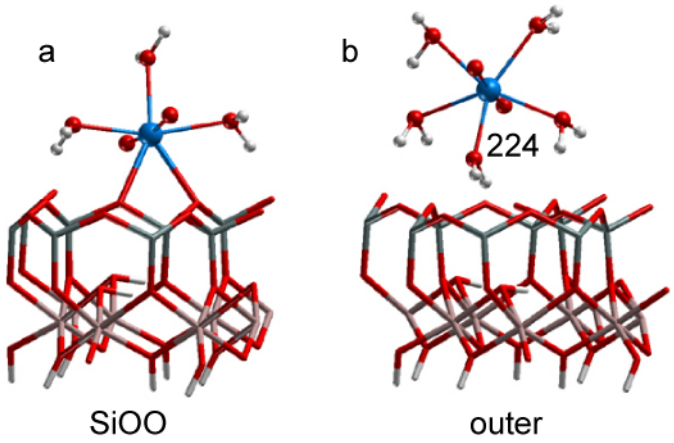

Figure 8.9. Optimized geometries of uranyl adsorption complexes on the kaolinite Si(t) (001) surface: (a) bidentate inner-sphere complex adsorbed at SiOO site, (b) outer-sphere complex.

shortening of that U-O_w bond, as for the Al(o) surface (Section 8.4). The other four aqua ligands exhibit common bond lengths U-O_w that vary from 243 to 252 pm (Table 8.9). A splitting of equatorial bond lengths of uranyl to aqua oxygen atoms appears for this model outer-sphere complex in contradiction to common assumptions;[121] recall that a similar result was calculated also for the outer-sphere species on Al(o) (Section 8.4).

At the Si(t)-KL surface, formation energies of both inner- and outer-sphere uranyl complexes are calculated positive (Table 8.9). Adsorption as inner-sphere complex is more endothermic than as outer-sphere complex, with energies of formation at 239 and 206 kJ mol^{-1}, respectively. These large values agree with the expectation that the Si(t) surface of kaolinite exhibits a low reactivity as long as charged defects are absent;[118,146] hence, adsorption of uranyl at this surface is unlikely in comparison to the Al(o) surface.

8.6 Adsorption of uranyl on bare (010) kaolinite surfaces

Uranyl surface complexes at two terminations of the (010) kaolinite surface as described in Section 7.5 and shown schematically in Figure 7.9 were optimized. Models of adsorption at AlOOH, AlOHOH, and AlOH-SiO sites with q=2 do not need a neutralization of the unit cell, while the model at the adsorption site AlOHOH (q=1), which is only singlydeprotonated, requires one negative charge on the opposite side of the slab for neutralization. This is achieved deprotonating one of the four SiOH groups which terminate the slab model at the "bulk" side.

Table 8.10 collects the main structural parameters for bidentate inner-sphere complexes adsorbed on the bare (010) kaolinite surface, as well as corresponding complexes adsorbed at AlOO and AlOOH sites on basal Al(o) kaolinite, which are chosen for comparison. Reaction

energies of the formation of adsorbed uranyl complexes including solvation corrections are calculated as described in Section 8.3.

Geometry parameters and energies of formation for all examined complexes of adsorption on S0 termination of (010) KL are presented in the middle part of Table 8.10. Note that three of the complexes, namely AlOOH, AlOHOH and AlOH-SiO (q=2), changed chemically during optimization: the adsorbed uranyl complex deprotonated to form uranyl monohydroxide, and the proton moved to a surface SiO^{-} or $AlOH^{-½}$ group, resulting in a SiOH or an $AlOH_2^{+½}$ group (Figure 8.10).

The complex adsorbed at the AlOOH site exhibits a similar U-O_t distance, 185 pm, as uranyl adsorbed on the (001) octahedral surface of kaolinite (Table 8.10). The uranyl complex adsorbed at the doubly deprotonated (q=2) AlOHOH and mixed AlOH-SiO sites show shorter uranyl bonds of 180-181 pm. Distances U-O_{surf} vary from 201 pm to 248 pm and both these extreme values are calculated for the complex adsorbed at AlOOH (q=2). Compared to uranyl adsorbed at the AlOO and AlOOH sites of (001) basal kaolinite, bonds from U to surface O^{-} and OH groups are shorter in case of the (010) surface. They are by ~ 15 pm shorter on average for U-O_{surf}(Al), 201 pm for S0 and 208 and 223 pm for the (001) surface, and by ~ 25 pm for U-OH(Al), which is 260 pm for the (001) surface and varies from 227 to 248 for the

Table 8.10. Calculated geometric and energetic characteristics of inner-sphere bidentate models of adsorption complexes of uranyl on two different terminations S0 and S1 of the edge (010) and the basal Al(o) (001) surfaces of kaolinite. Data for solvated uranyl as well as experimental results are given for comparison. q (in e) is the charge of the adsorption site. Distances in pm, energies in kJ mol^{-1}.

	Site	q	U-O_t	U-O_{surf}	U-Al	U-Si	U-O_w	U-O_{eq}	ΔE_{form}
	$UO_2(H_2O)_5^{2+}$		177					242	
(001), Al(o)	AlOO	2	185	208, 223	308		251, 253, 253	237	248
	AlOOH	1	184	210, 260	327		247, 248, 248	243	-46
(010), S0	AlOOH	2	185	201, 248	317		234[a], 251, 254	237	134
	AlOHOH	2	181	234, 236	321		237[a], 242, 251	240	141
	AlOH-SiO	2	180	230, 234	327	361	230[a], 250, 251	239	147
	AlOHOH	1	183	227, 238	333		248, 248, 253	243	-29
(010), S1	AlOOH	2	182	206, 227	316		253, 257, 258	240	214
	AlOHOH	2	181	231, 231	334		218[a], 253, 254	237	146
	AlOHOH	1	182	229, 230	332		250, 251, 257	243	-50
	UO_2^{2+}(aq.)[b]		177					241	
	exp.[c]		180	228(×2)	330		248(×3)	240	
	exp.[d]		180		310, 330			236–240	

[a] U-O_{OH} distance to the deprotonated aqua ligand where available.

[b] Ref. 53. [c] Ref. 22. [d] Ref. 25.

S0 termination of the (010) surface. This comparison points to a stronger binding of uranyl to the edge (010) surface compared to the basal Al(o) (001) surface.

Distances from U to Al atom vary from 317 to 333 pm for different complexes at the (010) S0 surface. The shortest one, 317 pm, is obtained for the site AlOOH. The corresponding adsorption site on the basal surface shows a U-Al distance of 327 pm. Models with doubly deprotonated (q=2) adsorption sites AlOHOH and AlOH-SiO exhibit U-Al distances of 321 pm and 327 pm, respectively. Adsorption at the singly deprotonated AlOHOH site yields a U-Al distance of 333 pm. The U-Si distance in the uranyl complex adsorbed at the mixed AlOH-SiO site amounts to 361 pm, which is much longer than the U-Al distances. Overall, all calculated U-Al distances are in the range of experimentally determined U-Al/Si distances, 310 and 330 pm.[24,25]

Despite all the differences in individual geometry parameters, the average equatorial distance U-O_{eq} varies only slightly for all four complexes, 237-243 pm. These values are inbetween U-O_{eq} values for sites AlOO (237 pm) and AlOOH (243 pm) for uranyl adsorbed on the basal kaolinite surface. The shortest U-O_{eq} of 237 pm corresponds to the complex at the AlOOH site with one deprotonated aqua ligand in the first solvation shell of uranyl. The complex at the AlOH-SiO site exhibits a similar U-O_{eq} distance of 239 pm. The longest U-O_{eq} distance of 243 pm is calculated for the site AlOHOH (q=1), the same U-O_{eq} was calculated for the site AlOOH at the basal surface. As a result, adsorption sites with q=2 for both (001) and S0 (010) surfaces exhibit U-O_{eq} values of 237–240 pm, which is in very good agreement with experimental values of 236–240 pm (Table 8.10).[22,25] Singly deprotonated adsorption sites at the Al(o) surface and termination S0 of the (010) surface feature slightly longer U-O_{eq} values, 243 pm, which nevertheless agree with experimental determinations of U-O_{eq}, if one takes the experimental uncertainty, ~4 pm, into account.[24,25]

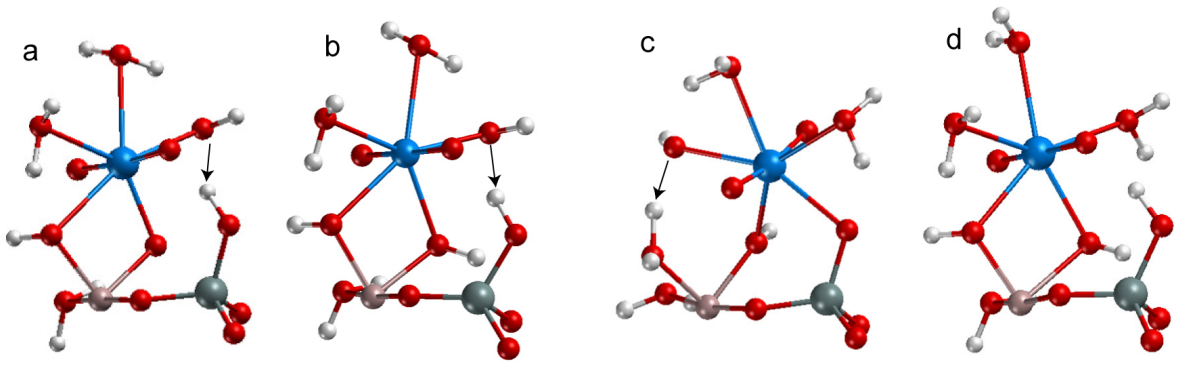

Figure 8.10. Optimized structures of uranyl inner-sphere complexes adsorbed in bidentate fashion on doubly deprotonated sites of the termination S0 of (010) kaolinite, q=2: (a) AlOOH, (b) AlOHOH, (c) AlOH-SiO; and on singly deprotonated sites, q=1, (d) AlOHOH.

The adsorption complex at the AlOOH site shows the longest U-O_t bond, 185 pm, which indicates the strongest interaction of uranyl with the surface. This complex exhibits also the smallest endothermicity of formation among all edge adsorption sites with q=2, 134 kJ mol^{-1}. The complex at the AlOH-SiO site exhibits a value ΔE_{form} = 147 kJ mol^{-1}, the least favorable among all the complexes adsorbed at the termination S0 of the (010) surface. All complexes adsorbed at the doubly deprotonated sites of termination S0 show formation energies considerably smaller than for the uranyl adsorption at the AlOO site on the basal (001) surface. This indicates a stronger adsorption of uranyl on the edge surface than on the basal Al(o) (001) surface. Model AlOHOH with q=1 and the complex at the singly deprotonated site AlOOH of the (001) surface have similar, exothermic energies of formation, -46 and -29 kJ mol^{-1}, respectively.

The second termination, S1, of the (010) kaolinite surface exhibits adsorption sites similar to termination S0: doubly deprotonated AlOOH and AlOHOH sites and a singly deprotonated AlOHOH site (Section 7.5). Geometry parameters of all examined complexes adsorbed at the S1 terminated (010) surface are given in the lower part of Table 8.10. Although both terminations, S0 and S1, as well as the adsorption sites, are rather similar, the results for S1 are different from those calculated for the termination S0. First of all, deprotonation of the aqua ligands from the first solvation shell of uranyl is obtained only for one adsorption complex – at the AlOHOH site (q=2) – which allows one to assume that the termination S1 is less reactive than termination S0. This is confirmed by the more endothermic energies for the formation of the adsorption complex formation of uranyl at termination S1 of the (010) surface (Table 8.10).

All three complexes adsorbed at termination S1 of the (010) surface exhibit similar uranyl U-O_t bond lengths, 181–182 pm. This result indicates a slightly weaker complexation

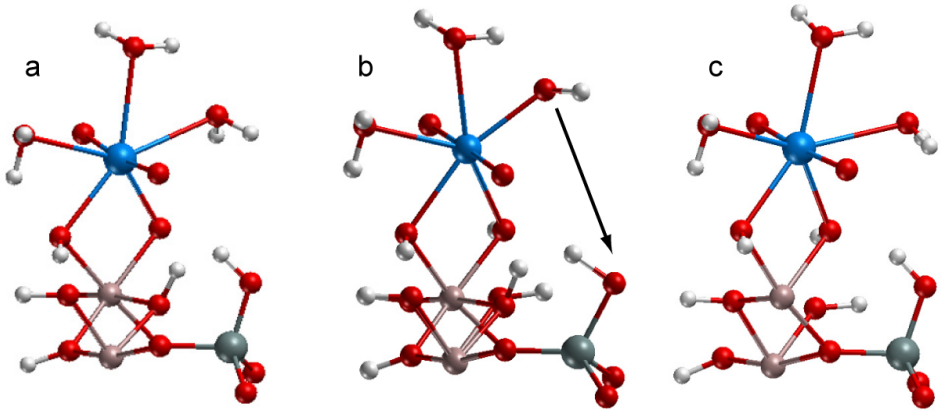

Figure 8.11. Optimized structures of uranyl inner-sphere complexes adsorbed in bidentate fashion on doubly deprotonated sites of the S1 termination of (010) kaolinite, q=2: (a) AlOOH, (b) AlOHOH; and on singly deprotonated sites, q=1, (c) AlOHOH.

of uranyl compared to termination S0 of the (010) surface. In turn, the energies of formation of uranyl inner-sphere complexes at the doubly deprotonated sites (q=2) at termination S1 of the (010) surface are more endothermic than those at termination S0; cf. 146–214 kJ mol^{-1} vs. 134-147 kJ mol^{-1}, respectively (Table 8.10). Distances U-O_{surf} vary from the shortest at site AlOOH, 206 pm, to 231 pm in the complex adsorbed at site AlOHOH (q=2). The shortest U-O_{surf} bond length, 206 pm, corresponds to the U-O_{surf}(Al) bond to the $O^{3/2-}$ surface group at the site AlOOH; U-O_{surf} bonds of ~230 pm (227 for AlOOH, 229–231 for both AlOHOH sites) relate to the U-OH(Al) bonds to the $OH^{1/2-}$ surface groups. Compared to uranyl adsorbed at the (001) basal surface of kaolinite, bonds from U to surface OH groups are ~30 pm shorter in case of termination S1 of the (010) surface, while U-O_{surf}(Al) bonds are only by 5 pm shorter: 206 pm for adsorption at termination S1 of the (010) surface and 213 pm on average for the Al(o) (001) surface (Table 8.10). The U-Al distances vary from 316 to 334 pm for S1, which is about the same range as for termination S0 (Table 8.10).

The average equatorial distances U-O_{eq} of uranyl complexes at doubly deprotonated sites (q=2) at termination S1 of the (010) surface, 237–240 pm, are comparable to those for termination S0 and to Al(o) (001) (237 pm). They all are in good agreement with experimental results of U-O_{eq}, ~240 pm.[22,25] Adsorption at the site AlOHOH (singly deprotonated) of termination S1 yields a relatively long U-O_{eq} value, 243 pm, just as for all other complexes at singly deprotonated sites (q=1) (Table 8.10).

8.7 Comparison of gas phase results to experiment

This section presents a preliminary comparison of computational results for "gas phase" models to available experimental data. Thus far, solvation of the surfaces, which may play a crucial role, was not accounted for. Therefore, a more detailed comparison of the obtained results with the experiment has to be postponed (Section 9.6), when also solvation is taken into account. Still, a comparison to experiment seems useful at this place.

The calculated results collected in Tables 8.7, 8.9 and 8.10 show that a short equatorial U-O bond of at most 230 pm, as seen in experiment,[22] is only obtainable at the basal Al(o) surface if a deprotonated hydroxyl group is involved in the adsorption site. Also, with the exception of the bidentate coordination to two O^- groups at the AlOO site, only a single short U-O bond is calculated. At site AlOO the two bonds to surface oxygen centers differ by 15 pm. As experimental results range from 310 to 330 pm for U-Al/Si contacts and from 234 to 240 pm for U-O_{eq} values,[24,25] one notes good agreement with the characteristics calculated for adsorption complexes at sites AlOOH (U-Al = 327 pm, U-O_{eq} = 243 pm) and AlOO (U-Al = 308 pm, U-O_{eq} = 237 pm). Whereas the partially deprotonated site AlOOH is in line with the experimental pH condition slightly above pH_{ZPC}, a two-fold depotonated site seems less

plausible, although deprotonation of surface hydroxyl groups is facilitated in the field of the uranyl ion.

Comparison of the optimized results for the (010) surface with available experimental data shows that most of the modeled complexes have similar characteristic geometrical parameters: U-O_{eq} distances fit the experimentally determined range of 236–240 (±4) pm (Table 8.10). The U-Al/Si distance was determined in an earlier experiment to 330 pm and in recent ones at 310 and 330 pm.[22,24,25] All models of inner-sphere bidentate uranyl complexes, adsorbed at doubly or singly deprotonated sites of the (010) edge surface and at the Al(o) basal surfaces yield U-Al distances between 308 and 334 pm. Experimentally determined U-Al/Si distances of 310 and 330 pm were derived by fitting a broad peak of the EXAFS spectrum between ~300 and 335 pm. In view of this finding, one can expect a rather broad distribution of these distances. In the earlier EXAFS experiment only one U-Al/Si distance of 330 pm was derived, also from a broad peak. Therefore, all optimized U-Al distances between 308 and 334 pm could contribute to the spectrum with different intensity. The uranyl bond lengths of the optimized complexes are 180–185 pm, which is comparable or longer than the experimental U-O_t bond length of 180±2 pm. Nevertheless, all optimized complexes of uranyl adsorbed at the edge (010) terminations, except one (AlOOH site at termination S0) show U-O_t bond lengths of 180–183 pm. This is in line with the experimental data, in view of the experimental uncertainty of 2 pm.

In summary, the main geometrical parameters of all complexes examined fit the experimental data. This allows one to assume, that many of these complexes may coexist at certain environmental conditions. On the other hand, one should not ignore the energy aspect. When analyzing the formation energies of adsorption complexes estimated by Eq. 8.4, the complexes fall into two groups. One group corresponds to a regime at lower pH and includes uranyl complexes at singly deprotonated sites (q=1). The other group comprises adsorbed complexes at doubly deprotonated sites (q=2) that represent conditions at higher pH, above pH_{ZPC}. Among the complexes of the first group the one most preferable by energy is the complex at site AlOHOH site of termination S1 of the (010) surface. In the group corresponding to elevated pH, bidentate complexes (q=2) at termination S0 of the (010) surface, adsorption at site AlOOH is energetically most favorable. Overall, from these simple gas phase surface models emerges the picture that adsorption complexes at edge surfaces are more favorable than complexes the basal surfaces.

9. Adsorption at solvated surfaces

Thus far only adsorption models of bare surfaces have been explored while solvation of the

surfaces was neglected. However, for realistic models, solvation is needed because it affects the charge distribution, the surface dipole layer, H-bonds, the polarization of the surface, etc. In quantum chemistry studies, solvation of complexes usually is accounted for by polarizable continuum models (PCM),[41,43,77] e.g. as done in the first part of the present thesis. For a better representation of solvation effects it is sometimes mandatory to include the water molecules of the first solvation shell in quantum chemical model, as done for uranyl complexes in the present work.[49,76,177] Another efficient approach to solvation is offered by hybrid methods (QM/MM) where one treats the complex of interest at a quantum chemical level and the solvent environment with a force field.[178] "*ab initio*" dynamical methods are appealing for studying systems with hundreds of atoms which include so many degrees of freedom that a statistical treatment is mandatory. With such an approach, solvation can explicitly by treated by including large amounts of water molecules in the model.[123,124,146] For example, *ab initio* MD methods (Car-Parinello MD) were used to study the solvation of edge surfaces of pyrophyllite.[123,124] Unfortunately *ab initio* MD methods are computationally demanding. In turn, systems of clays with solvation are easily treatable by MD (or Monte Carlo) methods that use an empirical force field approach. An MD study of uranyl adsorption on 2:1 aluminosilicates, with 240 water molecules per unit cell, ~4000 atoms in total, provides an example for this modeling strategy.[136,137] In the present thesis all adsorption models were explored at the QM level. Therefore solvation effects will also be estimated at that level. However, one needs to limit the number of (explicit) water molecules that are used for modeling solvation because these solvent molecules generate many weak interactions and considerably increase the time of calculation.

Thus, to estimate solvation effects on the adsorption of uranyl on kaolinite surfaces, adsorption complexes at surface models covered by a monolayer of water molecules were examined. A monolayer was chosen as a compromise because, on the one hand, it covers the surface completely and thus represents a first approximation of surface solvation; on the other hand, this approach keeps the models computationally treatable. First of all, bare surfaces of kaolinite covered by a water monolayer serve as a reference. Then, the same number of water molecules was included in the models to cover kaolinite surfaces together with adsorbed uranyl complexes. These models include a large number of weak interactions between water molecules and the surface, water-water interactions, and aqua ligands of the first solvation shell of uranyl interacting with other water molecules. Unfortunately, the LDA approach, thus far used in the present study of uranyl adsorption, does not describe well weak interactions.[156] Therefore, the subsequent models were treated with a GGA exchange-correlation functional (PW91).[155]

9.1 Comparison LDA versus GGA

GGA functionals are known to overestimate often bond lengths of heavy element compounds, although they predict energies very well.[89,179] To estimate the changes in geometric characteristics when switching from an LDA to a GGA approach, the investigated adsorption complexes on bare basal Al(o) and two terminations of (010) kaolinite surfaces were optimized also with the GGA PW91 functional. A comparison of LDA and GGA geometries and complex formation energies is shown in Table 9.1. First the main geometrical and energetic trends of GGA results for different adsorption complexes will be discussed; afterwards differences of these results to those obtained with the LDA approach will be commented on.

The main trends of structures of various adsorption complexes on the basal (001) surface did not change on going from an LDA to a GGA exchange-correlation functional. The most strongly bound complex on the basal Al(o) surface is uranyl adsorbed at the AlOO site; it shows two short U-O distances to the surface and three longer ones to the aqua ligands, together with the shortest U-Al distance of 311 pm in all PW91 calculations. Bidentate adsorption complexes at AlOOH and AlOHOH yield similar Al-O bonds as monodentate adsorbed species at AlO and AlOH sites, respectively. Outer-sphere models optimized at the GGA level still show a splitting of the bonds to the first ligand shell of uranyl. The aqua ligand positioned between the surface and the uranyl ion in outer-sphere complexes is attached to uranyl with a relatively short U-O_w bond, ~240 pm, while all other U-O_w contacts are in the range of 250–280 pm.

Complex formation energies are also affected by the change of the functional from LDA to GGA. Although the monodentate complex adsorbed at the AlOH site of the basal (001) surface is still the favored one (with the reference to the neutral surface) among all investigated inner-sphere complexes, its formation energy becomes close to that of the bidentate complex at the AlOHOH site (-269 kJ mol^{-1} and -253 kJ mol^{-1}, respectively). Furthermore, the outer-sphere complex which is modeled with an additional water ligand to balance the high surface reactivity ("outer + H_2O"), at the GGA level shows the lowest complex formation energy, -300 kJ mol^{-1}. Overall, all energies changed irregularly as joint result of two counteracting effects. For one, energies of structures optimized at the GGA level are lower than those obtained by the "single point" procedure GGA//LDA. On the other hand, the reprotonation energy of the defect is less exothermic (-755 vs -848 kJ mol^{-1}), when the full optimization is carried out at the GGA level (Table 8.5, Section 8.3).

Table 9.1. Calculated characteristics of inner-sphere and outer-sphere models of adsorption complexes of uranyl on bare basal (001) and edge (010) surfaces (terminations S0 and S1) of kaolinite optimized with LDA (VWN) and GGA (PW91) functionals. q (in e) is the charge of the adsorption site. Distances in pm, energies in kJ mol^{-1}.

	Site	q		U-O_t	U-O_{surf}	U-O_w	U-O_{eq}	U-Al	ΔE_{form} [a]
(001)	AlOO	2	LDA	185	208, 223	251, 253, 253	237	308	248
			GGA	187	213, 219	263, 266, 266	245	311	206
	AlOOH	1	LDA	184	210, 260	247, 248, 248	243	327	-46
			GGA	186	213, 264	257, 260, 262	251	332	-67
	AlOHOH	0	LDA	183	235, 259	242, 245, 251	246	346	-256
			GGA	186	243, 268	256, 256, 261	257	355	-253
	AlO	1	LDA	183	216	238, 250, 250, 260	242	361	-42
			GGA	184	224	251, 253, 270, 270	254	366	-50
	AlOH	0	LDA	183	244	236, 246, 248, 255	246	384	-323
			GGA	186	243	254, 258, 262, 267	257	398	-269
	outer	0	LDA	182	229[b]	241, 250, 267, 280[c]	247		-210
			GGA	184	242[b]	250, 256, 265, 281[c]	253		-237
	outer+H_2O	0	LDA	181	228[b]	241, 253, 254, 256	246		-223
			GGA	184	238[b]	249, 257, 263, 279	257		-300
(010) S0	AlOOH	2	LDA	185	201, 248	234,[d] 251, 254	237	317	134
			GGA	184	207, 239	261, 266, 266	248	320	202
			GGA [e]	187	204, 254	230,[d] 266, 268	244	322	140
	AlOHOH	2	LDA	181	234, 236	237, 242, 251	240	321	142
			GGA	183	241, 242	225,[d] 261, 263	246	336	181
	AlOH-SiO	2	LDA	180	230, 234	230,[d] 250, 251	239	327	147
			GGA	183	229, 237	249, 264, 267	249	347	210
			GGA [e]	182	235, 237	223,[d] 263, 269	245	338	190
	AlOHOH	1	LDA	183	227, 238	248, 248, 253	243	333	-29
			GGA	183	236, 242	255, 260, 263	251	342	-63
(010) S1	AlOOH	2	LDA	182	206, 227	253, 257, 258	240	316	214
			GGA	184	206, 234	265, 266, 266	247	324	210
	AlOHOH	2	LDA	181	231, 231	218,[d] 253, 254	237	334	146
			GGA	183	235, 237	220,[d] 264, 265	244	344	147
	AlOHOH	1	LDA	182	229, 230	250, 251, 257	243	332	-50
			GGA	183	233, 234	260, 261, 265	251	342	-50

[a] Complex formation energies are estimated as described in Section 8.3. [b] Bond lengths from U to aqua ligands oriented to the substrate surface. [c] The longest U-O_w distances were not included when calculating U-O_{eq}. [d] U-O bond length to a hydroxyl ligand, formed by aqua ligand deprotonation. [e] Adsorption of UO_2OH^+ for cases when deprotonation of aqua ligands of uranyl was obtained at the LDA level for solvated uranyl modeled as adsorbate.

Uranyl complexes adsorbed at the S1 (010) surface preserved their chemical identity when different exchange-correlation functionals are applied. The complex adsorbed at the AlOHOH (q = 2 e) site converged to an adsorbed UO_2OH^+ species, since one of the protons from an aqua ligand of the first solvation shell of uranyl moved to the surface. This happened for both optimization levels, LDA and GGA. Uranyl adsorbed at the AlOHOH (q = 1 e) site is the most favorable species at the LDA and at the GGA level for the S1 terminated (010) surface.

The properties of complexes adsorbed at the S0 termination of the (010) edge surface depend more strongly on the exchange-correlation functional applied. LDA and GGA models differ mainly in the deprotonation of an aqua ligand of the first solvation shell of adsorbed uranyl. At the LDA level of calculation, an aqua ligand deprotonates in complexes at the AlOOH and AlOH-SiO sites. This does not happen when these complexes are optimized with the GGA functional. Thus, besides effects on bond lengths and binding energies, the choice of the exchange-correlation functional can also qualitatively affect the adsorbed species, especially via a differences in the description of hydrogen bonds. In addition, for both these adsorption complexes, at the AlOOH and AlOH-SiO sites, modified starting geometries with deprotonated aqua ligands of uranyl were prepared and optimized at the GGA level; these calculations resulted in uranyl monohydroxide adsorbed at the S0 (010) surface. The corresponding geometrical results are also collected in Table 9.1 (marked as $PW91^d$).

Adsorption complexes of uranyl monohydroxide at the AlOOH and AlOH-SiO sites exhibit less endothermic formation energies than the corresponding adsorption complexes of uranyl (140 vs 202 kJ mol^{-1} for AlOOH, 190 vs 210 kJ mol^{-1} for AlOH-SiO). This indicates the high reactivity of the surface which tends to attract additional protons from the solvation shell of uranyl. Actually the deprotonation of an aqua ligand of uranyl, which should take place in solution at pH about 2–3, is facilitated in the presence of neighboring surface $AlOH^{-1/2}$ and SiO^- groups, due to their formal negative charges.

To compare the effect of the GGA approach on different adsorption complexes, Table 9.2 was set up: it focuses on differences with respect to LDA results (GGA–LDA). Only bidentate inner-sphere adsorption complexes on partially deprotonated sites are included in Table 9.2 since in the following only those will be studied, in accordance with experimental evidence. The basal octahedral surface of kaolinite yields two such complexes, adsorbed at the AlOO and AlOOH sites. In case of the two edge (010) terminations all the investigated complexes are of bidentate inner-sphere character, adsorbed at partially deprotonated sites with charges q = 1 e and q = 2 e. To estimate the pure GGA effect one should not compare minima optimized at the LDA and the GGA levels which correspond to different adsorbed species. Thus, only uranyl monohydroxide complexes adsorbed at the doubly deprotonated

AlOOH and AlOH-SiO sites of S0 were included in Table 9.2. The uranyl complexes adsorbed at the same sites, as optimized at the GGA level (Table 9.1), were excluded from comparison since they do not have a corresponding partner at the LDA level. In consequence, Table 9.2 contains nine adsorption complexes.

The uranyl bond lengths U-O_t of all adsorption complexes at partially deprotonated sites at kaolinite surfaces change by up to 2 pm on going from LDA to GGA results. Concomitantly, uranium bonds to surface oxygen centers elongate on average by 5 pm, commonly by 3–7 pm. In some cases the U-O_{surf} bond changes only marginally (all AlOOH sites), in others it is elongated by up to 9 pm (AlOHOH, q = 1 e, of S0). The average equatorial distance U-O_{eq} is elongated uniformly by 6–8 pm for all complexes inspected. The other parameters do not change uniformly, but exhibit different trends for each surface explored.

Geometrical parameters of the adsorbed bidentate complexes at the basal (001) Al(o) surface are uniformly affected by the change of the exchange-correlation functional. When changing from LDA to GGA results, the U-Al distance elongates at most by 5 pm, and the strongest elongation, 8 pm, is calculated for the parameter U-O_{eq}. This elongation compares very well with the elongation of U-O_{eq} by 7 pm for the solvated uranyl ion due to GGA effects (Table 9.2). At the GGA level, formation energies of adsorption complexes on the basal Al(o) kaolinite surface are lower by ~20 kJ mol^{-1} for the AlOOH site and by 40 kJ mol^{-1} for the AlOO site. When considering ΔE_{form}, one should not expect the usual trend of LDA to

Table 9.2. Calculated structural and energetic differences between LDA and GGA exchange-correlation functionals (Δ = GGA – LDA) for various adsorption sites of the Al(o) basal and different terminations of the edge (010) kaolinite surfaces. The charge q of the adsorption site is also shown. Distances in pm, energies in kJ mol^{-1}, charges in e.

Surface	Site	q	Adsorbate	U-O_t	U-O_{surf}	U-OH	U-O_{eq}	U-Al	ΔE_{form} [a]
$UO_2(H_2O)_5^{2+}$				1			7		
(001) Al(o)	AlOO	2	UO_2^{2+}	2	5, -4	-	8	3	-42
	AlOOH	1	UO_2^{2+}	2	3, 4	-	8	5	-21
(010) S0	AlOOH	2	UO_2OH^+	2	3, 6	-4	7	5	6
	AlOHOH	2	UO_2OH^+	2	7, 6	-12	6	15	39
	AlOH-SiO	2	UO_2OH^+	2	5, 4	-7	6	11	44
	AlOHOH	1	UO_2^{2+}	0	9, 4	-	8	9	-34
(010) S1	AlOOH	2	UO_2^{2+}	2	0, 7	-	7	8	-4
	AlOHOH	2	UO_2OH^+	2	4, 6	2	7	10	1
	AlOHOH	1	UO_2^{2+}	1	4, 1	-	8	10	0

[a] Complex formation energies are estimated as described in Section 8.3.

overestimate (binding) energies because formation energies represent *differences* of bond strengths (see Eq. 8.4).

The effects of the GGA functional on the structural parameters of uranyl complexes adsorbed on the S1 terminated (010) surface are similar to those for the basal Al(o) kaolinite surface. Yet, there is one exception: the U-Al distance is elongated by 8–10 pm in case of S1, compared to 3–5 pm in case of Al(o) surface. Complexes at the S1 terminated (010) surface are uniformly affected: U-O_{surf} bond lengths are slightly elongated (by 0–7 pm); also terminal U-O_t bonds increase (by 1–2 pm), while U-O_{eq} distances are elongated by 7–8 pm. Complex formation energies only marginally changed when GGA instead of LDA is applied to complexes at that surface (Table 9.2).

On the S0 surface mainly complexes of UO_2OH^+ were obtained. When UO_2^{2+} is adsorbed (AlOHOH site, q = 1 e), geometry changes due to the GGA functional are similar to those at the S1 terminated surface. In that case, complex formation is stabilized by 34 kJ mol^{-1}. A different situation arises when uranyl monohydroxide is formed during the optimization process. Seemingly, there is a bonding competition between the surface and the hydroxyl group, which is described differently at the LDA and GGA levels of theory. LDA structures of uranyl monohydroxide adsorbed on the S0 terminated (010) surface exhibit U-OH bond lengths of 230–235 pm, which are ~25 pm longer than typical U-OH bonds of uranyl monohydroxide (~210 pm).[103] GGA optimization of the same complexes yields shorter U-OH bonds, by 7–12 pm, resulting in U-OH bond lengths of ~225 pm. This is still longer (but only by 10 pm) than the corresponding value of the solvated UO_2OH^+ ion, 214 pm.[103] At the same time, U-O bonds to the surface and U-Al distances of these adsorption complexes elongate on average by 6 pm and 10 pm, respectively, as an effect of GGA. Thus, compared to LDA, at the GGA level, the bond to the hydroxyl ligand is stronger, while U-O_{surf} bonds get weaker. Complex formation is destabilized by ~40 kJ mol^{-1}.

As a result, the application of the GGA PW91 exchange-correlation functional for geometry optimization yields slight elongations (by ~2 pm) of the uranyl bonds and significant elongations, up to ~10 pm, of other characteristic distances (U-O, U-Al) compared to LDA. The U-O_{surf} bonds do not change uniformly, the U-OH bonds contract by up to 12 pm, U-O_{eq} values shorten by 7 pm on average for all complexes investigated. U-Al distances are elongated by up to 5 pm for adsorption on the basal Al(o) surface and by ~10 pm for the edge surfaces. GGA also stabilizes complex formation for uranyl, although not much (up to 40 kJ mol^{-1}), while a smaller driving force, by ~40 kJ mol^{-1}, is calculated for the formation of uranyl monohydroxide on the surfaces.

9.2 Solvation of basal (001) kaolinite surfaces

To explore approximately the main effects of solvation of kaolinite surfaces, a water monolayer was adsorbed. Thus, short-range solvation effects of the first "solvation layer" of the surface are explicitly accounted for.

The (2×2) supercell model of the basal (001) kaolinite surfaces has a surface area of ($2a \times 2b \times \sin\gamma$) = 1.88 nm^2, which was coated by 20 water molecules in order to cover the surface more or less completely. This number of water molecules was checked by optimizations of water films in smaller unit cells, starting from (1×1). The smallest unit cell, (1×1), was covered by 4 and 6 water molecules. Optimization showed that four water molecules do not fully cover the surface; their orientation depends on the periodic boundary conditions. On the other hand, the structure of the Al(o) surface covered by 6 water molecules shows some water molecules (1–2) which are not directly bound to the mineral surface; thus, these waters represent already part of a second solvation layer. Consequently, the (2×1) unit cell of Al(o) kaolinite was optimized with a coverage of 10 water molecules; for the (2×2) unit cell, a model with 20 water molecules was used to describe surface solvation. The resulting structures of the water overlayers of the (1×1) and (2×1) unit cells differed significantly, while the (2×2) unit cell exhibits approximately two units of the (2×1) model with small relaxation effects. Optimization overall yields an ordered structure for the water overlayer on the (001) Al(o) surface (Figure 9.1a), very similar to the results obtained in *ab initio* MD calculations (DFT, PW91, VASP).[146] That earlier study was carried out with a (2×1) unit cell with nine water molecules per unit cell adsorbed. To check whether the ordering of adsorbed water is a consequence of the boundary conditions of a too small unit cell, an additional calculation had been carried out for a (4×2) unit cell and 36 water molecules;[146] nevertheless, this test still led to the same ordered water overlayer. The structure of a water monolayer at the Al(o) kaolinite surface optimized in the present work is shown in Figure 9.1a. Each water molecule forms 3 H-bonds, to its neighbors as well as to the surface. There are two types of hydrogen bonds to the surface. One includes the surface oxygen as the electron donor and the water hydrogen as electron acceptor with an $O_{surf}\cdots H_w$ distance of ~170 pm, which is slightly longer than the value, 162 pm, obtained in the *ab initio* dynamical study (PW91-GGA).[146] The second type of hydrogen bond features water oxygen as an electron donor. It is weaker compared to the first one and therefore longer, 185–190 pm (180 pm in Ref. 146). Although the earlier study[146] and the present work were carried out at the same level of theory, the H-bond lengths are shorter in the former one. This likely is due to the fact that the number of water molecules per unit cell differed in the two investigations. Since the earlier study comprises a lower density of water molecules, water molecules on average are

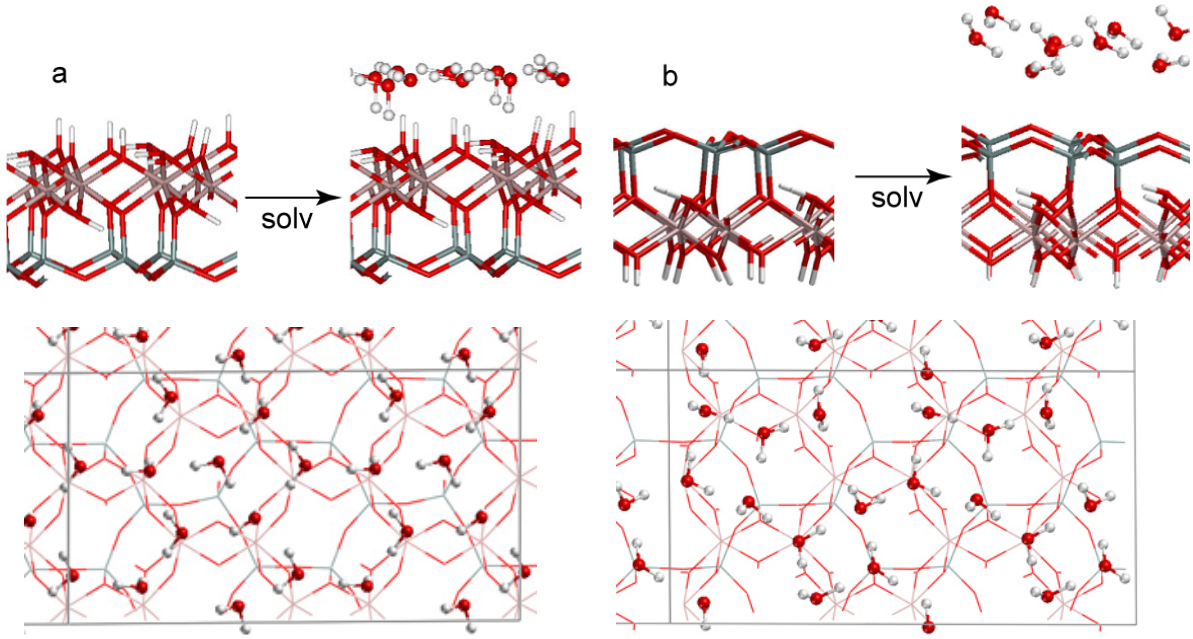

Figure 9.1. Models of the basal (001) kaolinite surfaces with a (2×2) unit cell, and their solvation by a water monolayer: (a) Al octahedral surface and (b) Si tetrahedral surface. Upper panels show side views, lower panels represent the top view of either solvated surface.

undercoordinated, leading to shorter hydrogen bonds. The hydrogen bond in the water dimer, optimized at the PW91-GGA level by VASP, exhibits an O···H bond length of 188 pm and a dimerization energy of 25 kJ mol^{-1}. Thus, the hydrogen bond of the first type is stronger than that in the water dimer since it is ~20 pm shorter. The second type of hydrogen bond between the surface and the water monolayer is comparable to that of a water dimer.

To estimate the solvation energy of the surface, or rather the energy of the hydrogen bonds of the water monolayer to the surface, the following formal reaction is introduced:

$$KL–(H_2O)_{20} \rightarrow KL(sp) + (H_2O)_{20}(sp) \qquad (9.1)$$

The kaolinite surface and the water monolayer were calculated separately without relaxation (sp – single point calculation). The interaction energy estimated in this way between the water layer and the surface amounts to 611 kJ mol^{-1}. The monolayer forms 20 hydrogen bonds per (2×2) unit cell to the surface. Eight of them are between surface O centers and water H atoms, $O_{surf}\cdots H_w$, and 12 are between water O centers and surface H atoms, $O_w\cdots H_{surf}$. Thus, the average energy of one H-bond is 30.5 kJ mol^{-1}, which is somewhat stronger than the H-bond in a water dimer (25 kJ mol^{-1}). Extending this approach, one can also approximately account for the H-bond energy between the water molecules in monolayer:

$$(H_2O)_{20}(sp) \rightarrow 20\ H_2O \qquad (9.2)$$

The energy needed to separate the adsorbed monolayer into 20 water molecules is estimated

Table 9.3. Comparison of average geometry parameters of bulk kaolinite, as well as of bare and solvated Al(o) basal kaolinite surfaces, optimized at the GGA level: Al-OH, O-H bond lengths, and H-bonds between layers in bulk kaolinite, and between the surface and the adsorbed water monolayer. Averaged characteristic bond lengths in pm.

Bond		bulk	Al(o)	Al(o) + 20 H_2O
Al-OH_{surf}	u	186	193	190
	l		194	197
O-H_{surf}	u	97	97	99
	l		98	98
H-bond		203		170-190

at 720 kJ mol^{-1}. Simple counting of the hydrogen bonds in the monolayer yields 30 H-bonds per unit cell. Thus, the average energy of H-bonds in the monolayer is 24 kJ mol^{-1}, very close to the value of 25 kJ mol^{-1} calculated for a water dimer.

Table 9.3 shows the average Al-OH and AlO-H bond lengths as well as the corresponding H-bonds for bulk kaolinite, the bare and the solvated surfaces. Other structural parameters were negligibly affected by solvation (less than 0.5 pm). Water molecules acting as electron donor in a hydrogen bond (longer bond of ~190 pm), form hydrogen bonds with "upright" surface hydroxyl groups. As a result, Al-uOH bonds shorten and AlO-H bonds are elongated by 2 pm on average. In case of the stronger H-bonds (170 pm) with the surface, with O_{surf} as electron donor, the surface O-H bond is not affected, while the Al-lOH bond is elongated by 3 pm, in contrast to the previous case.

The Si(t) kaolinite surface was solvated by the same amount of water molecules as the Al(o) surface. In contrast to results discussed above, no higher order of the water structure in the (2×2) unit cell was observed at that surface. The water molecules tend to form water clusters rather than to adsorb on the surface (Fig. 9.1b). As a result, structural changes for the Si(t) surface were found to be negligible (< 0.3 pm). The interaction energy between the surface and the water monolayer, estimated according to Eq. 9.1, in total is 25 kJ mol^{-1} per (2×2) unit cell only; this results indicates a very weak interaction only. Thus, these calculations showed the Si(t) surface of kaolinite not to be hydrophilic, while the Al(o) surface of kaolinite exhibits a strongly adsorbed water monolayer with an ordered structure, which might be a little disturbed when further layers of water are added.

9.3 Solvation of edge (010) kaolinite surfaces

The area of a (2×2) unit cell of the edge (010) surfaces of kaolinite is ($2a \times 2c \times \sin\beta$) = 1.5 nm^2, i.e. smaller than the surface area of the basal (2×2) unit cell. Unlike the more or less flat

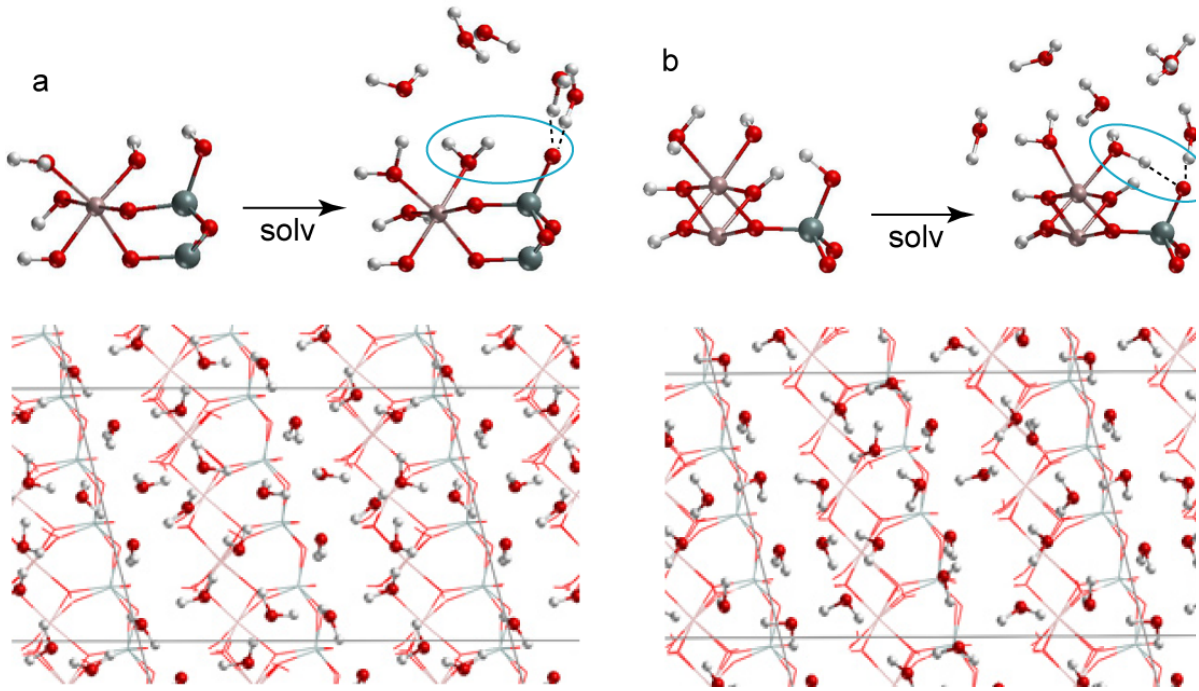

Figure 9.2. Reordering of the surface groups on the (010) kaolinite surfaces due to solvation. Formation of $AlOH_2^{+½}$-SiO^- instead of $AlOH^{-½}$-SiOH units for the terminations S0 (a) and S1 (b). Upper panels show side views, lower panels represent top views.

(001) surface, the (010) surfaces feature steps, hills, and holes; thus, the effective surface area is expected to be larger than the nominal value of 1.5 nm^2. To cover all the surface irregularities a larger amount of water molecules, 22, was used to solvate both terminations of the (010) kaolinite surface. In contrast to the solvation of the basal Al(o) surface, the water layers at the (010) terminations do not show any order. Also, a (2×2) optimization did not show any symmetry of the unit cell, thus a (2×2) overlayer was obtained. Some water molecules do not have direct contacts to the surface, but there also is no incipient second solvation layer. Thus, effectively, the water coverage represents a monolayer above that surface. Figures 9.2a and 9.2b illustrate the resulting structures of both terminations examined, S0 and S1, respectively. The main effect of solvation of the (010) kaolinite surfaces is the proton hopping of the SiOH groups to neighboring $AlOH^{-½}$ groups, forming a second $AlOH_2^{+½}$ group in the primitive unit cell and a negatively charged SiO^- group (Figure 9.2). A similar rearrangement of protons was observed in Car-Parinello MD simulations (DFT, PBE) of solvated edge surfaces of pyrophyllite.[123,124] Although proton hopping occurs at both terminations of the (010) surface, the resulting structures differ. Table 9.4 collects some characteristic structural parameters for both terminations, S0 and S1, of bare and solvated (010) surfaces. The first part of Table 9.4 shows Al-O and Si-O surface bond lengths. The $AlOH_2$ group, which already exists on the bare surface, exhibits an Al-O bond of 203 pm

Table 9.4. Calculated characteristic parameters of surface Al-O and Si-O groups, and of the (Al)HO···H···O(Si) fragment for bare and solvated S0 and S1 terminations of (010) kaolinite surfaces. Distances in pm, angles in degree.

bare surface	S0	S1	solvated surface	S0	S1
$Al\text{-}OH_2$	203	208	$Al\text{-}OH_2$	190	197
Al-OH	182	187		199	197
Si-OH	166	164	$Si\text{-}O^-$	162	161
AlHO···HOSi			$AlOH_2$···OSi		
O···H	219	165	O···H	299	153
∠O···H-O	133	161	∠O-H···O	135	167
O···O	289	264	O···O	374	255

for S0 and 208 pm for S1. Due to solvation these bonds shorten by ~10 pm. The Al-O bond of the AlOH surface group, which becomes $AlOH_2$ under solvation, correspondingly elongates from 182 pm to 199 pm for S0, and from 187 pm to 197 pm for S1. The Si-O bond is rather rigid; it changes at most by 4 pm and shortens after the proton moves to the neighboring aluminol group.

The second part of Table 9.4 collects the parameters of the hydrogen bonds in the fragment (Al)HO···H···O(Si). For the bare surface the proton is attached to the silanol group, resulting in the fragment (Al)HO···HO(Si). Solvation leads to a movement of the proton to the surface aluminol group and the fragment (Al)HOH···O(Si) is formed. Table 9.4 gives the main characteristics of the hydrogen bond, O···H distance, ∠O···H–O angle, and O···O distance. In case of the bare S0 termination of the (010) surface these three parameters are 219 pm, 133°, and 289 pm, respectively. After solvation, new surface groups appear, and the corresponding H-bond parameters are 299 pm, 135°, and 374 pm. The proton hopping at the S0 termination leads to an even weaker hydrogen bond compared to S1 termination. This hopping occurs via a water molecule of the solvation layer of the surface. The revealed SiO^- group is screened by two water molecules of the solvation overlayer with O···H distances of the hydrogen bonds at 150–170 pm (Fig. 9.2a).

For the bare S1 termination the three characteristic parameters in the surface fragment (Al)HO···HO(Si) are 165 pm, 161°, and 264 pm, respectively. After solvation they amount to 153 pm, 167°, and 255 pm. Upon solvation, the hydrogen bond becomes shorter, hence stronger, and the O···O distance shortens as well. In this case the proton moves directly along the surface without involving a water molecule (Fig. 9.2b). The SiO^- group at the S1 termination forms hydrogen bonds with one water molecule of the solvation overlayer (O···H = 150 pm) and one with the newly formed neighboring surface $AlOH_2$ group (O···H = 153

pm). For the (2×2) unit cell of the S1 termination of the (010) surface three out of four silanol groups transfer their protons to aluminol groups, while for the S0 terminated (010) surface all four silanol protons of the (2×2) unit cell move to form $AlOH_2$ surface groups. This different behavior is not unexpected since silanol groups at the bare S1 surface are already stabilized by a relatively strong hydrogen bond.

In analogy to the Al(o) surface (Section 9.2), one calculates the total interaction energy between the overlayer and the surface as

$$KL–(H_2O)_{22} \rightarrow KL(sp) + (H_2O)_{22}(sp) \quad (9.3)$$

This estimate of the adsorption energy of a water overlayer yields 1024 and 714 kJ mol^{-1} per (2×2) unit cell for S0 and S1, respectively. This difference is caused by different types of H-bonds to the surface. In case of S0 termination the resulting SiO^- groups are screened by water molecules of the solvation overlayer. This results in 7 bonds of the type $SiO^-\cdots HOH$ per (2×2) unit cell, which are rather strong (~160 pm). Because of the structural differences, SiO^- groups of the S1 termination are screened by neighboring surface $AlOH_2$ groups, resulting in a weaker interaction with the solvent. One can also estimate the energy of proton hopping along the surface by calculating single-point energies of the surface with the geometry fixed as obtained after solvation. The hopping energy is estimated from the formal reaction

$$KL \text{ (bare, relaxed)} \rightarrow KL \text{ (sp)} \quad (9.4)$$

The resulting proton hopping energies are 356 and 306 kJ mol^{-1} per (2×2) unit cell for S0 and S1, respectively. Since 4 and 3 protons are moved due to solvation on the S0 and S1 terminations, respectively, the values yield 89 and 102 kJ mol^{-1} for moving a single proton. One should keep in mind the rather rough procedure of reaching these estimates. In any case, the values corroborate the expectation that proton hopping should occur easily on the surface.

The observed rearrangement of the surface protons and the restructuring of the surface shows that solvation is important for a realistic description of edge surfaces. Consequently, it can affect the adsorption process and the type of the adsorption sites available.

9.4 Adsorption on solvated Al(o) kaolinite

From the results discussed above it is clear that the Si(t) surface of kaolinite hardly takes part in adsorption of metal cations, unless it is charged due to substitutions. Thus, the Si(t) surface was excluded from the investigation of uranyl adsorption at solvated kaolinite surfaces; only adsorption at the Al(o) basal and edge surfaces of kaolinite was studied. As discussed above (Section 9.2), solvation of the Al(o) surface was accounted for by an extended surface model with 20 water molecules per (2×2) unit cell, essentially representing the first solvent layer at that surface. As reference structure the solvated Al(o) surface of kaolinite was used (Section

Table 9.5. Calculated characteristics of bidentate inner-sphere and outer-sphere models of adsorption complexes of uranyl on solvated (001) Al(o) basal kaolinite. Data for solvated uranyl are given for comparison. Distances in pm, energies in kJ mol^{-1}.

Model	U-O_t	U-O_{surf}	U-Al	U-O_w	U-O_{eq}	ΔE_{form}
$UO_2(H_2O)_5^{2+}$	178				247	
bidenate						
AlOO	187	220, 222	315	247, 253, 271	243	218
AlOOH	187	220, 262	335	243, 246, 273	249	-67
AlOHOH	188	258, 265	362	239, 246, 261	254	-286
outer-sphere						
outer1, $1H_2O$[a]	187			239,[b] 250, 253, 261, 264	253	-237
outer2, $2H_2O$[a]	183			249, 251, 256, 260, 265	256	-226

[a] Number of the aqua ligands between the uranyl ion and the surface. [b] Distance to the aqua ligand oriented to the surface.

9.2). Initial structures for the optimization of uranyl adsorption complexes were modeled as follows: (*i*) the water monolayer was lifted above the surface, (*ii*) the adsorbate $UO_2(H_2O)_3^{2+}$ was added to the surface after pertinent deprotonation of surface sites to create various types of adsorption complexes, (*iii*) some water molecules (4 to 6) were shifted to form the cavity for uranyl in the solvation monolayer, (*iv*) the rearranged solvation layer was shifted down to cover the surface together with the adsorbate. In this way pure surface and adsorbate models are comparable, since the number of explicit water molecules in the model is preserved.

Table 9.5 collects the main structural parameters for bidentate uranyl inner-sphere and outer-sphere adsorption complexes on the Al(o) kaolinite surface, optimized at the PW91-GGA level with surface solvation effects included. Outer-sphere complexes will be discussed separately later in this section. For the investigated inner-sphere bidentate complexes Table 9.6 presents the geometry changes of the main characteristic distances due to the presence of the solvation overlayer. The U-O_t bonds were only weakly affected by solvation, the change in bond length due to solvation is at most 1–2 pm. While no change is observed for the strongly bound species at the AlOO site, the strongest change is calculated for the weakly bound complex at the protonated surface (AlOHOH). The bond distances from uranium to the surface are equilibrated and slightly elongated compared to the adsorption at the bare surface. In consequence, the U-Al distance is elongated by 3–7 pm when solvation is included in the model. However, the U-O_w distances to the aqua ligands are shortened by solvation, and, therefore, U-O_{eq} was calculated shorter by 2–3 pm. Note that the COSMO approach yields a similar shortening of U-O_{eq} for complexes of uranyl in solution.[76]

Overall, solvation does not change the general trends of properties of inner-sphere

complexes: U-Al and U-O_{eq} distances increase with the charge or degree of deprotonation of the adsorption site (Table 9.5). Formation energies for complexes adsorbed at the AlOO and AlOOH sites were only weakly affected by solvation. The propensity for forming a uranyl complex at the AlOHOH site was reduced by 33 kJ mol^{-1}. Thus, the main assumption of the earlier model approach (Section 8.4), namely that the solvation of the bare surface is approximately equivalent to the solvation of the surface with uranyl adsorbed, is essentially confirmed.

Next, outer-sphere complexes will be discussed. As first approximation, the outer-sphere complex at the solvated surface was modeled as described in the beginning of this section. This model is referred to as "outer1" in Table 9.5, since it corresponds to a geometry with a single aqua ligand between the uranyl ion and the surface (Fig. 9.3a). As for the outer-sphere complex without explicit surface solvation, also for this model with solvation there is one shorter U-O_w distance from uranium to an aqua ligand which is between uranyl and the surface, 239 pm, and longer distances, 250–264 pm, to the other four aqua ligands (Table 9.5). Thus, lack of solvation cannot held responsible for the splitting of the first solvation shell of uranyl outer-sphere complexes modeled at the bare surface.

To check the notion that, for an outer-sphere complex to resemble geometrically the free solvated uranyl ion, more than a single water molecule should be between uranyl and the surface, another model was constructed where solvated uranyl was attached to a monolayer of water adsorbed at the (001) Al(o) surface. Thus, the first solvation shell was assumed to be in contact with the first solvent monolayer which covers the Al(o) (001) surface; in that case,

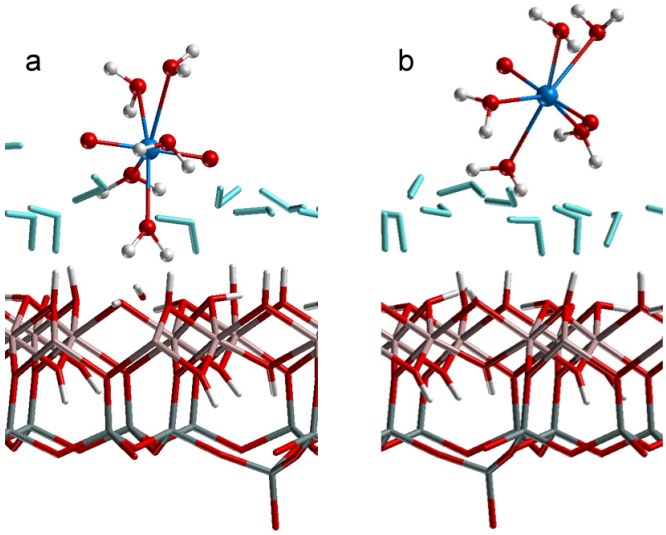

Figure 9.3. Outer-sphere adsorption complexes of uranyl at the (001) Al(o) kaolinite surface including surface solvation: (a) contact to the surface via a single aqua ligand; (b) contact to the surface via more than a single aqua ligand.

there are at least two water molecules between UO_2^{2+} and the surface (Fig. 9.3b). Optimized geometry parameters for that complex are given in Table 9.5 and the model is referred to as "outer2". This structure does not exhibit the strong splitting of U-O distances in the first ligand shell. All five U-O_w bonds are in the range of 249–265 pm. The U-O_t bond lengths differ for the two outer-sphere models due to the presence of hydrogen bonds between uranyl oxygen centers and water molecules in the model outer1; those bonds did not appear in model outer2. The U-O_t bond length of model outer1 is 187 pm, comparable to the U-O_t bond lengths of all other adsorbed solvated uranyl complexes (186–188 pm, Table 9.5), while model outer2 (Fig. 9.3b) features a U-O_t bond of 183 pm, comparable with U-O_t distances of outer-sphere models at the surface without solvation (Table 8.5).

As mentioned in Section 8.4 (charge distribution), U-O_t bonds in part elongate by hydrogen bonds that are formed between uranyl oxygen centers and neighboring surface hydroxyl groups, and in part due to charge donation from the surface. In the present case, water molecules of the solvation shell may form additional H-bonds with terminal O centers of uranyl. In the model outer1 uranyl is positioned inside the water monolayer, forming three H-bonds with water molecules with O···H bonds of 171, 186, and 205 pm. In model outer2 the uranyl terminal oxygen centers do not have the possibility to engage in any hydrogen bonds since uranyl is positioned above the solvation layer. Thus, the additional H-bonds in case of model outer1 allow one to rationalize the elongated U-O_t bonds compared to model outer2. The U-O_{eq} values of both models differ by 3 pm. The shorter one, 253 pm, corresponds to the model outer1, while the longer, 256 pm is calculated for model outer2. From Fig. 9.3 one can see that in model outer1 uranyl experiences the effect of a partial second solvation shell by aqua ligands which are supposed to solvate the kaolinite surface. In model outer2 uranyl is positioned higher above the surface since the uranyl ion and the surface were modeled to interact by their first solvation shells. Therefore, formally less members of the second solvation shell of uranyl are present in that model. As the contraction of U-O_{eq} due to surface solvation can be estimated by inner-sphere models to ~2 pm, one may roughly estimate second shell solvation effects for model outer2 also at 2 pm, which would shorten the U-O_{eq} value of model outer2 to 254 pm. This compares well to the U-O_{eq} value, 253 pm, calculated for the outer-sphere model complex with only one aqua ligand between the ion and the surface (outer1). Complex formation energies of both models are quite similar, -237 and -226 kJ mol^{-1} for models outer1 and outer2, respectively. These model calculations confirm the earlier assumption that more than one water molecule should be present between the adsorbed uranyl ion and the surface to reproduce the experimentally observed outer-sphere species. Thus, the experimentally detected outer-sphere complexes[20] may be assigned to species with at least two layers of water molecules between the surface and uranyl.

As one can see form this section, the adsorption models of uranyl on the well-defined, stable basal Al(o) surface are reasonable even without inclusion of surface solvation. The main geometry characteristics of bidentate inner-sphere complexes at the solvated surface exhibit the same trends as on the bare surface. However, for the outer-sphere models addition of surface solvation improves the results qualitatively. It also leads to an improved interpretation of the experimental observations, as will be seen in Section 9.6.

9.5 Adsorption on solvated (010) edge surfaces

Adsorption sites

As discussed above, surface solvation changes the (010) edge surfaces (Section 9.3). Instead of surface groups $AlOH^{-½}$ and SiOH, as on the bare surfaces, one obtains $AlOH_2^{+½}$ and negatively charged SiO^- groups due to the interaction with the solvent (Section 9.3). One should take into account these changes, when uranyl adsorption on edge kaolinite surfaces is

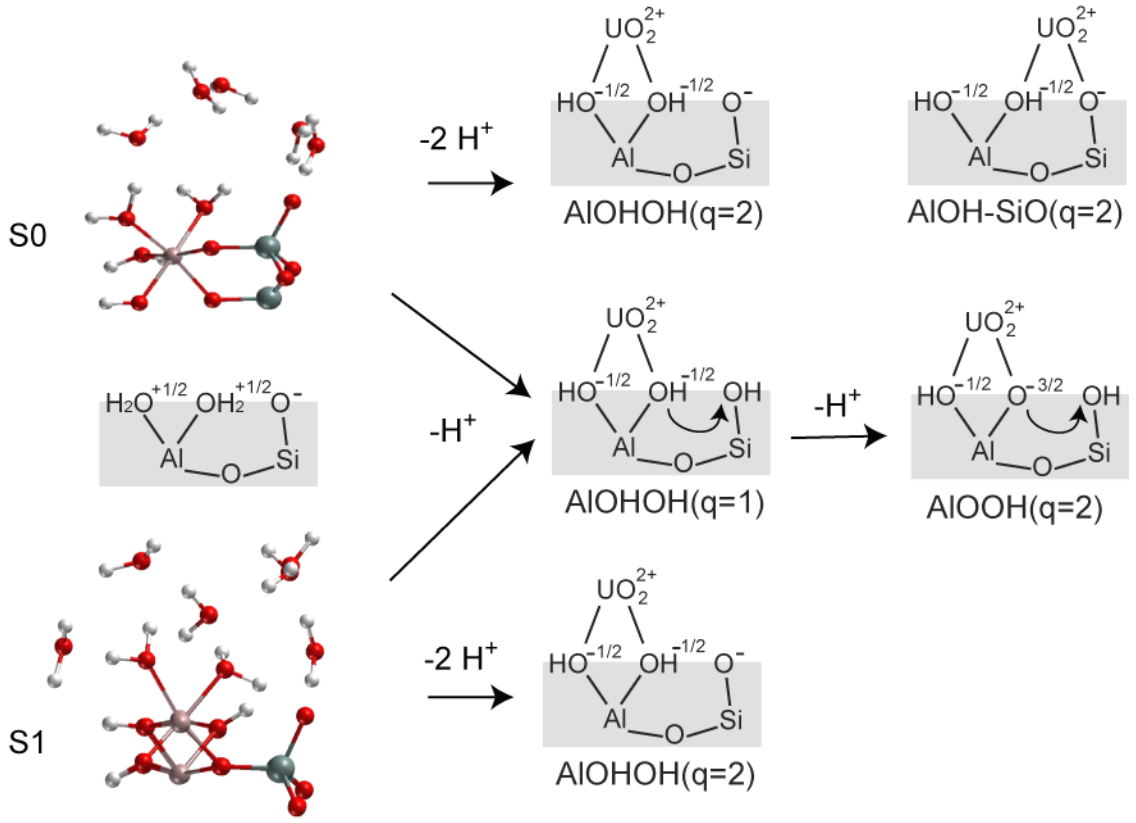

Figure 9.4. Scheme for preparing various sites for uranyl adsorption on solvated (010) surfaces. The first and the third rows describe doubly deprotonated AlOHOH and AlOH-SiO sites, created by removing a proton each from two surface $AlOH_2$ groups. The second row represents the formation of the singly deprotonated AlOHOH site by removing one proton and movement of another proton to a neighboring SiO group to create SiOH. The AlOOH site was created from the previous one by removing the second proton from one of the AlOH groups.

considered. Nevertheless, for consistency similar adsorption sites as on the bare (010) surface were modeled. Figure 9.4 sketches the procedure of the preparation of adsorption sites on the (010) surface of kaolinite. To form doubly deprotonated AlOHOH and AlOH-SiO sites two surface $AlOH_2$ groups were deprotonated (first and third rows in Fig. 9.4). To construct the alternative singly deprotonated AlOHOH (q = 1 e) site one proton was removed from an $AlOH_2$ group, while the proton of the second $AlOH_2$ group was moved to the neighboring silanolate group to create the second AlOH group of the site (second row in Fig. 9.4). Such a rearrangement of the surface protons is reasonable, since proton hopping between neighboring AlOH and SiOH surface groups is expected to be dynamic. In addition, it should be facilitated in the electric field of the uranyl dication. An AlOOH site (q = 2 e) was created from the site AlOHOH (q = 1 e) by removing a proton from one of the aluminol groups (Fig. 9.4).

Adsorption on the solvated S0 (010) surface

Adsorption complexes of uranyl at the solvated S0 termination of the (010) kaolinite surface are shown in Figure 9.5. Table 9.7 collects the geometry parameters and formation energies of the examined complexes (solv→ads block). Due to surface solvation the adsorbed species were changed. For all adsorption complexes at the S0 (010) surface one of the aqua ligands of uranyl is deprotonated, the proton being transferred to the surface. As a result, one obtains adsorbed hydroxylated species $[UO_2(OH)]^+$. In case of adsorption at aluminol sites one of the neighboring silanolate groups is protonated (Fig. 9.5a, b and d), while for the mixed site AlOH-SiO a neighboring aluminol AlOH group changes to $AlOH_2$ (Fig. 9.5c). Uranyl adsorption at the AlOHOH site (q = 2 e) leads to two deprotonated aqua ligands. In this reaction the nearest SiO^- group and another SiO^- group of the neighboring kaolinite layer are protonated. One of the protons first moves to a neighboring water molecule, and then one of the protons of the resulting H_3O^+ species is transferred to the silanolate group (see arrows in Fig. 9.5b). Overall, a neutral $UO_2(OH)_2$ moiety is adsorbed at the AlOHOH site with the charge q = 2 e.

The (2×2) unit cell of the solvated S0 (010) surface shows four negatively charged SiO^- and eight $AlOH_2^{+½}$ surface groups. Except for the changes (protonation of the silanolate group on the surface) due to adsorption of uranyl, as described above, all other $AlOH_2$–SiO fragments of the solvated S0 (010) surface are preserved, in contrast to the findings for the S1 termination (see below).

As mentioned above, geometry parameters of adsorbed complexes change significantly due to solvation (Table 9.7). In the following solvated adsorption complexes will be compared only with chemically identical complexes adsorbed on the bare S0 (010) surface. A comparison is meaningful only if on both surfaces, bare and solvated, the same species is

Table 9.7. Calculated structural and energetic characteristics of inner-sphere models of adsorption complexes of uranyl on the bare and solvated S0 termination of the (010) surface of kaolinite. Distances in pm, energies in kJ mol^{-1}. q (in e) is the charge of the adsorption site.

Site	q	U-O_t	U-O_{surf}	U-Al	U-Si	U-OH[a]	U-O_w	U-O_{eq}	ΔE_{form}	$\Delta^2 E_{form}$[b]
bare										
AlOOH	2	187	204, 254	322		230	266, 268	244	140	
AlOHOH	2	183	241, 242	336		225	261, 263	246	181	
AlOH-SiO	2	182	235, 237	373	338	223	263, 269	245	190	
AlOHOH	1	183	236, 242	342			255, 260, 263	251	-63	
solv→ads										
AlOOH	2	188	204, 258	332		230	250, 285	246	111	-29
AlOHOH	2	185	236, 254	351		223, 229	275	243	79	-102
AlOH-SiO	2	186	228, 257	397	344	219	247, 254	241	164	-26
AlOHOH	1	187	235, 259	355		229	244, 272	248	-159	-96
ads→solv										
AlOOH	2	188	204, 260	333		229	252, 285	246	105	-35
AlOHOH	2	183	230, 251	352		222	245, 271	244	118	-63
AlOH-SiO	2	186	226, 259	398	344	221	245, 254	241	172	-18
AlOHOH	1	187	235, 259	355		228	245, 272	248	-164	-101

[a] U-O_{OH} distance to OH ligands arising due to deprotonated aqua ligands. [b] Stabilization effect due to surface solvation.

obtained, either UO_2^{2+} or $[UO_2(OH)]^+$. Elongation of U-O_t by 2–4 pm due to solvation for the complexes adsorbed at the S0 terminated (010) kaolinite surface renders uranyl bonds (185–188 pm) comparable to those of adsorption complexes at the solvated basal Al(o) surface (~187 pm) although uranyl is not hydrolyzed at that surface. One of the two U-O_{surf} bonds to the surface is elongated due to solvation, while the second is slightly shortened (Table 9.7). As a result, all adsorption complexes at the solvated surface exhibit one shorter U-O_{surf} bond (204 pm for the site AlOOH and 228–236 pm for others) and one longer U-O_{surf} bond of about 254–259 pm. The latter is in the range of U-O_w distances, 244–285 pm. The shorter U-O_{surf} bonds are only a little longer than the U-OH bonds which were slightly shortened by solvation, to 219–230 pm. This trend is opposite to the behavior of the solvated ion $[UO_2(OH)]^+$, which yields elongated U-OH bonds (by 2 pm) when the COSMO solvation model is applied.[103] Thus, the U-O distances in the equatorial plane of uranyl show a splitting into two shorter ones, 221–235 pm (or three for the site AlOHOH), and three longer ones (or two for the site AlOHOH) of more than 245 pm. The shorter distances correspond to one U-O_{surf} bond and one (or two) U-OH bonds, the longer distances correspond to one U-O_{surf} bond and two (or one) U-O_w bonds. Such a splitting is in agreement with experimental findings[18,20,22,180] and is possible due to the presence of one or several hydroxyl groups as ligands of uranyl. Nonetheless, since U-O_{surf} distances are similar to U-OH bond lengths (~230 pm), experimentally they can not be easily distinguished. In this context, also note that

U-O_{surf} bonds do not show a characteristic lengths which may be identified unequivocally by EXAFS. Average equatorial U-O_{eq} distances decrease due to solvation, as expected,[73] yielding values of 241–248 pm, which are quite comparable with experimental distances.[18,20,22,24,180]

All U-Al/Si distances are substantially elongated due to solvation, mostly by 10–15 pm. For the site AlOH-SiO the U-Al distance is elongated even by 24 pm, while U-Si distances increase only by 6 pm. The resulting U-Al distance of 332 pm for uranyl adsorbed at the AlOOH site is rather close to experimental U-Al/Si values.[22,24,25] The U-Al distances in complexes adsorbed at the AlOHOH sites with q = 1 e and q = 2 e are rather similar and amount to 355 and 351 pm, respectively. Both are too long compared to experimental values, even if one takes into account that the GGA tends to overestimate such distances by ~10 pm (Section 9.1).

The formation energies, calculated according to Eq. 8.4 and including surface solvation effects, show a strong stabilization of the complexes relative to their analogues at the unsolvated surfaces. The decrease of ΔE_{form} due to surface solvation is given in the last

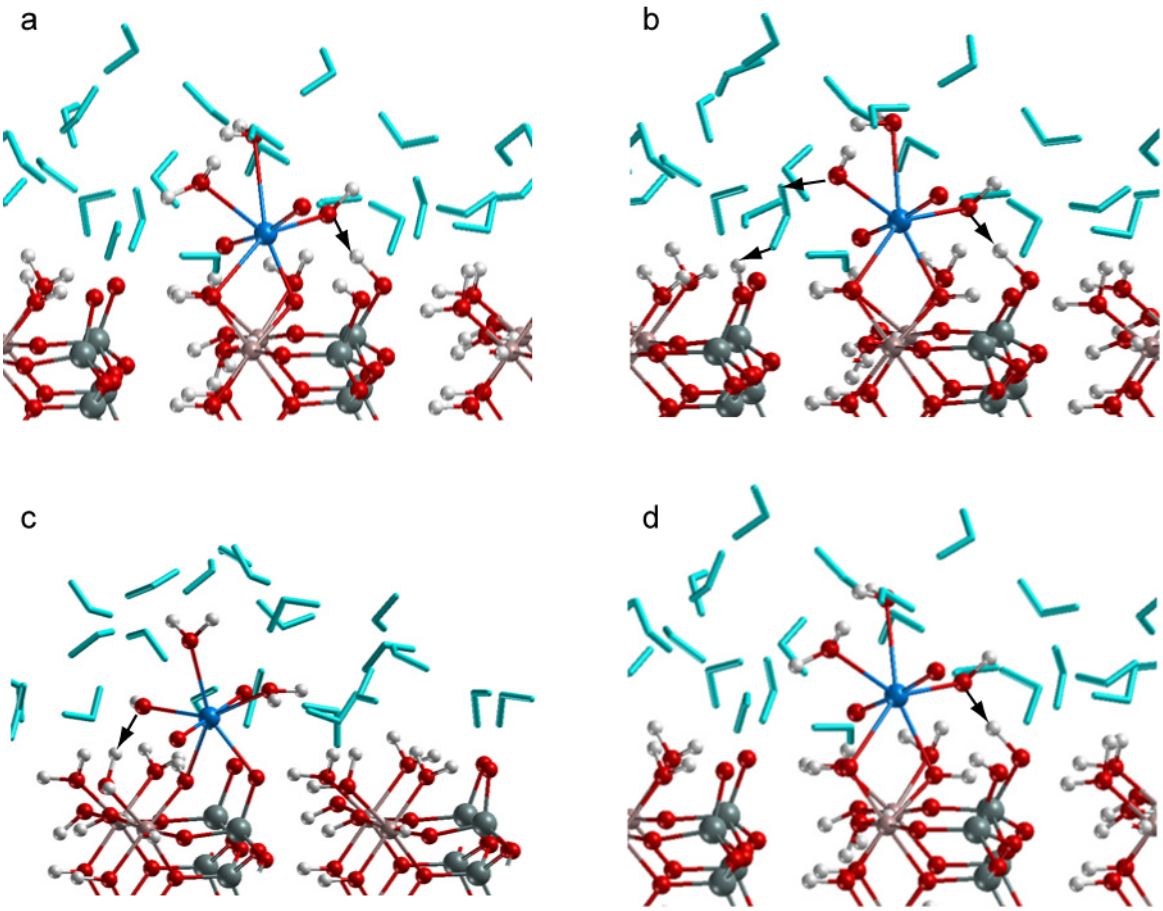

Figure 9.5. Optimized structures of uranyl inner-sphere complexes adsorbed in bidentate fashion on the solvated S0 termination of (010) kaolinite: doubly deprotonated sites (a) AlOOH, (b) AlOHOH, (c) AlOH-SiO, and (d) singly deprotonated AlOHOH site.

column of Table 9.7 (Δ^2E_{form}). The formation of adsorption complexes at the doubly deprotonated sites AlOOH and AlOH-SiO at S0 termination is favored by ~30 kJ mol^{-1}, while the adsorption complexes at the AlOHOH sites are even more stabilized, by ~100 kJ mol^{-1}. As a result, complexes adsorbed at the AlOOH and AlOHOH (q = 2 e) sites at S0 termination (ΔE_{form} = 111 and 79 kJ mol^{-1}, respectively) become more favorable than uranyl adsorption at the mixed site AlOH-SiO (164 kJ mol^{-1}). Thus, the mixed AlOH-SiO site, the only one involving a surface silanol group, can be excluded as possible adsorption site because of its relatively high formation energy. All complex formation energies for models with q = 2 e are still endothermic, as they are referenced to the neutral kaolinite surface. If the partially deprotonated surface is taken as a reference, the formation of adsorption complexes will be more favorable. The complex formation energy for the singly deprotonated site AlOHOH (q = 1 e) is also stabilized by ~100 kJ mol^{-1}. Indeed, it becomes highly exothermic, -159 kJ mol^{-1}, due to solvation effects.

As mentioned above, for all complexes at the S0 termination, uranyl monohydroxide is calculated as the species actually adsorbed. The only exception is uranyl adsorbed at the doubly deprotonated site AlOHOH, where an $UO_2(OH)_2$ species is formed. Thus, it is of interest to estimate also the energy of adsorption of $[UO_2(OH)(H_2O)_4]^+$, which is a useful reference species at about neutral pH of the solution:

$$S\text{-}(OH)_2 + UO_2(OH)(H_2O)_4^+ \rightarrow S\text{-}(O)(OH)\text{-}UO_2(OH)(H_2O)_2 + H_2O + H_3O^+ \qquad (9.4)$$

Eq. 9.4 for the formation of uranyl adsorption complexes is written in the same spirit as previously Eq. 8.4; it differs only by the deprotonation energy of the solvated uranyl ion, which is estimated by a gas phase VASP calculation with solvation corrections applied (COSMO model, calculated with the program ParaGauss) at 67 kJ mol^{-1} This energy is higher than the one calculated by Ray et al.[113] since thermodynamic corrections are neglected here. Thus, formation of the uranyl monohydroxide complex at the S0 termination of the (010) kaolinite surface is favored by 67 kJ mol^{-1} compared to the formation of the uranyl complex.

To investigate the effect of the model construction on the properties of the adsorption complexes, an alternative approach was invoked. Whereas in this first procedure the adsorbate was positioned on the solvated surface, in the second procedure the water monolayer was added to the adsorption complexes equilibrated at the bare surface. Thus, in the construction of model complexes the order solvation → adsorption was changed to adsorption → solvation. The results of this latter approach are shown in the lower part of Table 9.7 (model ads→solv). With the exception of the adsorption complex at the site AlOHOH (q = 1 e), all results are very similar in geometry and energy to the corresponding complexes modeled with the approach solvation → adsorption. Uranyl bonds and U-O_{eq} changed only weakly, while all

other U-O and U-Al distances change by 2 pm at most. The formation energies of the complexes changed by less than 8 kJ mol^{-1}, which is also rather small. As mentioned, the only marked deviation was obtained for the complex at the site AlOHOH (q = 2 e). In that complex uranyl looses two protons of its first solvation shell in the model solv→ads and only one in the strategy ads→solv. Therefore, the former complex exhibits longer uranyl bonds (by 2 pm) and two rather short U-O bonds to the hydroxyl groups (~226 pm). Complex formation is favored by 40 kJ mol^{-1} for the $UO_2(OH)_2$ adsorbate compared to uranyl monohydroxide.

Adsorption on the solvated S1 (010) surface

Uranyl complexes adsorbed at the S1 termination of the (010) kaolinite surface are shown in Figure 9.6. There are two main differences compared to uranyl complexes adsorbed at the solvated S0 terminations of edge surfaces. First, complexes at S1 termination do not deprotonate. Even the complex at the site AlOHOH (q = 2 e), which formed uranyl monohydroxide as adsorbate on the bare S1 (010) surface, yields adsorbed uranyl at the solvated S1 (010) surface. Secondly, all SiO^- groups of the solvated surface are reprotonated from neighboring $AlOH_2$ groups as an effect of uranyl adsorption, with the only exception of the complex at the site AlOHOH (q = 2 e) (Fig. 9.6b). Hence, units AlOH-SiOH appear, as on the bare S1 (010) surface, instead of $AlOH_2$-SiO moieties, which are present at the solvated S1 (010) surface (Section 9.3). To rationalize the chemically different behavior of the S0 and S1 terminations of the (010) edge surface, one should note the structural differences between the surface fragments AlOH···HOSi (Section 9.3). Due to the short distances from AlOH to SiOH groups of the S1 (010) surface, proton hopping between them can occur directly and more easily, without mediation of a solvent molecule (Section 9.3). On the solvated S1 (010) surface only three protons among four in the (2 × 2) unit cell are moved to form $AlOH_2^{+1/2}$

Table 9.8. Calculated characteristics of inner-sphere models of adsorption complexes of uranyl on the bare and solvated S1 termination of the (010) surface of kaolinite. q (in e) is the charge of the adsorption site. Distances in pm, energies in kJ mol^{-1}.

Site	q	U-O_t	U-O_{surf}	U-Al	U-OH[a]	U-O_w	U-O_{eq}	ΔE_{form}	$\Delta^2 E_{form}$[b]
bare									
AlOOH	2	184	206, 234	324		265, 266, 266	247	210	
AlOHOH	2	183	235, 237	344	220	264, 265	244	147	
AlOHOH	1	183	233, 234	342		260, 261, 265	251	-50	
solv→ads									
AlOOH	2	185	209, 241	326		250, 260, 273	246	25	-185
AlOHOH	2	184	218, 228	339		250, 261, 266	244	121	-26
AlOHOH	1	184	240, 246	348		243, 258, 261	249	-235	-185

[a] U-O_{OH} distance to OH ligands arising due to deprotonated aqua ligands. [b] Stabilization effect due to surface solvation.

groups. As mentioned already, in the presence of uranyl nearly all the silanolate groups get protonated.

The complex at the site AlOHOH (q = 2 e) is the only one which changed its chemical identity from uranyl monohydroxide to uranyl due to solvation. It also exhibits the least favorable energy of formation, 121 kJ mol^{-1} at the solvated surface. The alternative strategy of constructing complexes at solvated surfaces was also applied for that species. When the water monolayer is added to the complex optimized in the gas phase (adsorption → solvation strategy), again adsorbed uranyl, not monohydroxide, results, but the adsorption site changes. One of the aluminol groups of the initially constructed AlOHOH site deprotonates, resulting in an AlOOH site. Thus, the two strategies of constructing the adsorption complexes at solvated surfaces lead to the same adsorbate species UO_2^{2+}, but different adsorption sites, AlOHOH and AlOOH. Thus, it is shown that available adsorption sites do not only depend on

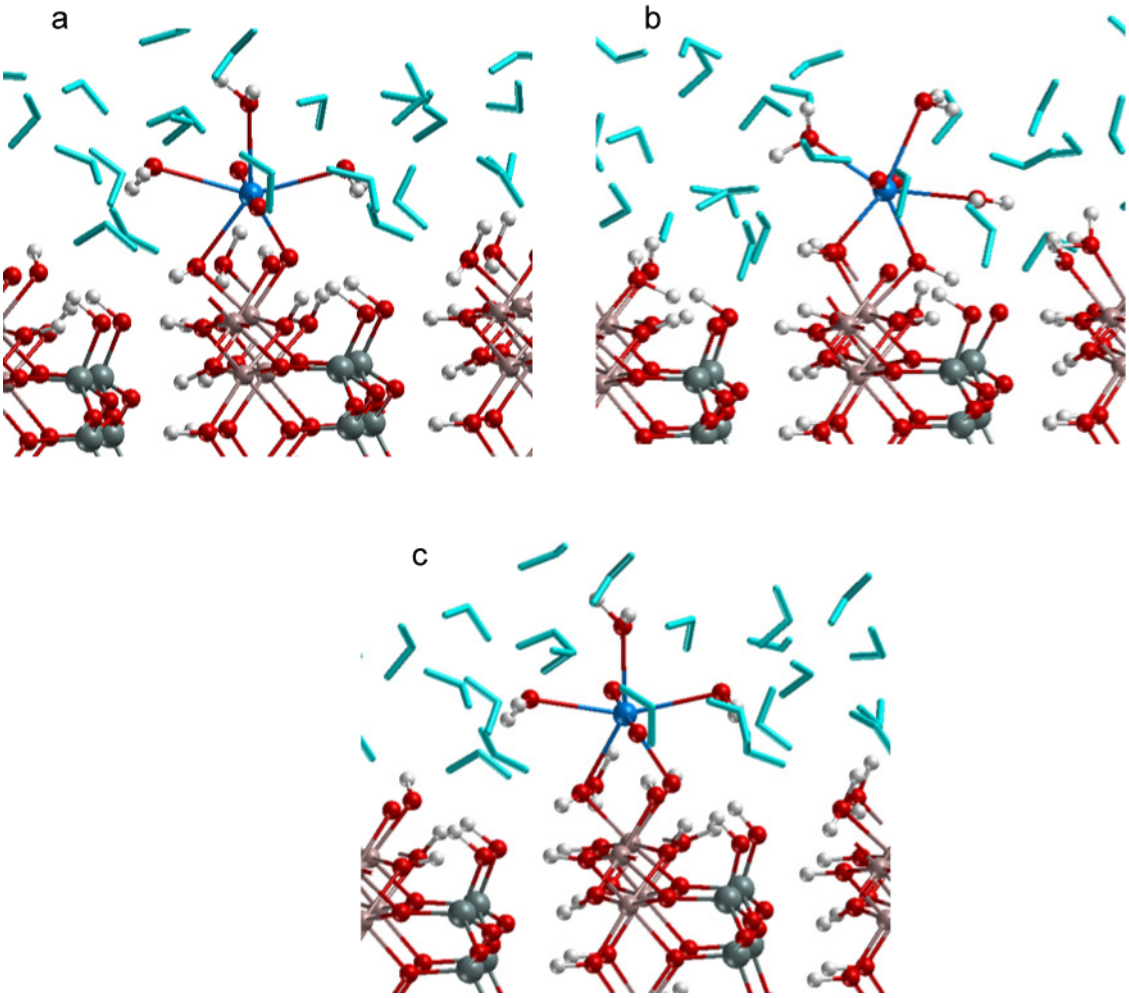

Figure 9.6. Optimized structures of uranyl inner-sphere complexes adsorbed in bidentate fashion on the solvated S1 termination of (010) kaolinite: doubly deprotonated sites (a) AlOOH, (b) AlOHOH, and (c) singly deprotonated AlOHOH site.

pH conditions, but are also affected by the adsorbed ion.

Geometrical changes due to solvation are not uniform for the three adsorption complexes investigated on the S1 (010) surface (Table 9.8). The uranyl U-O_t bond elongates by 1 pm for all complexes, but all other parameters do not exhibit a uniform trend. The U-O_{surf} bonds are elongated for the complexes adsorbed at the sites AlOOH and AlOHOH (q = 1 e), but shorten for the complex at the doubly deprotonated site AlOHOH. The U-Al distance exhibits the same trend: it elongates by 2–6 pm for the complexes at the sites AlOOH and AlOHOH (q = 1 e), but contracts by 5 pm at the site AlOHOH (q = 2 e).

As one can see, the uranyl bonds at the S1 termination are shorter than those obtained for adsorption complexes on the surfaces S0 (010) and Al(o) (001). They amount to 184–185 pm only, while on the other surfaces they vary from 185 pm to 188 pm (Tables 9.5, 9.7). Invoking bond order conservation, these shorter uranyl bonds may be rationalized by the lower number of hydrogen bonds to the surrounding water molecules. For complexes at the sites AlOOH and AlOHOH (q = 2 e) only two such H-bonds are formed with O···H distances of 174 and 187 pm, while for AlOHOH (q = 1 e) three hydrogen bonds appear, one of 186 pm and two longer ones, 196 and 237 pm. In contrast, uranyl adsorbed on the solvated surfaces S0 (010) and Al(o) (001) is engaged in three or four hydrogen bonds, some of which, more than one for each case, are rather short, ~180 pm.

Among the U-O_{surf} bonds shown in Table 9.8 there are only three shorter ones, one to the AlO group of the AlOOH adsorption site, 209 pm, and two bonds to AlOH surface groups of the site AlOHOH (q = 2 e) site, 218 pm and 228 pm. All other U-O bonds in the equatorial plane of uranyl are longer, from 240 and 273 pm, including U-O_w bonds. U-Al distances are somewhat shorter than in the complexes adsorbed on the S0 (010) surface; they vary from 326 pm to 348 pm. These shorter distances can be rationalized by the lack of hydrolysis of adsorbed uranyl at the S1 terminated surface. Thus, there are no additional hydroxyl ligands, that compete with surface bonds, as in the case of adsorption at the S0 termination. The U-Al distance of 348 pm appears at the singly deprotonated site AlOHOH and seems rather long compared to typical EXAFS results of 330 pm.[22,24] The other two U-Al distances, 326 pm and 339 pm, correspond to the sites AlOOH and AlOHOH (q = 2 e) and are in the range of experimentally observed U-Al/Si distances. The calculated U-O_{eq} values of 244–249 pm are in the same range as for the surfaces S0 (010) and Al(o) (001) and thus are not suited to discriminate adsorption at different facets or terminations. Overall, they are slightly shortened due to solvation, by 1-2 pm (Table 9.8).

Surface solvation affects the formation energies favorably, by 185 kJ mol^{-1} for the uranyl complexes at the sites AlOOH and AlOHOH (q = 1 e). Both are the lowest formation

energies among the complexes adsorbed at sites of the same charges, among all kaolinite surfaces examined. The formation of the complex at the site AlOOH (q = 2 e) of the S1 terminated (010) surface requires only 25 kJ mol^{-1}, while adsorption at the site AlOHOH (q = 1 e) is exothermic, by 235 kJ mol^{-1}In contrast, uranyl adsorption at the site AlOHOH (q = 2 e) has a similar formation energy, 121 kJ mol^{-1}, as calculated for the complexes of various adsorbed $[UO_2(OH)]^+$ species at the S0 termination of the (010) surface.

Overall, surface solvation leads to longer uranyl U-O_t bonds and smaller U-O_{eq} values for uranyl complexes on kaolinite surfaces. Other structure parameters change irregularly. The main structural effect of solvation for adsorption on the S0 termination of the (010) surface is the deprotonation of an aqua ligand of the first solvation shell of uranyl, which leads to adsorbed hydroxylated species, $[UO_2(OH)]^+$. This does not happen on the S1 surface. When $[UO_2(OH)]^+$ is formed, one of the U-O_{surf} bonds elongates considerably and, in consequence, U-Al distances increase by 10–15 pm. On the S1 termination of the (010) surface the U-Al distance does not vary much, at most 6 pm (Table 9.8). The second effect of the deprotonation of an aqua ligand of uranyl is a pronounced splitting of the U-O bonds in equatorial plane, resulting in two (or three) shorter U-O bonds, one of which is directed to the surface and another one (or two) to the hydroxyl ligand, and three (or two) longer bonds to surface groups and to aqua ligands. As the distances U-O_{surf} and U-OH are very similar, they cannot be distinguished from the contacts to hydroxyl ligands and to the surface. Thus, one is also not able to differentiate the various adsorbate species, UO_2^{2+} and $[UO_2(OH)]^+$. A splitting of U-O bonds also appears in experiment and typically indicates inner-sphere adsorption. Adsorption complexes are always stabilized by solvation. The stabilization effect varies significantly, from 26 to 185 kJ mol^{-1}. Obviously, solvation must not be neglected when modeling adsorption on edge surfaces. It can change not only structural parameters and complex formation energies, but may even modify the chemical identity of the adsorbate.

9.6 Comparison with experiment

So far, computational results of uranyl adsorption on kaolinite surfaces have been discussed. Modeling of uranyl adsorption on bare (001) basal surfaces showed, as expected, that the Si(t) surface is less reactive than the Al(o) surface. Therefore, it was excluded from further consideration. Adsorption on the bare (010) edge surfaces of kaolinite was calculated to be more favorable than on the basal surface Al(o). Finally, solvation effects for the surface were accounted for by inclusion of a water monolayer into the slab model. As a result, adsorption complexes changed their structural parameters and some of them even their chemical nature to yield different adsorbate species. In this section these computational results will be compared to available experimental data, also with the goal to identify the nature of uranyl

species adsorbed on kaolinite. Since the computational models show that surface solvation changes not only the geometry of the complexes, but also the behavior of the surface groups and the nature of the uranyl species adsorbed, only results from models with solvation will be used in this comparison. Next, an overview of EXAFS results for uranyl adsorption on different clay and other relevant mineral surfaces will be given. Results of other experimental techniques will be also considered. Then, the computational findings will be related to appropriate experimental data and an interpretation will be suggested.

The majority of experiments on uranyl adsorption on clay minerals are carried out with powder substrates.[22,24,25,180,181,182] Thus, it is, at least in part, unclear on which of the facets of the clay minerals adsorption takes place. Ideally cleaved (001) planes are assumed to represent the major surface area,[115,116] and therefore, can be regarded to be more probable for adsorption. In contrast, edge surfaces are believed to exhibit a higher reactivity.[183] Also, significant edge surface areas, often up to 30% of the total surface area, are observed by atomic force microscopy (AFM) and scanning electron microscopy (SEM) inspections of clay crystallites.[120]

Experimental conditions vary for different minerals. Also, adsorption of uranyl is known to depend on the pH of solution.[20,22,24,25] Therefore, the experimental pH is usually adjusted such that uranyl is almost completely adsorbed. The pH value allowing strong and complete adsorption varies from 3.5 for silica gel[18] and montmorillonite[20] to 8.5 for kaolinite.[24] The uranyl concentration is usually chosen at 10^{-5} to 10^{-6} M. Another important factor which strongly affects adsorption is the atmosphere. To prevent the formation of carbonate complexes due to contact with air, N_2 or Ar atmospheres are chosen.[22,24,25,184] Nevertheless, many experiments are done under air to better represent environmental conditions.[18,20,22,180]

Structurally, two types of sorbed species are distinguished in experiments, inner- and outer-sphere complexes.[121] Inner-sphere complexes are characterized by a splitting of the equatorial U-O distances and/or sufficiently short U-Al/Si distances to be detectable by EXAFS.[121] Physisorption as outer-sphere complexes seems to be the preferred mode of adsorption at low pH values around 3–4,[20,21] resulting in (proper) outer-sphere complexes that are characterized by a single equatorial U-O distance and short U-O_t bonds, similar to the corresponding values of solvated uranyl, U-O_t = 177 pm, U-O_{eq} = 241 pm,[185] and no detectable U-Al/Si distance. The presence of U-U contacts, as observed in some EXAFS experiments[20,22,24] is considered as a hint of polynuclear species of uranyl sorbed on the surface. The detection of U-C distances implies that carbonate complexes of uranyl are adsorbed.[180] Additional helpful information from EXAFS experiments are the coordination numbers related to the interatomic distances resolved. They should be used only as a guide line since they are uncertain by ~20 %.[20,22] Products of uranyl hydrolysis should contribute to

the adsorption as well at not too low pH (≥ 3), but there is no direct evidence in any EXAFS experiment. Unfortunately, experiments thus far did not deliver energy parameters, e.g. adsorption energies for uranyl adsorption on clay minerals. Despite some experimental results related to the parameters listed above, the definite chemical nature of adsorbed species as well as the adsorption sites on the surfaces are largely unknown and can hardly be determined directly by experiments.

Nevertheless, one can try to classify the available experimental data to extract a better characterization of possible surface species. This discussion mainly relies on geometrical parameters obtained from EXAFS experiments. Most of the interpretations of the experiments on uranyl adsorption on phyllosilicate surfaces are done by comparing these results to

Table 9.9. Available EXAFS results for uranyl adsorption at clay and related minerals: amorphous silica and alumina, silica gel, α- and γ-Al_2O_3, montmorillonite and kaolinite. Experimental conditions (pH, atmosphere, etc.) are given, CO_2 refers to aerobic conditions. Distances in pm, coordination numbers in parentheses.

Surface	pH, atm.	U-O_t	U-O		U-Al/Si	U-C	U-U	U-O_{eq}	Ref.
Silica	6.5, CO_2	176	226(3.5)	248(1.7)	308(1.0)		397(1.8)	233(5.2)	20
Silica gel	3.5, CO_2	180	227(2.2)	252(3.2)				242(5.4)	18
	4.5, CO_2	179	226(2.6)		272(0.5)				18
α-Al_2O_3(110)	6, N_2	178	222(2.0)	242(3.0)				234(5.0)	184
γ-Al_2O_3	5, N_2	181			339(0.7)		392(1.0)	246(4.7)	19
γ-Al_2O_3	6.5, CO_2	181	232(2.6)	247(3.1)			401(0.4)	240(5.7)	20
γ-$Al(OH)_3$	6.5, CO_2	180			333(1.0)		421(0.9)	240(6.2)	182
Montm.									
STx-1[a]	5, N_2	178			343(0.6)			236(6.2)	19
	7, N_2	178			340(0.6)			234(5.9)	19
SAz-1[b]	4, CO_2	178						242(6.6)	20
	6.4, CO_2	177	230(3.0)	248(2.7)				239(5.7)	20
SWy-2[c]	7, CO_2	180	235(4.0)	254(2.0)	346(0.2)[d]	288(1.0)		241(6.0)	180
SAz-1	7, CO_2	181	234(2.0)	253(2.0)	337(0.2)	284(1.0)		244(4.0)	180
Kaolinite	7.5, Ar_2	180	222(2.1)	249(2.9)	~330		387(2.0)	238(5.0)	22
	7, CO_2	180	227(2.1)	249(2.9)	~330		388(1.0)	240(5.0)	22
	5, CO_2	179			310, 330			237(5.0)	24
	8.5, CO_2	181			308, 328		391(0.5)	241(5.0)	24
	8.5, N_2	180			309, 329			236(5.0)	24
	7, CO_2	177			306, 326			234(5.0)	25
	8.5, CO_2, HAs	178			308, 327			235(5.0)	25

[a] $Ca_{0.33}Al_{1.67}(Mg,Fe)_{0.33}Si_4O_{10}(OH)_2$. [b] $Ca_{0.88}Al_{2.96}Mg_{1.32}Si_8O_{20}(OH)_4$.
[c] $Ca_{0.52}[Al_{3.23}Fe(III)_{0.46}Mg_{0.56}]Si_8O_{20}(OH)_4$. [d] U-Fe distance was defined.

findings on uranyl adsorption on alumina surfaces or on silica gel and amorphous silica.[20] Table 9.9 collects available EXAFS results of uranyl sorption on silica,[18,20] alumina,[20,181,182,184] montmorillonite,[19,20,180] and kaolinite.[22,24,25]

The most important characteristic parameters of adsorption complexes resolved in EXAFS are the distances U-O_t and U-O_{eq}. The only result for an outer-sphere complex on montmorillonite[20] exhibits U-O_t of 178 pm and U-O_{eq} of 242 pm, which is in agreement with the corresponding results for the solvated uranyl ion, U-O_t = 177 pm, U-O_{eq} = 241 pm.[185] The uranyl U-O_t bonds for inner-sphere adsorption on different minerals vary from 177 to 181 pm for the same systems and similar experimental conditions (montmorillonite, kaolinite, Table 9.9). This variation is slightly larger than the experimental uncertainty of ±2 pm. In turn, the U-O_{eq} values can be found to be split into shorter distances of ~226–235 pm and longer distances of ~243–254 pm, indicating inner-sphere adsorption; however, U-Al/Si distances remain unresolved in some cases. The resolved U-Si distance for silica is rather short (272, 308 pm), while the distances U-Al or U-Fe (for montmorillonite) are about 333–346 pm. Measured U-Al/Si distances of 310 and 330 pm for uranyl adsorption on kaolinite are comparable to U-Si and U-Al distances for silica and alumina surfaces (of gibbsite and corundum), respectively. On the other hand, due to elevated reactivity of Al edge sites relative to Si ones,[186] and the stoichiometric excess of Al_2O_3 in kaolinite[30] silanol groups are expected to be unlikely as adsorption sites for uranyl. Surprisingly, U-U distances are resolved for many systems,[20,22,24] except for montmorillonite. For kaolinite U-U distances vary from 387 pm to 391 pm, in agreement with the experimentally determined U-U distance of the dinuclear complex $[(UO_2)_2(OH)_2]^{2+}$ in solution, 387 pm.[187] For alumina and silica longer U-U distances, 392–421 pm, have been determined.[19,20,182] Although most experiments were carried out in air, U-C distances, at 284–288 pm, were resolved only for uranyl adsorbed on montmorillonite at pH = 7.[180] None of the available EXAFS spectra for adsorption complexes on kaolinite or other minerals exhibit U-C bonds. For U-O_{eq} averaged over all resolved U-O contacts of uranyl complexes adsorbed as inner-sphere species, the distance U-O_{eq} correlates with the presence of U-U and U-C contacts. If U-U and U-C distances were not observed by EXAFS, U-O_{eq} amounts to about 234–236 pm and once 239 pm (Table 9.9). When U-U or U-C contacts are present, U-O_{eq} is determined at 240–246 pm. Thus, the formation of polynuclear or carbonate complexes of uranyl adsorbed on the surface enlarges the average equatorial distance U-O_{eq}. In contrast to complexes in solution, this change of U-O_{eq} should not be interpreted as a change of the coordination number.[72,73,76]

Time-resolved laser fluorescence spectroscopy (TRLFS) also provides information on adsorption complexes of actinides on clay minerals.[28,30,183] Uranyl adsorption on kaolinite,[30] gibbsite,[28] and muscovite[183] was investigated by means of TRLFS. Two characteristic features

of TRLFS spectra are usually discussed in the literature: the peak positions and the fluorescence life times. Different life times are associated with different surface species for two reasons: (*i*) the number of aqua ligands around uranyl affects the quenching of the fluorescence,[30] or (*ii*) coexisting mono- and polynuclear adsorbed species exhibit a different quenching behavior.[28,183] In contrast to many other ligands, hydroxyl is expected to affect the peak positions and the shape of fluorescence spectra.[28,30] The experiments listed above do not detect any changes in the peak positions and the shapes of the spectra although different life times are observed for the various species. This finding can be rationalized by assuming that the first coordination shell of uranyl contains the same number of hydroxyl groups.[28,30]

Results for uranyl adsorption on kaolinite have to be discussed in more detail, since they are of central interest in this thesis. An earlier EXAFS study of Thompson et al.[22] on uranyl adsorption on kaolinite at pH values of 6–7.9 determined two shorter equatorial U-O bonds of 226–229 (±2) pm and three longer ones of 247–249 (±2) pm, together with a U-Al/Si distance of ~330 pm.[22] This U-Al/Si distance is rather close to the case of uranyl adsorption on gibbsite (333 pm)[182] and rather far from the observed U-Si distances for uranyl adsorbed on silica gel[18] or amorphous silica[20] (< 310 pm, Table 9.9). Actually, one more peak was observed in the study of Thompson et al.,[22] at ~300 pm, which was tentatively also assigned as a U-Al/Si distance. An alternative source of this peak could be a multiple-scattering feature.[22] Nevertheless, the authors were confident, that this peak corresponds to an U-Al/Si distance, but they considered both values, 300 and 330 pm, as very approximate.[22]

A recent study of Reich et al.[24] reported comparable results, where uranyl bond lengths of 179-181 pm and unresolved U-O_{eq} distances of 236–241 pm have been determined. In this study, two U-Al/Si distances were identified, a shorter one at ~310 pm and a longer one at ~330 pm,[24] which were interpreted as indicative for sorption at edge sharing Al octahedra or Si tetrahedra. An alternative interpretation assigns these results to a mixture of two adsorption complexes.[25] This scenario is supported by a recent TRLFS study[30] of uranyl adsorption at kaolinite, where two different fluorescence life times were detected that were attributed to bidentate surface complexes which differ by the number of aqua ligands around uranyl. Similar TRLFS findings for uranyl on gibbsite[28] and muscovite[183] have been interpreted as a consequence of coexisting mono- and polynuclear sorption complexes. A very recent EXAFS study by Křepelová et al.[25] on uranyl adsorption on kaolinite in the presence of humic acids confirms the results of Reich et al.,[24] but surprisingly resolved a rather short uranyl bond of 177–178 pm, comparable to that of the free uranyl ion. Although the experiment was done in the presence of air and humic acids, no U-C distance was resolved. Due to the presence of U-Al contacts it was concluded that uranyl adsorbs directly at the surface rather than via humic

acids. Also, no U-U contacts were detected. Correspondingly, the U-O_{eq} distances in this experiment amounted to 233–235 pm. As noticed above, a longer U-O_{eq} of 241 pm was resolved in the experiment of Reich et al.[24] only in the case when a U-U distance was observed (CO_2, pH = 8.5).

Since in this thesis single uranyl ions adsorbed on kaolinite surfaces have been modeled, the results should preferentially be compared to those experiments which do not exhibit U-C or U-U distances and were performed at anaerobic conditions. In this section only bidentate complexes adsorbed at the partially deprotonated solvated surfaces of kaolinite as the most probable are considered, although monodentate species can be excluded as a short U-Al/Si contact of 330 pm, as commonly observed in EXAFS experiments, was never calculated for monodentate complexes. The shortest U-Al distance calculated for a monodentate adsorption complex of uranyl is ~360 pm (Section 8.4). All optimized solvated bidentate inner-sphere complexes of uranyl adsorbed at Al(o) (001) and S0 and S1 terminations of (010) surfaces are listed in Table 9.10. The bidentate inner-sphere uranyl complexes are divided into two groups according to the charge of the adsorption site: singly deprotonated sites, q = 1 e, and doubly deprotonated sites, q = 2 e. Formally these different charges, assigned to the sites, correspond to different pH regimes. At pH = pH_{ZPC} the surface is neutral and only small a amount of positively charged sites is expected to be present. At this pH, the existence of doubly deprotonated sites (q = 2 e) can be excluded. With increasing pH first the number of singly charged sites (q = 1 e) will increase. With further growing pH these sites will more and more be replaced by doubly deprotonated sites (q = 2 e) and fully deprotonated surface areas. Thus, sites of charge q = 1 represent a situation at about pH_{ZPC} = 5.5[121] or slightly above, while doubly deprotonated sites will dominate at higher pH. On the other hand, adsorbed uranyl species at sites with q = 2 e could also form by deprotonation of surface hydroxyl groups in the field of uranyl. This process is also facilitated with increasing pH.

Recall that all solvated complexes inspected were optimized at the GGA level of theory which is known to yield elongated structural parameters compared to LDA. For actinide species, LDA structures, in turn, compare well with experiment.[89,179] Therefore, uranyl U-O_t bonds typically are calculated too long by 2 pm and the average equatorial U-O_{eq} distance is overestimated by 7 pm (Section 9.1). The overestimation of U-Al distances at the GGA level depends on the kaolinite surface studied. It is 5 pm the Al(o) (001) surface and 10 pm for the (010) surfaces. These average corrections will be taken into account in further discussion, when comparison with experimental data is introduced. Note, however, that these differences between GGA and LDA distances are also affected by solvation.

In the following calculated results will be compared with experiment and a final interpretation will be given. First, sites with q = 1 e will be discussed, starting with energy

aspects of uranyl adsorption at singly deprotonated sites, to be followed by a comparison of calculated structures with available EXAFS results. Next, complexes adsorbed at sites with q = 2 e will be addressed which correspond to a higher pH regime. Some conclusions about preferred sites and differences between adsorption at basal and edge surfaces can be drawn based on complex formation energies; however, it will be shown that these energies are not decisive. The subsequent structural comparison will result in a better interpretation of experimental EXAFS and TRLFS results. The most important conclusions will briefly be summarized at the end of this chapter.

The comparison of experimental and computational results is started with the adsorption complexes at sites of charge q = 1 e (Table 9.10). The formation of adsorption complexes on the (010) surface is energetically favorable compared to (001), especially strongly on the S1 termination (-235 kJ mol^{-1}). The formation energy ΔE_{form} of uranyl complexes at the S0 termination is calculated at -159 kJ mol^{-1}. This is significantly less exothermic than for the S1 termination, but more exothermic than complexation at the Al(o) surface, -67 kJ mol^{-1} (Table 9.10). Thus, the S1 termination of the (010) surface seems to be the most reactive surface among the systems studied that are intended to model uranyl adsorption at lower pH. The highly exothermic formation energies of uranyl complexes adsorbed at singly deprotonated

Table 9.10. Calculated characteristics (interatomic distances in pm, complex formation energies ΔE_{form} in kJ mol^{-1}) of inner-sphere models of adsorption complexes of uranyl on different surface of kaolinite, including surface solvation. Experimental results are given for comparison.

Site	Surface	Adsorbate	U-O_t	U-Al(Si)	U-O	U-O_{eq}	ΔE_{form}
q = 1 e							
AlOOH	(001) Al(o)	UO_2^{2+}	187	335	220,[a] 243, 246, 262,[a] 273	249	-67
AlOHOH	(010) S0	UO_2OH^+	187	355	229,[b] 235,[a] 244, 259,[a] 272	248	-159
AlOHOH	(010) S1	UO_2^{2+}	184	348	240,[a] 243, 246,[a] 258, 261	249	-235
q = 2 e							
AlOO	(001) Al(o)	UO_2^{2+}	187	315	220,[a] 222,[a] 247, 253, 271	243	219
AlOOH	(010) S0	UO_2OH^+	188	332	204,[a] 230,[b] 250, 258,[a] 285	246	111
AlOHOH		UO_2OH^+	185	351	223,[b] 229,[b] 236,[a] 254,[a] 275	243	79
AlOH-SiO		UO_2OH^+	186	397(344)	219,[b] 228,[a] 247, 254, 257[a]	241	164
AlOOH	(010) S1	UO_2^{2+}	185	326	209,[a] 241,[a] 250, 260, 273	246	25
AlOHOH		UO_2^{2+}	184	339	218,[a] 228,[a] 250, 261, 266	244	121
exp.	conditions						
Kaolinite[c]	CO_2, pH 5		179	310, 330		237(5.0)	
Kaolinite[c]	N_2, pH 8.5		180	309, 329		236(5.0)	
Kaolinite[d]	CO_2, pH 7		177	306, 326		234(5.0)	
Kaolinite[e]	CO_2, pH 7		180	~330	227(2.1), 249(2.9)	240(5.0)	

[a] U-O_{surf} bond to the surface. [b] U-OH bond to hydroxyl group. [c] Ref. 24. [d] Ref. 25. [e] Ref. 22, a U-U distance of 388 pm with coordination number 1 was also resolved.

sites of the (010) surface can not directly be compared to those with q = 2 e because the energy difference is dominated by the large reprotonation energy of the charge compensating defect (Section 8.3). Still, it is meaningful to compare complexes with the same charge as the same type of model and compensation procedure is used (Section 8.3). Comparison of geometries of complexes at singly deprotonated sites (q = 1 e) shows elongated U-O_t bonds compared to solvated uranyl, to 184–187 pm,. The U-Al distances, 348 pm and 355 pm, calculated for complexes adsorbed on the (010) surface are somewhat long compared to experimental values, 330 pm, even if one accounts for the GGA overestimation which is 10 pm in this case. Note that the U-Al distance does not represent a chemical bond; therefore it may certainly be off by 10 pm due to uncertainties of the models. In contrast, uranyl adsorbed on the AlOOH site of the solvated Al(o) surface shows a U-Al distance of 335 pm. In the case of the Al(o) surface, GGA values overestimate U-Al distances up to 5 pm only (Section 9.1); thus the U-Al result agrees well with the experimental value of 330 pm.[22,24,25] The two shorter U-O bonds of ~230 pm seen in experiment[22] are present only for the complex at the AlOHOH site for the S0 termination of the (010) surface, 229 and 235 pm (Table 9.10). As discussed in Section 9.1, the U-O bonds do not change uniformly when one uses the GGA approach instead of LDA. Thus, it is difficult to estimate which of the shorter U-O bonds fit the experimental range. Still, in all three complexes adsorbed at singly deprotonated sites, there are shorter U-O distances of 220–246 pm and longer ones of 258–273 pm. Thus, the "splitting" of the equatorial shell of O atoms coordinated to uranyl, as found by EXAFS, is also present in the calculated structures. For the average value U-O_{eq} of 248–249 pm an estimate arrives at 241–242 pm, after a GGA correction by -7 pm, which is somewhat larger than the experimental values, 236–240 pm. On the one hand, this result is rather close to the experimental values of ~240 pm, which were resolved only when U-U contacts were seen (Table 9.9).[22,24] As already mentioned, when EXAFS does not indicate U-U and U-C contacts, U-O_{eq} bonds are shorter on average, 234–237 pm. Therefore, the computational results (241–242 pm after GGA correction) should be compared with these shorter U-O_{eq} values; then they are a bit long, by ~4 pm. Thus, the results calculated for all these complexes hardly fit the experiments. Recall that these complexes adsorbed at singly deprotonated sites should represent a situation at a pH close to pH_{ZPC} which, however, is rarely covered by experiments.[24]

The second group of adsorption complexes with q = 2 e corresponds to a higher pH of the solution. The discussion will follow the same lay-out as the one just given for complexes with q = 1 e. Adsorption on the basal surface at the AlOO site is the least favorable, as it is calculated endothermic by 219 kJ mol^{-1} (Table 9.10). However, one can not exclude it from the consideration for kinetic reasons. Although adsorption on edge kaolinite surfaces is

thermodynamically more favorable, kinetically uranyl can first reach the basal facets of kaolinite, since this type of surfaces represents by far the larger part of the surface area. This same argument can also be applied to the partially deprotonated AlOOH site with q = 1 e of the Al(o) surface.

Among all uranyl complexes on the (010) kaolinite surface, that at the mixed AlOH-SiO site yields the most endothermic energy of formation, 164 kJ mol^{-1}. Mixed sites, containing silanol and aluminol surface groups, are a minority and apparently they also are not energetically favorable. Thus, neither thermodynamics nor kinetics provides arguments to take these sites into account. Consequently, mixed sites are excluded from further considerations. This conclusion corroborates an earlier molecular modeling study that determined a higher acidity for Al sites compared to Si ones.[186] Thus, pertinent negative centers favorable for adsorption are formed preferentially by deprotonated aluminol sites.

The more favorable adsorption sites on the solvated S0 and S1 terminations of (010) kaolinite surfaces are AlOHOH and AlOOH, respectively. Formation of uranyl complexes at the AlOHOH site on the S0 termination requires 79 kJ mol^{-1}. Even less energy, only 25 kJ mol^{-1}, is required to form the AlOOH site by deprotonation of the S1 termination and to adsorb uranyl. Recall that the most preferable surface termination was not unequivocally determined; see Section 7.4. Thus, both terminations should be assumed to form in contact with aqueous solution. It is unknown which of them contributes the larger surface area. As a result, according to energetic aspects, three complexes (q = 2 e) corresponding to a higher pH regime are determined as the more probable ones, one for each type of surface: AlOO sites on the basal (001) surface for kinetic reasons as well as for thermodynamic reasons AlOHOH sites on the S0 termination and AlOOH sites on the S1 termination of edge (010) kaolinite surfaces.

These computational results on possibly preferred adsorption complexes have now to be compared to the experimental information on structures. In this comparison one has to take into account that the formal reaction of adsorption (Eq. 8.4) includes single or double deprotonation steps of the surface groups, that require different mechanisms and energies for the (001) and (010) surfaces. The basal Al(o) (001) surface of kaolinite contains $(Al)_2OH$ surface groups, from which one or two are deprotonated to create the investigated adsorption sites. The S0 and S1 terminations of the edge (010) surface exhibit $AlOH^{-1/2}$, $AlOH_2^{+1/2}$, and SiOH surface groups, which can be modified under solvation. The deprotonation energies of all these groups are difficult to estimate. Sometimes, to create models of appropriate sites, surface protons were also manually "moved" from $AlOH_2$ groups to a neighboring silanolate group (see Section 9.5). In summary, it is a meaningful procedure to compare optimized

structures of adsorption complexes with experimental structural parameters and to use relative energies of surface complexes only as an additional guideline.

When comparing calculated inner-sphere complexes adsorbed at kaolinite surfaces to experimental results (Section 9.4), one notes the rather long calculated uranyl U-O_t bonds. While U-O_t is typically 180 pm in experiment, 2 pm longer than for the free uranyl ion, calculated U-O_t bonds for most complexes at the GGA level are 184–187 pm. The latter results agree well with the U-O_t distances of uranyl adsorbed at gibbsite (188–190 pm)[188] and TiO_2 (187–190 pm),[134] calculated at the GGA level. Applying a GGA correction of -2 pm (Section 9.1) yields estimates of 182–185 pm, which are still longer than the experimental values. Moskaleva et al.[135] calculated similar U-O_t values, 184–185 pm, at the LDA level for uranyl inner-sphere complexes at AlOO sites of the α-Al_2O_3 (0001) surface. Therefore, such an overestimation of U-O_t bonds is observed in all density functional calculations on periodic slab models of uranyl adsorption on mineral surfaces. As mentioned in Section 8.4, this overestimation may be due to charge transfer from the surface and to hydrogen bonds which uranyl oxygen centers are calculated to form with surface hydroxyl groups and surrounding water molecules. On the other hand, these H-bonds should be also present in experiment. Thus, there is currently no fully convincing rationalization for the notable calculated elongation of U-O_t bonds.

Many of the inspected adsorption complexes of uranyl on kaolinite exhibit a "splitting" of the equatorial U-O shell, comparable to the experimental results observed by Thompson et al.[22] for kaolinite. Experimentalists usually assign the shorter U-O values to the bonds of uranium to the surface. The EXAFS coordination numbers of the shorter U-O bonds vary from 2 to 3, although for bidentate complexes there are only two contacts of uranium to the reactive surface groups. The present study found that due to the high reactivity of edge kaolinite surfaces the aqua ligands of the first solvation shell of uranyl can deprotonate, leading to hydroxyl ligands. As a result, one (or two) short U-OH bonds appear in addition to the short uranyl contacts to the surface. This finding tentatively helps to rationalize why EXAFS experiments sometimes show a coordination number of 3 for the shorter U-O distances (Table 9.9 for silica and montmorillonite). Although direct experimental evidence of hydroxyl ligands in adsorption complexes of uranyl is still lacking, one may tentatively transfer this concept to all clay minerals that exhibit similar reactive groups on their edges. Moreover, at experimental pH conditions, uranyl hydroxide species are present in solution and thus may directly adsorb. The calculated shorter U-O_{surf} and U-OH bond lengths are rather close (about 230 pm). Therefore, one should not expect that experiments will be able to differentiate between them. Since a hydroxyl group is quite a strong ligand, bond competition between an OH group and the surface leads to an elongation of one of the U-O_{surf} bonds and

thus of the U-Al distances. This, in turn, would require a change in the interpretation of experiments: short U-O bonds have to be assigned to either U-O_{surf} or U-OH bonds, while longer ones can also originate from U-O_{surf} contacts.

Next, a comment on the interpretation of TRLFS results of uranyl adsorption on kaolinite is in order because it directly refers to the presence of OH groups in the first solvation shell of uranyl.[30] As aqua ligands quench the fluorescence, the two different life times that have been detected,[30] have been assigned to two types of surface species that differ by the number of water molecules in the first solvation shell of uranyl. Furthermore, the two species are expected to feature the same number of hydroxyl groups because all fluorescence peaks of both species coincide.[30] In contrast, varying numbers of hydroxyl groups have been demonstrated to change the spectral features.[28,30,189] Different adsorbates found in the present thesis, UO_2^{2+} and $[UO_2(OH)]^+$, represent adsorption complexes with different numbers of aqua ligands in the first coordination shell of uranyl (three for UO_2^{2+}, two for $[UO_2(OH)]^+$). In addition, these adsorbates exhibit different numbers of hydroxyl groups in the first coordination shell of uranyl: none for UO_2^{2+} and one for $[UO_2(OH)]^+$. This result is at variance with the interpretation of Křepelová et al.[30] who excluded a change in the number of hydroxyl groups (see above). The same argument, namely that the same number of hydroxyl ligands of uranyl can be inferred from similar shapes of TRLFS spectra, was also invoked in a TRLFS study of uranyl adsorption on gibbsite,[28] which referred to earlier TRLFS studies on the characterization of hydroxyl complexes of uranyl.[189] (However, one may argue that this latter study[189] does not make such strong claims as implied by the more recent TRLFS investigations.[28,30]) That earlier study[189] analyzed fluorescence spectra of uranyl at different pH (from 2 to 11) of solutions with a total content of UO_2^{2+} species which varied from 0 to 99.95 % (according to speciation); the different life times detected were assigned to the species UO_2^{2+}, $[UO_2(OH)]^+$, $[UO_2(OH)_2]$, $[(UO_2)_2(OH)_2]^{2+}$, $[UO_2(OH)_3]^-$, and $[(UO_2)_3(OH)_5]^+$.[189] The spectral features (peak positions and intensities) of a pure uranyl perchlorate solution and solutions with hydrolysis products indeed differ from each other.[189] The situation changes crucially, when one measures the same spectra of uranyl solutions with hydrolysis products in the presence of PO_4 ligands.[189] As soon as phosphate ligands are admitted, the TRLFS spectra acquire a shape very similar to those seen for different uranium minerals (phosphates, arsenates),[190] for adsorption of uranyl on kaolinite or gibbsite,[28,30] with and without humic acids in solution.[30] The emission wavelengths in all cases listed above are very close to each other and show a red shift compared to a pure uranyl (without hydrolysis products) solution in perchlorate medium.[28,30,190] Thus, characteristic spectral features of $[(UO_2)_n(OH)_m]^{2n-m}$ species with different n and m are not pronounced or hidden when the explored solution contains carbonate (CO_2) or humic acids or surface adsorption sites (clay)

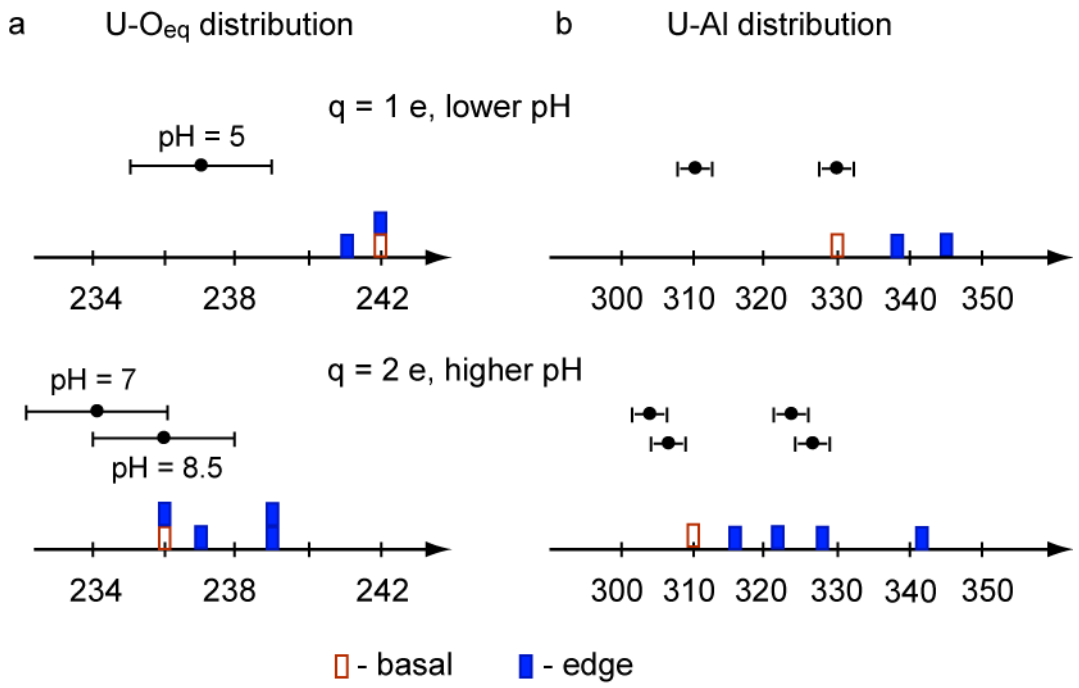

Figure 9.7. Distribution of (a) U-O_{eq} and (b) U-Al distances for the bidentate uranyl complexes investigated that are adsorbed at the basal (empty symbols) and edge (filled symbols) surfaces of kaolinite. The results shown have been adjusted for GGA corrections: -7 pm to U-O_{eq}, -5 pm to U-Al for Al(o) surface, -10 pm to U-Al for (010) surfaces (see text). Experimental results are indicated as dots and horizontal error bars. Data for pH = 5 and 8.5 are from Ref. 24, for pH = 7 from Ref. 25. The two panels show separate distributions for lower (q = 1 e) and higher (q = 2 e) pH regimes.

as potential ligands of uranyl. Therefore, adsorbed species with different numbers of hydroxyl ligands in the first coordination shell of uranyl can coexist, even if the TRLFS peak positions are similar for short- and long-lived species.

Figure 9.7 compares average equatorial U-O_{eq} bonds and U-Al distances of bidentate inner-sphere complexes of uranyl at various kaolinite surfaces (excluding the AlOH-SiO site, see above) to experimental results. All values for U-O_{eq} given in Fig. 9.7 are corrected by -7 pm, as GGA results on average overestimate U-O_{eq} compared to LDA which is known to fit experimental structures of actinide complexes better.[89,179] As was mentioned, GGA results overestimate U-Al distances, depending on the type of surface (Section 9.1). For the Al(o) (001) surface it is -5 pm, for (010) surfaces it amounts to -10 pm. Those corrections were established in Section 9.1 and applied in Figure 9.7. That figure contains two panels, for singly deprotonated (q = 1 e) and doubly deprotonated adsorption sites (q = 2 e). Experimental data measured at different pH (from 5 to 8.5)[24,25] are given with error bars. A comment on the various pH regimes and the differently charged adsorption sites is appropriate. One notices that the distance of complexes adsorbed at higher pH (sites with q =

2 e) agree significantly better with experimental data than the complexes at singly deprotonated sites (q = 1 e) which are expected to be prevalent at lower pH of solution. Inspection of Figure 9.7 shows that complexes adsorbed at sites with q = 1 e have unlikely been observed in available EXAFS experiments as they exhibit longer U-O_{eq} and U-Al distances. (On the other hand, the few experimental results available[24,25] do not show a clear trend for U-O_{eq} and U-Al with increasing pH, see Fig. 9.7) As mentioned, complexes with q = 1 e can be intermediate species that transform to adsorption complexes at sites with q = 2 e by deprotonation of surface groups which is facilitated in the presence of uranyl.

The distribution of U-O_{eq} distances from the various complexes (Fig. 9.7a) shows two groups of values. The shorter U-O_{eq} values of 236–239 pm correspond to sites on both basal and edge surfaces that are doubly deprotonated (q = 2 e). They agree very well with experimental results for systems where no U-U and U-C bonds were resolved (234–237 pm, Table 9.9). The second group, involving longer U-O_{eq} distances of 241–242 pm, results from singly deprotonated adsorption sites (q = 1 e). As mentioned earlier in the discussion of adsorption on singly deprotonated sites, these U-O_{eq} distances are slightly longer than the experimental values, by ~4 pm (see above). Since the mean experimental uncertainty for U-O_{eq} values is ±2 pm,[22,24,25] calculated U-O_{eq} values of 236–242 pm on average can be considered also compatible with the experimentally defined range of 234–237 (±2) pm.

For the U-Al distances one can perform only an approximate comparison to experiment as U-Al distances do not represent bonds, thus should be more affected by details of the models. From the distribution of U-Al distances (Figure 9.7b) one notes several distances that are close to experimental values. The shorter calculated distances correspond to the AlOO adsorption site at the basal surface (310 pm) and to the AlOOH site of the S0 termination of the (010) surface (316 pm). These results compare very well with the shorter experimental distance, ~310 pm.[24,25] The second set of U-Al distances slightly below the experimental value of 330 pm[24,25] (322–330 pm) is computed for AlOOH adsorption sites at basal and edge surfaces. Also the AlOHOH site of the S1 termination of (010) surface exhibits a calculated U-Al distance of 329 pm. The distribution of U-Al distances shows that complexes at sites involving AlO groups agree better with experiment than complexes at sites with only AlOH groups (right filled rectangles around 340–345 pm in Fig. 9.7b). Note that in the present study the two experimentally determined U-Al distances of ~310 and ~330 pm were never obtained for the same model of the adsorption complex. Thus, one is led to conclude that these two distances, differing by 20 pm, correspond to different complexes or different sets of species, preferentially adsorbed at AlOO and AlOOH sites.

In summary, at least five surface complexes modeled computationally agree

Table 9.11. EXAFS results in comparison with calculated characteristics[a] (interatomic distances in pm) of inner-sphere models of uranyl adsorption complexes on different solvated surfaces of kaolinite that are compatible with EXAFS data. Shown are raw GGA data and corrected data to estimate LDA results (see text).

	Site	Surface	Adsorbate	$U\text{-}O_{eq}$		U-Al	
				raw	corr.[b]	raw	corr.[b]
q = 1 e	AlOOH	(001) Al(o)	UO_2^{2+}	249	242	335	330
q = 2 e	AlOO	(001) Al(o)	UO_2^{2+}	243	236	315	310
	AlOOH	(010) S0	UO_2OH^+	246	239	332	322
	AlOOH	(010) S1	UO_2^{2+}	246	239	326	316
	AlOHOH		UO_2^{2+}	244	237	339	329
exp.		conditions					
	Kaolinite[c]	CO_2, pH 5			237(5.0)		310, 330
	Kaolinite[c]	N_2, pH 8.5			236(5.0)		309, 329
	Kaolinite[e]	CO_2, pH 7			234(5.0)		306, 326
	Kaolinite[d]	CO_2, pH 7			240(5.0)		~330

[a] PW91 GGA results. [b] Corrections are -2 pm for $U\text{-}O_t$, -7 pm for $U\text{-}O_{eq}$, -5 pm for U-Al in case of Al(o) surface, and -10 pm for U-Al in case of (010) surfaces (see Section 9.1). [c] Ref. 24. [d] Ref. 25. [e] Ref. 22.

satisfactorily with experiment, namely complexes adsorbed at the AlOO and AlOOH sites of the Al(o) surface, at the AlOOH sites of the S0 termination, as well as at the AlOOH and AlOHOH sites of the S1 termination of the edge (010) surface. To facilitate this summary, Table 9.11 compares computed results for these five adsorption complexes (raw and GGA corrected results) with experimental data. Recall that the corrected data are estimates of LDA results which are assumed to agree better with experiment. Silanol sites were excluded as possible adsorption sites because the corresponding complexes were calculated to require relatively high energies of formation, but structural features also did not match available experimental results (see above). The "splitting" of the equatorial shell of U-O distances, as observed in some experiments,[20,22,180] may indicate the presence of hydroxyl groups in the first coordination shell of uranyl in addition to shorter bonds to surface O centers. The bond lengths of uranyl to hydroxyl ligands and to some surface O centers are similar and shorter than $U\text{-}O_w$ bonds, hence should be difficult to discriminate by experiment. Two of the five complexes listed in Table 9.11, those at the AlOO site of the basal Al(o) surface and at the AlOOH site of the S0 termination, exhibit U-Al distances (310 and 316 pm, respectively) that are compatible with the experimental shorter value, 310 pm, whereas all other complexes were calculated to exhibit longer U-Al distances. Obviously, there are not just one or two specific adsorption sites for uranyl on kaolinite, but a set of complexes should exist in equilibrium. They all are characterized by qualitatively similar structural parameters and lead

to broad peaks in EXAFS spectra,[22,24,25] which average over this manifold of structures. The present computational results also are compatible with the interpretation of TRLFS experiments.[30] Furthermore, the present study suggests an extension of the original interpretation which implied the existence of two adsorbed species with different numbers of aqua ligands around uranyl.[30] In this new view, the set of comparable adsorption complexes may formally be separated into subgroups according to the number of aqua (and/or hydroxyl) ligands of uranyl. The first group contains those complexes where UO_2^{2+} as adsorbate exhibits three aqua ligands; this statement implicitly assumes that uranyl has a coordination number of 5, as revealed in EXAFS experiments (Table 9.9). The second group corresponds to the adsorbate $[UO_2(OH)]^+$ and thus exhibits only two aqua ligands and one hydroxyl group which nevertheless can be expected to leave the TRLFS spectra essentially unmodified.

Summary

Environmental chemistry of radioactive elements plays an important role in the modern world due to the risk assessment of radionuclide migration in nature. Of special concern in this respect are long-living isotopes of U, Pu, and Np in their different oxidation states. Uranium mining sites and especially repositories for radioactive waste exhibit the highest risk. To prevent unnecessary contamination of nature one needs to predict and subsequently prevent the distribution of these hazardous elements. Controlling and/or prohibiting the release of radionuclides to the environment require a fundamental understanding of their chemical and physical properties, as well as of the key processes that determine their transport. Of central importance in this respect are the complexation of radionuclides with inorganic and organic ligands in solution, the formation of colloids, and their sorption at mineral surfaces. This thesis is dedicated to the actinide element U which forms more than 95 % of the radioactive waste. Here the most stable oxidation state VI is discussed. Uranium (VI) in solution forms the stable dication UO_2^{2+}, uranyl, which is highly mobile (Section 1). In the present work two important topics of environmental chemistry of uranyl were treated: the complexation of UO_2^{2+} with humic acids (HAs) and the sorption of uranyl at clay mineral surfaces.

The first part of this thesis focused on uranyl complexation by alcoholic and phenolic groups of HAs (Sections 2-4). Humic acids are a part of natural organic matter, which is structurally not well defined. Carboxylic groups are considered to be the most reactive groups in HAs and thus responsible for uranyl complexation. Nevertheless, up to 15 % of all reactive

groups of HAs are phenolic OH groups, which also may contribute to complexation. To examine the role of phenolic OH groups blocking experiments were done, resulting in ambiguous conclusions. On the one hand, a decreased loading capacity of HA with chemically blocked phenolic OH groups was determined, compared to unmodified HA, which allowed to conclude that phenolic OH groups contribute to uranyl complexation. On the other hand, an EXAFS analysis of both systems found no structural differences between uranyl bound by modified and unmodified HAs, which lead to some doubt regarding the participation of phenolic groups in uranyl complexation.

First-principles density functional calculations were carried out throughout this thesis. The scalar relativistic second-order Douglas-Kroll-Hess all-electron approach to the Dirac-Kohn-Sham problem, as implemented in the code PARAGAUSS (Section 2.1), was used to study uranyl complexation with aliphatic and phenolic OH reactive groups of humic substances. As representative models of phenolic and alcoholic reactive groups of HAs small phenols and alcohols were used (Section 2.3). Complexes of neutral and deprotonated single ligands of uranyl were optimized in solution. Uranyl complexes with deprotonated phenolic and alcoholic RO^- ligands show uranyl bonds U-O_t of 180–181 pm and average equatorial U-O distances U-O_{eq} of 237–238 pm. Complexes with neutral ROH ligands exhibit U-O_t values of 178 pm and U-O_{eq} of 236–239 pm (Section 3.1). These results are rather similar to those for complexes with carboxylic groups (U-O_t = 179 pm, U-O_{eq} = 237 pm). Due to the experimental uncertainty of 1–2 pm in the uranyl bond and 2 pm in U-O_{eq}[13,15,31] these small variations in bond lengths are not easily resolved in experiment. Complexation with phenolic and alcoholic groups of HAs seems to be unlikely due their rather high pK_a values (10–15), at environmental pH (~6–7). The present thesis suggests an alternative mechanism, which includes complexation of uranyl by OH groups and subsequent deprotonation, which is facilitated in the field of the uranyl ion (Section 3.3). It is shown that this mechanism is energetically more favorable. Thus, this computational study supports the experimental suggestion that phenolic OH groups contribute to uranyl complexation and rationalizes the failure of EXAFS in detecting an effect due to blocking of phenolic OH groups by the similarity of phenolate and carboxylate complexes (Section 4).

The second part of this thesis (Sections 5-9) addresses for the first time the adsorption of the uranyl ion on clay mineral surfaces. Kaolinite was chosen as a simple exemplary clay mineral with a relatively small unit cell. This mineral contributes to the clay mineral content of opalinus clay, one of the potential host rocks appropriate for radioactive waste disposal. Not much is known about uranyl adsorption on kaolinite at the atomic level. Experimentally it

was shown, that uranyl adsorbs strongly on kaolinite at a pH higher than 6 under anaerobic conditions.[22] In the presence of air uranyl desorbs at pH values larger than 8 due to formation of soluble carbonate complexes.[24] EXAFS experiments pointed out that uranyl adsorbed as inner-sphere complex on kaolinite, as was confirmed by the presence of two U-Al/Si distances of 310 and 330 pm.[24,25] A TRLFS study found two life times indicating the co-existence of two surface complexes of adsorbed uranyl.[30] Important open issues were the preferred surface facets of adsorption, the chemical identity of the adsorbed complexes, and their structures.

The periodic plane-wave based projector augmented wave approach as implemented in the program VASP was used for investigating uranyl adsorption on kaolinite surfaces (Section 6). First, uranyl adsorption on bare basal (001) kaolinite surfaces, the hydroxylated Al(o) and the Si(t) surface, was studied (Section 7). To avoid charged unit cells, neutralization via defects was invoked (Section 8.2). The corresponding energy cycle was constructed to estimate energies of adsorption.

At the (001) Si(t) surface, formation energies of both inner- and outer-sphere uranyl complexes were calculated endothermic, 239 and 206 kJ mol^{-1}, respectively (Section 8.5). These large values agree with the expectation that the Si(t) surface of kaolinite exhibits a low reactivity as long as charged defects are absent; hence, adsorption of uranyl at this surface is unlikely.

The Al(o) (001) kaolinite surface is more reactive due to a pH dependant surface charge resulting from deprotonation of surface hydroxyl groups. A number of adsorption complexes (inner- and outer-sphere) with different coordination modes (mono- and bidentate) were explored for various adsorption sites at the Al(o) surface (Section 7.3). For inner-sphere complexes, only two deprotonated sites (AlOO and AlOOH) yield main geometry characteristics comparable to those observed in the experiments, although their formation energies with respect to the neutral surface were estimated to be endothermic. Uranyl complexes adsorbed on neutral sites and outer-sphere complexes yield highly exothermic formation energies. Monodentate complexes show the most favorable energy of formation (Section 8.4). Nonetheless, these formation energies should be used with ~~due~~ care since they take the neutral surface as a reference and depend on the reprotonation energy of the defect used for charge neutralization (Section 8.3). At higher pH the Al(o) surface will be partially deprotonated, facilitating uranyl adsorption due to electrostatic attraction. As a simple model of surface solvation the (001) Al(o) surface was covered by a monolayer of water. As judged from these models, surface solvation of adsorption complexes at the Al(o) kaolinite does not

have a strong effect on structural or energetic parameters. The distances U-O_{surf} and U-Al as well as U-O_t were elongated due to solvation, while the average equatorial U-O_{eq} distance was slightly shortened. The main trends and results of comparison with EXAFS data remained unchanged due to solvation.

For outer-sphere complexes at (001) surfaces U-O distances to aqua ligands vary considerably. These computational results are at variance with the common expectation that outer-sphere complexes essentially preserve the structure of solvated uranyl with similar bond lengths U-O_w to the aqua ligands. For outer-sphere complexes a short U-O_w bond, 225–230 pm, was calculated to the aqua ligands that are in direct contact with the surface, while the other U-O_w bonds were determined in the usual range, 240–250 pm (Section 8.4). By these results, one is led to conclude that experimentally detected adsorbed outer-sphere species with a similar geometry as solvated uranyl are associated with more than a single layer of aqua ligands between uranyl and the mineral surface. That hypothesis was checked by models including surface solvation. Two outer-sphere models were constructed at the solvated Al(o) surface, one with a single aqua ligand between uranyl and the surface, and another with two layers of waters between the adsorbate and the surface (Section 9.4). The "splitting" of the bond distances of the first ligand shell of uranyl vanished for the second model, thus confirming the assumption that the experimentally observed outer-sphere species feature more than a single water layer between uranyl and the surface.

As a representative edge surface, the (010) surface of kaolinite was studied. Since the structure of the edge surfaces is unknown, several terminations of the (010) surface were suggested. From model considerations two of them were found to exist more likely in solution (Section 7.4). First, uranyl adsorption on bare edge surfaces was investigated (Section 8.6). Since experimentally only inner-sphere complexes of uranyl adsorbed on kaolinite are characterized, this study was restricted to bidentate complexes of uranyl adsorbed on partially deprotonated sites of the two more favorable terminations (S0 and S1) of the (010) surface (Section 7.5). Results for monodentate complexes at the Al(o) (001) surface showed that this type of coordination yield normally longer U-Al distances than observed in experiment. Energetically all the complexes adsorbed on the S0 and S1 terminations of the edge (010) surface are more favorable than corresponding species on the basal Al (o) (001) surface.

Solvation of the edge (010) surface affects the surface structure (Section 9.3). Neighboring surface groups SiOH-AlOH on S0 and S1 terminations of the (010) surface change to SiO-$AlOH_2$. Uranyl adsorption on solvated surfaces is stabilized strongly by up to 100 kJ mol^{-1}, in contrast to the result for the Al(o) basal surface. Also in some cases the

chemical identity of the adsorbate complex is changed. Thus, surface solvation plays a crucial role in the adsorption on edge surfaces. All inspected adsorption complexes on the S0 termination of the (010) surface transform to adsorbed uranyl monohydroxide by loss of a proton of one of the aqua ligands of uranyl. The shell of equatorial U-O bonds is divided in shorter and longer U-O bonds. Shorter U-O lengths correspond to one (of two) of the surface AlO groups and to the hydroxyl ligand. In turn, longer U-O bonds are formed to aqua ligands and a second surface group. Thus, experimentally determined short U-O bonds characterizing inner-sphere adsorption may not only be attributed to short U-O_{surf} contacts to the surface, but also to the presence of hydroxyl ligands. Unfortunately, U-O_{surf} and uranyl bonds to OH ligands are indistinguishable by EXAFS. In contrast, models of complexes adsorbed on the ideal S1 termination did not undergo a hydrolysis reaction. The different behavior of the two terminations of (010) kaolinite surfaces is tentatively rationalized by structural differences.

Finally, structural parameters of all bidentate inner-sphere complexes of uranyl adsorbed on the solvated (001) and (010) surfaces were compared with available experimental data (Section 9.6). As a result, at least five surface complexes were found to exhibit satisfactory qualitative agreement of structural parameters with those observed in EXAFS.[22,24,25] A mixed adsorption site containing silanol and aluminol groups is unlikely for uranyl adsorption due to the least favorable complex formation energy as well as deviating structural characteristics. Thus, the models favor neutral or partially deprotonated aluminol sites for uranyl adsorption, and deprotonation of these sites can be facilitated in the field of uranyl. One adsorption complex among the five most probable structures yields UO_2OH^+ as adsorbed species which therefore exhibits two instead of three aqua ligands in the first solvation shell of uranyl. Thus, this complex may be responsible for longer decay times observed in TRLFS experiment.[30] The short-lived species then correspond to adsorbed uranyl with three aqua ligands in the first coordination shell. The presence of OH ligands may explain also relatively high coordination numbers (up to 3) of shorter U-O bonds indicated by EXAFS.[20,22] None of the present models yielded simultaneously the two experimentally determined characteristic U-Al/Si values, ~310 and 330 pm,[24,25] suggesting these two distances to correspond to different adsorption species. Furthermore, a rather short U-Al distance of 310–316 pm is calculated only for uranyl, adsorbed at the AlOO site of the basal Al(o) kaolinite surface and at the AlOOH site of the S1 termination of the (010) surface. The EXAFS peak around 330 pm, interpreted as U-Al distance[24,25] is reproduced in this study in fair agreement with three complexes at partially protonated sites. These findings suggest that there is an equilibrium of different adsorption species that coexist on the surface.

Overall, this thesis demonstrates that scalar-relativistic density functional methods provide a reliable approach to model accurately actinide environmental chemistry in solution and at mineral surfaces. As was shown, solvation effects may play a crucial role in uranyl adsorption, especially on clay mineral edge surfaces. Thus, an adequate solvation model is important for treating more reactive surfaces. Improved solvation models including thermodynamic corrections are highly desirable for more accurate studies of the sorption process and especially for a quantitative determination of adsorption energies. Attention should be paid to this topic in future method developments. While force field methods are efficient enough to treat actinide adsorption at more complex mineral surface in a dynamic way, a corresponding treatment by accurate quantum mechanical approaches at present is too demanding to cope with model systems of reliable size. Although it is still a challenge for a computational treatment to establish an adequate model of realistic environmental conditions, calculations of simplified models of uranyl complexation can provide important insights and may help to rationalize experimental findings, as has been demonstrated in this thesis.

Appendix A – Basis sets

This appendix summarizes all atomic basis sets used in this thesis. The program ParaGauss employs products of primitive Gaussian functions of the form $\exp(-\alpha_i r^2)$ and real spherical harmonic functions Y_l^m for the representation of the molecular orbitals. In the following tables the exponents α_i will be listed for the atoms hydrogen, carbon, oxygen, and uranium. The size of the basis sets are given in the notation introduced in Section 2.1, i.e. (n_0s, n_1p, n_2d, n_3f) and [N_0s, N_1p, N_2d, N_3f] for primitive and contracted sets, respectively.

In addition, the size of the auxiliary basis sets to represent the charge density is given in the form (n_0s, n_1r^2, m_1p, m_2d, m_3f). The exponents of the corresponding *s*- and r^2-type "fitting functions" are generated from the orbital basis (see Section 2.1). The exponents for higher angular momenta *p*, *d*, and *f* are added each as a geometric series with a progression of 2.5, starting with 0.1, 0.2, and 0.3 au, respectively; typically, five "polarization exponents" are used for each angular momentum. The corresponding exponents are given in the following table.

Exponents for polarization fitting functions

	p	d	f
α_1	0.10000000	0.20000000	0.30000000
α_2	0.25000000	0.50000000	0.75000000
α_3	0.62500000	1.25000000	1.87500000
α_4	1.56250000	3.12500000	4.68750000
α_5	3.90625000	7.81250000	11.71875000

Hydrogen (Z = 1): (6s, 1p) basis set

Ref. 91a,c

Contraction (6s, 1p) → [4s, 1p]

Fitbasis (6s, $1r^2$, 5p)

	s	p
α_1	0.08989100	1.00000000
α_2	0.25805300	
α_3	0.79767000	
α_4	2.82385400	
α_5	12.40955800	
α_6	82.63637400	

Carbon (Z = 6): (9s, 5p, 1d) basis set

Ref. 91a,b

Contraction (9s, 5p, 1d) → [5s, 4p, 1d]

Fitbasis (9s, $5r^2$, 5p, 5d)

	s	**p**	**d**
α_1	0.15659000	0.12194000	0.60000000
α_2	0.51190000	0.38554000	
α_3	2.41804900	1.20671000	
α_4	6.17577600	4.15924000	
α_5	16.82356200	18.84180000	
α_6	50.81594200		
α_7	178.35083000		
α_8	782.20479500		
α_9	5240.63525800		

Oxygen (Z = 8): (9s, 5p, 1d) basis set

Ref. 91a,b

Contraction (9s, 5p, 1d) → [5s, 4p, 1d]

Fitbasis (9s, $5r^2$, 5p, 5d)

	s	**p**	**d**
α_1	0.30068600	0.21488200	1.15000000
α_2	1.00427100	0.72316400	
α_3	4.75680300	2.30869000	
α_4	12.28746900	7.84313100	
α_5	33.90580900	34.85646300	
α_6	103.65179300		
α_7	364.72525700		
α_8	1599.70968900		
α_9	10662.28494000		

Uranium (Z = 92): (24s, 19p, 16d, 11f) basis set

Ref. 90

Contraction (24s, 19p, 16d, 11f) → [10s, 7p, 7d, 4f]

Fitbasis (24s, $9r^2$, 5p, 5d, 5f)

	s	**p**	**d**	**f**
α_1	0.02058815	0.15790660	0.03447413	0.11032550
α_2	0.04313320	0.40899790	0.08774074	0.30254220
α_3	0.08254175	0.90591220	0.21542030	0.73748150
α_4	0.31243190	2.29137600	0.51211640	1.69235400
α_5	0.65236340	4.64911000	1.20507700	3.75266500
α_6	1.85772200	11.13758000	2.55673600	8.17341700
α_7	3.33603700	22.85757000	5.22965900	17.51736000
α_8	8.81990900	52.73747000	10.89752000	38.22365000
α_9	15.37485000	113.71170000	22.23856000	86.84438000
α_{10}	37.71001000	270.72840000	45.78370000	219.08110000
α_{11}	69.22380000	649.75080000	94.63173000	703.26150000
α_{12}	172.98510000	1673.81000000	205.18560000	
α_{13}	370.13750000	4676.74500000	474.04020000	
α_{24}	849.55400000	14437.84000000	1215.79900000	
α_{15}	1981.83800000	50135.61000000	3707.24200000	
α_{16}	4869.81100000	200185.00000000	16079.47000000	
α_{17}	12511.46000000	948314.40000000		
α_{18}	33651.45000000	5589055.00000000		
α_{19}	95179.62000000	30062560.00000000		
α_{20}	285123.90000000			
α_{21}	912190.10000000			
α_{22}	3147013.00000000			
α_{23}	12113820.00000000			
α_{24}	48171220.00000000			

Appendix B – Data for bulk kaolinite

Table B1. Unit cell parameters for bulk kaolinite calculated at LDA and GGA (PW91) levels.

	a	***b***	***c***	***α***	***β***	***γ***
LDA	5.115	8.878	7.188	92	105.2	89.8
GGA	5.209	9.042	7.451	92	105.2	89.8

Table B2. Cartesian coordinates of the bulk kaolinite structure, optimized at the LDA and GGA (PW91) levels.

	LDA			GGA		
	x	**y**	**z**	**x**	**y**	**z**
Al	1.00081	4.26822	3.20434	1.00806	4.34052	3.28205
Al	0.97574	7.25282	3.17786	0.98403	7.37921	3.25305
Al	3.57418	8.70855	3.20434	3.59587	-0.18036	3.29414
Al	3.51783	2.81251	3.17785	3.57184	2.85833	3.26513
Si	0.17769	2.96244	0.45184	0.17123	3.01940	0.50403
Si	0.25241	5.88077	0.46527	0.25349	5.98966	0.50367
Si	2.75106	7.40272	0.45185	2.79256	7.54086	0.48422
Si	2.79450	1.44048	0.46528	2.84130	1.46878	0.51576
O	0.02936	3.03959	2.04188	0.01898	3.10652	2.11362
O	0.38685	5.79407	2.05351	0.39979	5.90506	2.11149
O	-1.44894	4.17284	6.70915	-1.56244	4.23777	7.01075
O	-0.51015	1.74189	6.86580	1.40653	2.06752	-0.00174
O	-0.48373	6.56598	6.71312	-0.50503	6.63416	7.00115
O	2.60274	7.47994	2.04193	2.64032	7.62799	2.09381
O	2.92897	1.35373	2.05356	2.98759	1.38417	2.12358
O	1.12445	8.61318	6.70910	1.05890	8.75923	6.99093
O	2.06327	6.18222	6.86581	4.02788	6.58898	-0.02155
O	2.05842	2.12566	6.71313	2.08278	2.11327	7.01323
O	0.02418	8.52472	2.10243	0.01144	8.66345	2.17908
O	-0.98895	1.33168	4.08937	-1.03997	1.35064	4.20448
O	-0.59240	4.05648	4.08398	-0.59922	4.10670	4.19361
O	-0.58067	7.45648	4.13057	-0.59090	7.60762	4.22975
O	2.56629	4.08438	2.10243	2.59925	4.14256	2.19116
O	1.58442	5.77202	4.08937	1.58136	5.87210	4.18466
O	1.98099	8.49682	4.08398	2.02212	8.62816	4.17379
O	1.96144	3.01615	4.13056	1.99691	3.08674	4.24183
O	0.02418	8.52472	2.10243	0.46568	0.46464	2.20003
H	0.48574	0.49438	2.14427	-0.75956	1.36611	5.13406
H	-0.70820	1.35753	5.02847	-0.79624	4.34149	5.11620
H	-0.80256	4.26558	5.02096	-0.79251	7.18689	5.08106
H	-0.74750	7.05640	5.01036	3.08702	4.98611	2.18022
H	3.05912	4.93472	2.14427	1.86178	5.88758	5.11425
H	1.86517	5.79787	5.02847	1.79156	-0.17940	5.12829
H	1.73955	-0.17476	5.02096	1.79529	2.66600	5.09314
H	1.79460	2.61607	5.01036	1.00806	4.34052	3.28205

Bibliography

[1] B. M. Thompson, P. A. Longmire, D. G. Brookings, *Applied Geochem*. **1986**, *1*, 335.

[2] I. Grenthe, R. J. M. Fuger, R. J. Konings, A. B. Lemire, A. B. Muller, C. Nguyen-Tsung Cregu, H. Wanner; *Chemical Thermodynamics of Uranium*; H. Wanner, I. Forest eds.; Elsevier: Amsterdam, 1992.

[3] P. I. Mitchell, J. V. Batlle, A. B. Downes, O. M. Condren, L. L. León Vintró, J. A. Sánchez Cabeza, *Appl. Radiat. Isot*. **1995**, *46*, 1175.

[4] C. Degueldre, J. M. Paratte, *J. Nucl. Mater*. **1999**, *273*, 1.

[5] *Kristallin-I, Safety Assessment Report*, Nagra Technical Reports NTB 93-22E, National Cooperative for the Disposal of Radioactive Waste: Wettingen (Switzerland), 1994.

[6] Endlagerung hochradioaktiver Abfälle in Deutschland, *Untersuchung und Bewertung von Regionen mit potenziell geeigneten Wirtsgesteinsformationen*. BGR, Hannover/Berlin, April 2007.

[7] P. J. Finck, hearing on Nuclear Fuel Reprocessing, June 16, 2005. Before the House Committee on Science, Energy Subcommittee. U. S. Department of Energy, Argonna National Laboratory.

[8] „Sicherheitsanforderungen an die Endlagerung wärmeentwickelnder radioaktiver Abfälle“, Entwurf, Bundesministerium für Umwelt, Naturschutz und Reaktorsicherheit, Bonn, 2008. http://www.bmu.de/atomenergie_ver_und_entsorgung/downloads/doc/42047.php

[9] *Project Opalinus Clay, Safety Report*, Nagra Technical Reports NTB 02-05, National Cooperative for the Disposal of Radioactive Waste: Wettingen (Switzerland), 2002.

[10] S. Sachs, K. Schmeide, T. Reich, V. Brendler, K. H. Heise, G. Bernhard, *Radiochim. Acta* **2005**, *93*, 17.

[11] M. A. Denecke, *Coord. Chem. Rev*. **2006**, *250*, 730.

[12] K. Schmeide, T. Reich, S. Sachs, *Inorg. Chim. Acta* **2006**, *359*, 237.

[13] K. Schmeide, S. Sachs, M. Bubner, T. Reich, K. H. Heise, G. Bernhard, *Inorg. Chim. Acta* **2003**, *351*, 133.

[14] V. Vallet, H. Moll, U. Wahlgren, Z. Szabó, I. Grenthe, *Inorg. Chem.* **2003**, *42*, 1982.

[15] A. Rossberg, L. Baraniak, T. Reich, C. Hennig, G. Bernhard, H. Nitsche, *Radiochim. Acta* **2000**, *88*, 593.

[16] M. A. Denecke, T. Reich, S. Pompe, M. Bubner, K. H. Heise, H. Nitsche, P. G. Allen, J. J. Bucher, N. M. Edelstein, D. K. Shuh, *J. Phys*. **1997**, IV 7, C2:637.

[17] T. Reich, H. Moll, M. A. Denecke, G. Geipel, G. Bernhard, H. Nitsche, P. G. Allen, J. J. Bucher, N. Kaltsoyannis, N. M. Edelstein, D. K. Shuh, *Radiochim. Acta* **1996**, *74*, 219.

[18] T. Reich, H. Moll, T. Arnold, M. A. Denecke, C. Hennig, G. Geipel, G. Bernhard, H. Nitsche, P. G. Allen, J. J. Bucher, N. M. Edelstein, D. K. Shuh, *J. Electron. Spectrosc.* **1998**, *96*, 237.

[19] C. Hennig, T. Reich, R. Dähn, A. M. Scheidegger, *Radiochim. Acta* **2002**, *90*, 653.

[20] E. R. Sylvester, E. A. Hudson, P. G. Allen, *Geochim. Cosmochim. Acta* **2000**, *64*, 2431.

[21] A. Dent, J. D. F. Ramsay, S. W. Swanton, *J. Colloid Interface Sci.* **1992**, *150*, 45.

[22] H. Thompson, G. Parks, J. Brown. In *Adsorption of Metals by Geomedia*; E. Jenne, ed.; Academic Press: San Diego, 1998, p. 350.

[23] C. Den Auwer, E. Simoni, S. Conradson, C. Madic, *Eur. J. Inorg. Chem*. **2003**, *21*, 3843.

[24] T. Reich, T. Ye. Reich, S. Amayri, J. Drebert, N. L. Banik, R. A. Buda, J. V. Kratz, N. Trautmann, AIP Conf. Proc. **2007**, *882*, 179.

[25] A. Křepelová, T. Reich, S. Sachs, J. Drebert, G. Bernhard, *J. Colloid Interface Sci.* **2008**, *319*, 40.

[26] Z. Szabó, H. Moll, I. Grenthe, *J. Chem. Soc. Dalton Trans*. **2000**, *18*, 3158.

[27] M. Morgenstern, R. Klenze, J. I. Kim, *Radiochim. Acta* **2000**, *88*, 7.

[28] N. Baumann, V. Brendler, T. Arnold, G. Geipel, G. Bernhard, *J. Colloid Interface Sci.* **2005**, *290*, 318.

[29] Z. M. Wang, J. M. Zachara, P. L. Gassman, C. X. Liu, O. Qafoku, W. Yantasee, J. G. Catalan, *Geochim. Cosmochim. Acta* **2005**, *6*, 1391.

[30] A. Křepelová, V. Brendler, S. Sachs, N. Baumann, G. Bernhard, *Environ. Sci. Technol*. **2007**, *41*, 6142.

[31] S. Pompe, K. Schmeide, M. Bubner, G. Geipel, K. H. Heise, G. Bernhard, H. Nitsche, *Radiochim. Acta* **2000**, *88*, 553.

[32] H. Moll, G. Geipel, T. Reich, G. Bernhard, Th. Fanghänel, I. Grenthe, *Radiochim. Acta* **2003**, *91*, 11.

[33] S. P. Pasilis, J. E. Pemberton, *Inorg. Chem*. **2003**, *42*, 6793.

[34] F. Quilès, A. Burneau, *Vib. Spectrosc*. **1998**, *18*, 61.

[35] T. Payne, G. Lumpkin, T. Waite. In *Adsorption of Metals by Geomedia*; E. Jenne, ed.; Academic Press: San Diego, 1998; p. 75.

[36] Y. Arai, M. McBeath, J. Bargar, J. Joye, J. Davis, *Geochim. Cosmochim. Acta* **2006**, *70*, 2492.

[37] A. Křepelová, S. Sachs, G. Bernhard, *Radiochim. Acta* **2006**, *94*, 825.

[38] C. J. Chisholm-Brause, J. M. Berg, K. M. Little, R. A. Matzner, D. E. Morris, *J. Colloid Interface Sci.* **2004**, *277*, 366.

[39] M. Pepper, B. E. Bursten, *Chem. Rev*. **1991**, *91*, 719.

[40] N. Rösch, S. Krüger, M. Mayer, V. A. Nasluzov. In *Recent Developments and Applications of Modern Density Functional Theory*; J. M. Seminario ed.; Elsevier: Amsterdam, 1996, p. 497.

[41] N. Rösch, A. V. Matveev, V. A. Nasluzov, K. M. Neyman, L. Moskaleva, S. Krüger. In *Relativistic Electronic Structure Theory-Applications*; P. Schwerdtfeger ed.; Elsevier: Amsterdam, 2004, p. 676.

[42] G. Schreckenbach, P. J. Hay, R. L. J. Martin, *Comp. Chem*. **1999**, *20*, 70.

[43] V. Vallet, P. Macak, U. Wahlgren, I. Grenthe, *Theor. Chem. Acc.* **2006**, *115*, 145.

[44] T. Privalov, B. Schimmelpfennig, U. Wahlgren, I. Grenthe, *J. Phys. Chem. A* **2003**, *107*, 587.

[45] S. Spencer, L. Gagliardi, N. C. Handy, A. G. Ioannou, C. K. Skylaris, A. Willets, A. M. Simper, *J. Phys. Chem. A* **1999**, *103*, 1831.

[46] T. Fleig, H. J. Jensen, J. Olsen, L. Visscher, *J. Chem. Phys*. **2006**, *124*, 104106.

[47] V. Vallet, U. Wahlgren, B. Schimmelpfennig, H. Moll, Z. Szabó, I. Grenthe, *Inorg. Chem*. **2001**, *40*, 3516.

[48] R. A. Zielinsli, D. T. Chafin, E. R. Banta, B. J. Szabo, *Environ. Geol*. **1997**, *32*, 124.

[49] A. Kremleva, S. Krüger, N. Rösch, *Inorg. Chim. Acta* **2009**, *362*, 2542.

[50] A. Kremleva, S. Krüger, N. Rösch, *Langmuir* **2008**, *24*, 9515.

[51] A. Kremleva, S. Krüger, N. Rösch, in preparation.

[52] M. Åberg, D. Ferri, J. Glaser, I. Grenthe, *Inorg. Chem*. **1983**, *32*, 3986.

[53] U. Wahlgren, H. Moll, I. Grenthe, B. Schimmelpfennig, L. Maron, V. Vallet, O. Gropen, *J. Phys. Chem. A* **1999**, *103*, 8257.

[54] D. Hagberg, G. Karlström, B. O. Roos, L. Gagliardi, *J. Am. Chem. Soc*. **2005**, *127*, 14250.

[55] C. Nguyen-Trung, D. A. Palmer, G. M. Begun, C. Peiffert, R. E. J. Mesmer, *J. Solution Chem*. **2000**, *29*, 101.

[56] Jr. C. F. Baes, R. E. Mesmer. *The Hydrolysis of Cations*; Wiley: New York, 1976, p.174.

[57] G. R. Choppin, *Radiochim. Acta* **1988**, *44/45*, 23.

[58] G. R. Choppin, *Radiochim. Acta* **1992**, *58/59*, 113.

[59] D. L. Clark, D. E. Hobart, M. P. Neu, *Chem. Rev*. **1995**, *95*, 25.

[60] L. Maya, *Inorg. Chem*. **1982**, *21*, 2895.

[61] K. Nash, S. Fried, A. M. Friedman, J. C. Sullivan *Environ. Sci. Technol*. **1981**, *15*, 834.

[62] Y. P. Chin, P. M. Gschwend, *Geochim. Cosmochim. Acta* **1991**, *55*, 1309.

[63] *Humus Chemistry: Genesis, Composition, Reactions*; F. J. Stevenson ed.; John Wiley & Sons, Inc.: New York, 1994.

[64] B. A. Dempsey, C. R. O'Melia, *Aquatic and Terrestrial Humic Materials*; R. F. Christman and E. T. Gjessing eds.; Ann. Arbor Sci. Publ., Michigan, 1983.

[65] G. R. Choppin, L. Kullberg, *J. Inorg. Chem*. **1978**, *40*, 651.

[66] G. R. Choppin, B. Allard. In *Handbook on the Physics and Chemistry of the Actinides*; A. J. Freeman, C. Keller eds.; Elsevier: Amsterdam, 1985, p. 407.

[67] Z. Szabó, I. Grenthe, *Inorg. Chem*. **2000**, *39*, 5036.

[68] A. Günther, G. Geipel, G. Bernhard, *Polyhedron* **2007**, *26*, 59.

[69] P. Lagrange, M. Schneider, J. Lagrange, *Polyhedron* **1994**, *13*, 861.

[70] P. Lagrange, M. Schneider, J. Lagrange, *J. Chim. Phys*. **1998**, *95*, 2280.

[71] S. Sachs, G. Bernhard, *Radiochim. Acta* **2005**, *93*, 141.

[72] S. Krüger, F. Schlosser, S. R. Ray, N. Rösch. In *Lecture Series on Computer and Computational Sciences*; T. Simos, G. Maroulis eds.; Koninklijke Brill NV: Leiden, 2006, p. 904.

[73] F. Schlosser, *A Relativistic Density Functional Study of Actinide Complexation in Aqueous Solution*, Doctoral Thesis, Technische Universität München, 2006.

[74] V. Vallet, U. Wahlgren, B. Schimmelpfennig, Z. Szabó, I. Grenthe, *J. Am. Chem. Soc*. **2001**, *123*, 11999.

[75] H. Bolvin, U. Wahlgren, H. Moll, T. Reich, G. Geipel, Th. Fanghänel, I. Grenthe, *J. Phys. Chem. A* **2001**, *105*, 11441.

[76] F. Schlosser, S. Krüger, N. Rösch, *Inorg. Chem*. **2006**, *45*, 1480.

[77] M. S. K. Fuchs, A. M. Shor, N. Rösch, *Int. J. Quantum Chem*. **2002**, *86*, 487.

[78] B. I. Dunlap, N. Rösch, *Adv. Quantum Chem*. **1990**, *21*, 317.

[79] T. Belling, T. Grauschopf, S. Krüger, F. Nörtemann, M. Staufer, M. Mayer, V. A. Nasluzov, U. Birkenheuer, A. Hu, A. V. Matveev, A. M. Shor, M. S. K. Fuchs-Rohr, K. M. Neyman, D. I. Ganyushin, T. Kerdcharoen, A. Woiterski, A. B. Gordienko, S. Majumder, N. Rösch, PARAGAUSS, version 3.0, Technical University of Munich, 2004.

[80] O. D. Häberlen, N. Rösch, *Chem. Phys. Lett*. **1992**, *199*, 491.

[81] M. Douglas, N. M. Kroll, *Ann. Phys*. **1974**, *82*, 89.

[82] G. Jansen, B. A. Hess, *Phys. Rev. A* **1989**, *39*, 6016.

[83] M. Mayer, S. Krüger, N. Rösch, *J. Chem. Phys*. **2001**, *115*, 4411.

[84] M. García-Hernández, C. Lauterbach, S. Krüger, A. Matveev, N. Rösch, *J. Comp. Chem*. **2002**, *23*, 834.

[85] S. H. Vosko, L. Wilk, M. Nusair, *Can. J. Phys*. **1980**, *58*, 1200.

[86] T. Ziegler, *Chem. Rev*. **1991**, *91*, 651.

[87] A. D. Becke, *Phys. Rev. A* **1988**, *38*, 3098.

[88] J. P. Perdew, *Phys. Rev. B* **1986**, *33*, 8822.

[89] A. Görling, S. B. Trickey, P. Gisdakis, N. Rösch. In *Topics in Organometallic Chemistry*; J. Brown, P. Hoffman eds.; Springer: Heidelberg (Germany), 1999, p.109.

[90] T. Minami, O. Matsuoka, *Theo. Chim. Acta* **1995**, *90*, 27.

[91] (a) F. B. Van Duijneveldt, IBM Res. Rep. 1971, RJ 945. (b) S. Huzinaga, J. Andzelm, M. Klobukowski, E. Radzio-Andzelm, Y. Sakai, H. Tatewaki, *Gaussian Basis Sets for Molecular Calculations*, Elsevier, Amsterdam, 1984 [O: d exponent 1.15; C: d exponent 0.60]. (c) M. J. Frisch, J. A. Pople, J. S. Binkley, *J. Chem. Phys*. **1984**, *80*, 3265 [H: p exponent 1.0].

[92] M. Garcia-Hernandez, C. Willnauer, S. Krüger, L. Moskaleva, N. Rösch, *Inorg. Chem.* **2006**, *45*, 1356.

[93] A. D. Becke, *J. Chem. Phys.* **1988**, *88*, 2547.

[94] A. Klamt, G. Schürmann, *J. Chem. Soc. Perkin Trans*. **1993**, *2*, 799.

[95] J. Andzelm, C. Kölmel, A. Klamt, *J. Chem. Phys*. **1995**, *103*, 9312.

[96] V. Barone, M. Cossi, *J. Phys. Chem. A* **1988**, *102*, 1995.

[97] C. Amovilli, V. Barone, R. Cammi, E. Cances, M. Cossi, B. Mennucci, C. S. Pomelli, J. Tomasi, *J. Adv. Quantum Chem*. **1998**, *32*, 227.

[98] A. Bondi, *J. Phys. Chem*. **1964**, *68*, 441.

[99] J. L. Pasqual-Ahuir, E. Silla, *J. Comput. Chem*. **1990**, *11*, 1047.

[100] E. Silla, I. Tuñón, J. L. Pasqual-Ahuir, *J. Comput. Chem*. **1991**, *12*, 1077.

[101] D. A. McQuarrie, J. D. Simon, *Molecular Thermodynamics*; University Science Books: Sausalito, 1999.

[102] J. E. Huheey, *Inorganic Chemistry: Principles of Structure and Reactivity*; Harper and Row: New York, 1983, p. 527.

[103] R. S. Ray, *A Relativistic Density Functional Study of Uranyl Hydrolysis and Complexation by Carboxylic Acids in Aqueous Solution*, Doctoral Thesis, Technische Universität München, 2009.

[104] G. J. Tawa, I. A. Topol, S. K. Burt, R. A. Caldwell, A. A. Rashin, *J. Chem. Phys*. **1998**, *109*, 4852.

[105] M. W. Palascak, G. C. Shields, *J. Phys. Chem*. **2004**, *108*, 3692.

[106] D. M. Chipman, F. J. Chen, *J. Chem. Phys*. **2006**, *124*, 144507.

[107] C. P. Kelly, C. J. Cramer, D. G. Truhlar, *J. Chem. Theory Comput*. **2005**, *1*, 1133.

[108] C. P. Kelly, C. J. Cramer, D. G. Truhlar, *J. Phys. Chem. A* **2006**, *110*, 2493.

[109] J. R. Jr. Pliego, J. M. Riveros, *J. Phys. Chem. A* **2002**, *106*, 7434.

[110] V. S. Bryantsev, M. S. Diallo, W. A. Goddard III, *J. Phys. Chem. B* **2008**, *112*, 9709.

[111] D. D. Perrin, *Dissociation Constants of Organic Bases in Aqueous Solution*; Butterworths: London, 1965.

[112] I. Grenthe, J. Fuger, R. J. Lemire, A. B. Muller, C. Nguyen-Trung, H. Wanner, NED-TDB *Chemical Thermodynamics of Uranium*, Nuclear Energy Agency, Organization for Economic Cooperation and Development, Elsevier Science, Amsterdam, 1992.

[113] R. S. Ray, S. Krüger, N. Rösch, accepted in *Inorg. Chim. Acta*.

[114] S. Guggenheim, *Clays Clay Miner.* **1995**, *43*, 255.

[115] B. Velde. In *Origin and Mineralogy of Clays*; B. Velde ed.; Springer-Verlag: New York, 1995, p. 8.

[116] D. L. Sparks, *Environmental Soil Chemistry*; Academic Press: San Diego, 2003.

[117] G. Sposito, *The Surface Chemistry of soils*; Oxford Univ. Pres: New York, 1984.

[118] G. Sposito, N. T. Skipper, R. Sutton, S. Park, A. Soper, J. A. Greathouse, Proc. Natl. Acad. Sci. USA (colloquium paper) 1999, Vol. 96, pp. 3358.

[119] B. Bickmore, D. Bosbach, M. Jr. Hochella, L. Charlet, E. Rufe, *Am. Mineral.* **2001**, *86*, 411.

[120] M. Zbik, R. Smart, *Clays Clay Miner.* **1998**, *46*, 153.

[121] W. Stumm, *Chemistry of the Solid-water Interface. Processes at the Mineral-water and Particle-water Interface in Natural Systems*; Wiley: New-York, 1992.

[122] J. Kameda, A. Yamagishi, T. Kogure, *Am. Mineral.*, **2005**, *90*, 1462.

[123] S. V. Churakov, *Geochim. Cosmochim. Acta* **2007**, *71*, 1130.

[124] S. V. Churakov, *J. Phys. Chem. B* **2006**, *110*, 4135.

[125] C. M. Koretsky, D. A. Sverjensky, N. Sahai, *Am. J. of Sci.* **1998**, *298*, 349.

[126] B. R. Bickmore, K. M. Rosso, K. L. Nagy, R. T. Cygan, C. J. Tadanier, *Clays Clay Miner.* **2003**, *51*, 359.

[127] E. Wieland, W. Stumm, *Geochim. Cosmochim. Acta* **1992**, *56*, 3339.

[128] T. Hiemstra, W. H. Van Riemsdijk, G. H. Bolt, *J. Colloid Int. Sci.* **1989**, *133*, 91.

[129] C. M. Marquardt. In *Migration of Actinides in the System Clay, Humic Substances, Aquifer*; C. M. Marquardt ed.; Forschungszentrum Karlsruhe GmbH: Karlsruhe, 2008.

[130] N. L. Banik, R. A. Buda, S. Burger, J. V. Kratz, N. Trautmann, *Radiochim. Acta* **2007**, *95*, 569.

[131] S. Amayri, N. L. Banik, M. Breckheimer, R. A. Buda, S. Bürger, J. Drebert, A. Jermolaev, J. V. Kratz, B. Kuczewski, D. Kutscher, T. Ye. Reich, T. Reich, N. Trautmann. In *Migration of Actinides in the System Clay, Humic Substances, Aquifer*; C. M. Marquardt ed.; Forschungszentrum Karlsruhe GmbH: Karlsruhe, 2008, p.141.

[132] F. P. Bertetti, R. T. Pabalan, M. G. Almendarez. In *Adsorption of metals by geomedia*; E. Jenne, ed.; Academic Press: San Diego, 1998, p. 132.

[133] T. E. Payne, G. R. Lumpkin, T. D. Waite. In *Adsorption of metals by geomedia*; E. Jenne, ed.; Academic Press: San Diego, 1998, p. 75.

[134] H. Perron, C. Domain, J. Roques, R. Drot, E. Simoni, H. Catalette, *Inorg. Chem*. **2006**, *45*, 6568.

[135] L. Moskaleva, V. Nasluzov, N. Rösch, *Langmuir* **2006**, *22*, 2141.

[136] J. A. Greathouse, R. T. Cygan, *Phys. Chem. Chem. Phys.* **2005**, *7*, 3580.

[137] J. A. Greathouse, R. T. Cygan, *Environ. Sci. Technol.* **2006**, *40*, 3865.

[138] A. C. Hess, V. R. Saunders, *J. Phys. Chem.* **1992**, *96*, 4367.

[139] J. D. Hobbs, R. T. Cygan, K. L. Nagy, P. A. Schultz, M. P. Sears, *Am. Mineral.* **1997**, *82*, 657.

[140] L. Benco, D. Tunega, J. Hafner, H. Lischka, *Am. Mineral.* **2001**, *86*, 1057.

[141] D. Bougeard, K. S. Smirnov, *Phys. Chem. Chem. Phys.* **2007**, *9*, 226.

[142] P. Boulet, H. C. Greenwell, S. Stackhouse, P. V. Coveney, *THEOCHEM* **2006**, *762*, 33.

[143] D. Tunega, G. Haberhauer, M. H. Gerzabek, H. Lischka, *Langmuir* **2002**, *18*, 139.

[144] C. H. Bridgeman, A. D. Buckingham, N. T. Skipper, M. C. Payne, *Mol. Phys.* **1996**, *89*, 879.

[145] D. Tunega, L. Benco, G. Haberhauer, M. H. Gerzabek, H. Lischke, *J. Phys. Chem. B* **2002**, *106*, 11515.

[146] D. Tunega, M. H. Gerzabek, H. Lischka, *J. Phys. Chem. B* **2004**, *108*, 5930.

[147] K. S. Smirnov, D. Bougeard, *J. Phys. Chem. B* **1999**, *103*, 5266.

[148] M. Arab, D. Bougeard, K. S. Smirnov, *Phys. Chem. Chem. Phys.* **2003**, *5*, 4699.

[149] M. Arab, D. Bougeard, K. S. Smirnov, *Phys. Chem. Chem. Phys.* **2004**, *6*, 2446.

[150] (a) G. Kresse, J. Furthmüller, *Phys. Rev. B* **1996**, *54*, 11169. (b) G. Kresse, J. Hafner, *ibid.* **1994**, *49*, 14251. (c) G. Kresse, J. Hafner, *ibid.* **1993**, *47*, 558. (d) G. Kresse, J.

Hafner, *ibid.* **1993**, *48*, 13115. (e) G. Kresse, J. Furthmüller, *Comp. Mat. Sci.* **1996**, *6*, 15.

[151] http://cms.mpi.univie.ac.at/vasp/vasp/node152.html.

[152] J. P. Perdew, A. Zunger, *Phys. Rev. B* **1981**, *23*, 5048.

[153] A. Görling, S. B. Trickey, P. Gisdakis, N. Rösch. In *Topics in Organometallic Chemistry*; Brown, J., Hofmann, P., eds.; Springer: Heidelberg, 1999, Vol. 4, p. 109.

[154] W. Koch, M. C. Holthausen, *A Chemist's Guide to Density Functional Theory*; Wiley-VCH: Weinheim, 2000.

[155] J. P. Perdew, Y. Wang, *Phys. Rev. B* **1992**, *45*, 13244.

[156] F. Sim, A. St-Amant, I. Papai, D. R. Salahub, *J. Am. Chem. Soc.* **1992**, *114*, 4391.

[157] P. E. Blöchl, *Phys. Rev. B* **1994**, *50*, 17953.

[158] G. Kresse, D. Joubert, *Phys. Rev. B* **1999**, *59*, 1758.

[159] A. H. MacDonald, S. H. Vosko, *J. Phys. C* **1979**, *12*, 2977.

[160] H. J. Monkhorst, J. D. Pack, *Phys. Rev. B* **1976**, *13*, 5188.

[161] M. Methfessel, A. T. Paxton, *Phys. Rev. B* **1989**, *40*, 3616.

[162] R. A. Young, A. W. Hewat, *Clays Clay Miner.* **1988**, *36*, 225.

[163] D. Bish, *Clays Clay Miner.* **1993**, *41*, 738.

[164] M. R. Antonio, L. Soderholm. In *The Chemistry of the Actinide and Transactinide Elements*; L. R. Morss, N. M. Edelstein, J. Fuger, eds.; Springer: Dordrecht, 2006; Vol. 5, p. 3086.

[165] L. Pauling, *Am. Chem. Soc.* **1929**, *51*, 1010.

[166] W. F. Bleam, *Rev. Geophys.* **1993**, *31*, 51.

[167] (a) P. Hartmann, W. G. Perdock, *Acta Crystallographica* **1955**, *8*, 49. (b) P. Hartmann, W. G. Perdock, *Acta Crystallographica* **1955**, *8*, 521. (c) P. Hartmann, W. G. Perdock, *Acta Crystallographica* **1955**, *8*, 525.

[168] G. N. White, L. W. Zelazny, *Clay Clay Miner.* **1988**, *36*, 141.

[169] I. D. Brown, D. Altermatt, *Acta Cryst.* **1985**, *B41*, 244.

[170] R. T. Cygan, K. L. Nagy, P. V. Brady. In *Adsorption of Metals by Geomedia*; E. Jenne, ed.; Academic Press: San Diego, 1998, p. 383.

[171] E. Tertre, S. Castet, G. Berger, M. Loubet, E. Giffaut, *Geochim. Cosmochim. Acta* **2006**, *70*, 4579.

[172] M. Garçia-Hernandez, C. Willnauer, S. Krüger, L. V. Moskaleva, N. Rösch, *Inorg, Chem.* **2006**, *45*, 1356.

[173] K. H. Lim, O. Zakharieva, A. M. Shor, N. Rösch, *Chem. Phys. Letters* **2007**, *444*, 280.

[174] G. Henkelman, A. Arnaldsson, H. Jónsson, *Comput. Mater. Sci.* **2006**, *36*, 254.

[175] S. L. Dubarev, G. A. Botton, S. Y. Savrasov, C. J. Humphreys, A. P. Sutton, *Phys. Rev. B* **1998**, *57*, 1505.

[176] Chosen according to a parametrization of ionization potentials of UO_2^+ and UO_2. R. Ramakrishnan and A. V. Matveev, private communication.

[177] R. S. Ray, S. Krüger, N. Rösch, *Dalton Trans.* **2009**, *18*, 3590.

[178] M. S. Gordon, J. M. Mullin, S. R. Pruitt, L. B. Roskop, L. V. Slipchenko, *J. Phys. Chem. B* **2009**, *113*, 9646.

[179] W. Koch, M. C. Holthausen, *A Chemist's Guide to Density Functional Theory*, 2nd ed.; Wiley-VCH: Weinheim, 2000.

[180] J. G. Catalano, G. E. Jr. Brown, *Geochim. Cosmochim. Acta* **2005**, *69*, 2995.

[181] A. Froideval, M. Del Nero, C. Gaillard, R. Barillon, I. Rossini, J. L. Hazemann, *Geochim. Cosmochim. Acta* **2006**, *70*, 5270.

[182] T. Arnold, A. C. Scheinost, N. Baumann, V. Brendler, FZD-IRC Annual report, 2006.

[183] T. Arnold, S. Utsunomiya, G. Geipel, R. C. Ewing, N. Baumann, V. Brendler, *Environ. Sci. Technol*. **2006**, *40*, 4646.

[184] M. A. Denecke, J. Rothe, K. Dardenne, P. Lindqvist-Reis, *Phys. Chem. Chem. Phys.* **2003**, *5*, 939.

[185] (a) U. Wahlgren, H. Moll, I. Grenthe, B. Schimmelpfennig, L. Maron, V. Vallet, O. Gropen, *J. Phys. Chem. A* **1999**, *103*, 8257. (b) P. G. Allen, J. J. Bucher, D. K. Shuh, N. M. Edelstein, T. Reich, *Inorg. Chem*. **1997**, *36*, 4676.

[186] P. V. Brady, R. T. Cygan, K. L. Nagy. In *Adsorption of Metals by Geomedia*; E. Jenne, ed.; Academic Press: San Diego, 1998; p. 371.

[187] H. Moll, T. Reich, Z. Szabó, *Radiochim. Acta* **2000**, *88*, 411.

[188] E. Veilly, J. Roques, M.-C. Jodin-Caumon, B. Humbert, R. Drot, E. Simoni, *J. Chem. Phys*. **2008**, *129*, 244704.

[189] V. Eliet, G. Bidoglio, N. Omenetto, L. Parma, I. Grenthe, *J. Chem. Soc. Faraday Trans.* **1995**, *91*, 2275.

[190] G. Geipel, G. Bernhard, M. Rutsch, V. Brendler, H. Nitsche, *Radiochim. Acta* **2000**, *88*, 757.